Somatic genetics analysis of sleep in adult mice

Guodong Wang[1,2,3,10], Qi Li[1,2,10], Junjie Xu[1,2,4], Shuai Zhao[5], Rui Zhou[1,2,6], Zhenkang Chen[7], Wentong Jiang[1,2,3], Xue Gao[1,2], Shuang Zhou[1,2,4], Zhiyu Chen[1,2], Quanzhi Sun[1,2], Chengyuan Ma[8], Lin Chen[1,2], Bihan Shi[1,2], Ying Guo[1,2], Haiyan Wang[1,2], Xia Wang[1,2], Huaiye Li[1,2], Tao Cai[1,2], Yibing Wang[1,2], Zhineng Chen[5], Fengchao Wang[1,2*] & Qinghua Liu[1,2,9*]

[1]National Institute of Biological Sciences (NIBS), Beijing 102206, China; [2]Tsinghua Institute of Multidisciplinary Biomedical Research, Tsinghua University, Beijing 102206, China; [3]Graduate School of Peking Union Medical College, Chinese Academy of Medical Sciences, Beijing 100730, China; [4]College of Life Sciences, Beijing Normal University, Beijing 100875, China; [5]Institute of Automation, Chinese Academy of Sciences, Beijing 100080, China; [6]College of Biological Sciences, China Agriculture University, Beijing 100094, China; [7]Children's Medical Center Research Institute, UT Southwestern Medical Center, Dallas, TX 75235, USA; [8]Chinese Institute of Brain Science, Beijing 102206, China; [9]International Institute for Integrative Sleep Medicine (WPI-IIIS), University of Tsukuba, Tsukuba 305-8575, Japan.

[10]These authors contributed equally to this study

[Running Title: Somatic genetics analysis of sleep in adult mice]

[Key words: adult brain chimeric (ABC), AAV-PHP.eB, knockout (KO), somatic genetics analysis, Cre/loxP recombination, CRISPR/Cas9, sleep phenotypes]

* Corresponding authors:

liuqinghua@nibs.ac.cn (lead contact); wangfengchao@nibs.ac.cn

SUMMARY

Classical forward and reverse mouse genetics approaches require germline mutations and, thus, are unwieldy to study sleep functions of essential genes or redundant pathways. It is also time-consuming to conduct electroencephalogram/electromyogram-based mouse sleep screening owning to labor-intensive surgeries and genetic crosses. Here, we describe a highly accurate SleepV (video) system and adeno-associated virus (AAV)-based adult brain chimeric (ABC)-expression/knockout (KO) platform for somatic genetics analysis of sleep in adult mice. A pilot ABC-expression screen identifies CREB and CRTC1, of which constitutive or inducible expression significantly reduces quantity and quality of non-rapid eye movement sleep. Whereas ABC-KO of exon 13 of *Sik3* by AAV-Cre injection in *Sik3-E13*$^{flox/flox}$ adult mice phenocopies *Sleepy (Sik3*$^{Slp/+}$*)* mice, ABC-CRISPR of *Slp/Sik3* reverses hypersomnia of *Sleepy* mice, indicating a direct role of SLP/SIK3 kinase in sleep regulation. Multiplex ABC-CRISPR of both orexin/hypocretin receptors causes narcolepsy-like episodes, enabling one-step analysis of redundant genes in adult mice. Finally, ABC-expression/KO screen identifies Ankrd63 and NR1 as two potentially new sleep regulators. Therefore, this somatic genetics approach should facilitate high-throughput analysis of sleep regulatory genes, especially for essential or redundant genes, in adult mice by skipping the mouse development and genetic crosses.

42 **INTRODUCTION**

43 Despite of significant advance in understanding the neural pathways that control executive
44 sleep/wake switching (Liu and Dan, 2019; Saper et al., 2010; Saper et al., 2005; Scammell et al.,
45 2017; Weber and Dan, 2016), the molecular mechanisms of mammalian sleep regulation are largely
46 unclear (Allada et al., 2017; Sehgal and Mignot, 2011; Webb and Fu, 2021). It remains to be
47 identified which genes constitute the core sleep regulatory pathways, and where these molecular
48 pathways may function in the mouse brain. However, it is very costly and time-consuming to
49 conduct large-scale mouse sleep screening for two main reasons: 1) both forward and reverse
50 genetics approaches require germline mutations and genetic crosses (3 months/cross); 2) the
51 electroencephalogram (EEG)/electromyogram (EMG)-based sleep analysis requires labor-intensive
52 and invasive surgeries.

53 Accumulating evidence suggest that sleep is essential for survival in invertebrate and
54 vertebrate animals (Bentivoglio and Grassi-Zucconi, 1997; Rechtschaffen et al., 1989; Shaw et al.,
55 2002; Vaccaro et al., 2020). Thus, it is plausible that core sleep regulatory genes may be essential
56 for survival in mice. It is estimated that about one third of ~23,000 mammalian genes are essential
57 genes (Dickinson et al., 2016), which often encode structural proteins, housekeeping enzymes, or
58 signaling proteins with critical roles at multiple stages of development (Tian et al., 2018). However,
59 classical mouse genetic approaches are unwieldy to study the sleep functions of essential genes
60 owing to early lethality caused by germline mutations.

61 Conditional knockout (KO) mice are commonly used to bypass early lethality and analyze the
62 temporal and/or tissue-specific functions of essential genes (Gierut et al., 2014). Typically, this
63 strategy involves crossing of tissue-specific Cre recombinase or tamoxifen-dependent Cre^{ERT2}
64 expressing transgenic mice with conditional flox mice that contain two loxP sites flanking a critical
65 exon(s) of target gene (Feil et al., 1996; Gierut et al., 2014). The Cre/loxP-mediated site-specific
66 recombination will exercise the critical exon(s) and disrupt the target gene in a tissue-specific

67 and/or temporal manner. However, this time-consuming (1 to 2 years) approach requires
68 construction of appropriate Cre transgenic and flox mouse strains, but also multiple genetic crosses
69 to generate sufficient number of conditional KO mice for comprehensive sleep analysis (Gierut et
70 al., 2014).

71 Given the vital importance of sleep in physiology and survival, it is likely that redundant
72 pathways exist for sleep regulation. Thus, ablation of a gene of interest may cause mild or no sleep
73 phenotype owning to genetic redundancy. Additionally, mice with germline mutations may adapt
74 or compensate for sleep phenotypes before the EEG/EMG-based sleep analysis that is normally
75 conducted in adult mice. Moreover, it is a costly and tedious process to generate double or triple
76 KO mice by conventional germline genetics methods. A combination of triple-target CRISPR/Cas9
77 and modified embryonic stem cell technologies facilitates biallelic KO of redundant genes for sleep
78 phenotype analysis in a single generation, but it does not work for essential genes (Sunagawa et al.,
79 2016).

80 Recombinant adeno-associated viruses (AAVs) have been widely used as vehicles for gene
81 expression, knockdown/knockout and gene therapy in the central nervous system (CNS) (Borel et
82 al., 2014; Suzuki et al., 2016; Yang et al., 2016). To bypass the blood-brain barrier (BBB) and
83 spatially restrict gene expression, these applications often require local AAV injection into specific
84 regions of the mouse brain (Castro et al., 2021; Hunker et al., 2020; Zell et al., 2020). Alternatively,
85 intravenous administration of AAVs provides a non-invasive strategy for systemic gene delivery
86 into the CNS (Choudhury et al., 2016; Deverman et al., 2016; Foust et al., 2009). In particular,
87 Gradinaru and colleagues have used the Cre-recombination-based AAV-targeted evolution
88 (CREATE) to isolate AAV9 variants, such as AAV-PHP.B and AAV-PHP.eB, which can
89 efficiently bypass BBB and transduce the majority of adult brain neurons and astrocytes in certain
90 mouse strains (Chan et al., 2017; Deverman et al., 2016). Both AAV-PHP.B and AAV-PHP.eB
91 have been successfully used to deliver systemic gene expression (Liu et al., 2021; Luoni et al.,

92 2020; Silva-Pinheiro et al., 2020), or target gene ablation by CRISPR/Cas9 across the adult mouse
93 brain neurons (Torregrosa et al., 2021; Xiao et al., 2021; Yamaguchi and de Lecea, 2019).
94 Here, we systematically assembled, optimized and utilized this AAV-PHP.eB-based adult
95 brain chimeric (ABC)-expression/KO platform for somatic genetics analysis of sleep in adult mice
96 **(Figure 1)**. We also developed a highly accurate, non-invasive and fully automated SleepV (video)
97 system for high-throughput mouse sleep screening. By skipping the mouse development and
98 genetic crosses, this somatic genetics approach, coupled with the SleepV system, should facilitate
99 highly efficient analysis of sleep regulatory genes, especially for essential or redundant genes, in
100 adult mice.
101
102 **RESULTS**
103 **Development of ABC platform for somatic genetics analysis of sleep in adult mice**
104 Sleep and wakefulness are two alternate physiological states of the brain, which globally
105 impact the molecular, synaptic and cellular activities across the whole brain (Cirelli and Tononi,
106 1998; de Vivo et al., 2017; Diering et al., 2017; Elliott et al., 2014; Tononi and Cirelli, 2014; Wang
107 et al., 2018). Thus, homeostatic sleep regulation likely involves the majority of neurons and
108 possibly astrocytes across the adult mouse brain (Tononi and Cirelli, 2014; Wang et al., 2018). It
109 has been reported that retro-orbital injection of 10^{11} vector genomes (vg) of single-stranded AAV-
110 PHP.eB systemically transduced approximately 40% to 80% of adult brain neurons and astrocytes
111 (Chan et al., 2017). Therefore, we hypothesized that AAV-PHP.eB-mediated ABC-expression or
112 knockout of sleep regulatory genes should theoretically result in significant sleep phenotypes
113 **(Figure 1)**.
114 To verify the efficiency of this AAV delivery system, we performed retro-orbital injection of
115 12-week old C57BL/6J mice with dual AAV-PHP.eB (10^{12} vg/mice), AAV-CBh-Cre and AAV-
116 EF1α-DIO-H2B-eGFP **(Figure 1-figure supplement 1A)**. Thus, only brain cells co-transduced

with both AAVs could exhibit the Cre-dependent expression of histone H2B-GFP fusion proteins. As shown by co-immunostaining of GFP and NeuN, a pan-neuronal marker protein **(Figure 1-figure supplement 1B and C)**, these two viruses efficiently co-transduced the majority of the adult brain neurons two weeks after AAV administration. Quantification of double positive cells showed high percentage of GFP-expressing neurons across nine different brain regions, ranging from averaging 56.6% in the hippocampus to 88.7% in the thalamus **(Figure 1-figure supplement 1D)**. More importantly, ABC-expression of the GFP reporter did not affect the sleep-wake architecture in the AAV-PHP.eB-injected mice relative to no virus injected control mice **(Figure 1-figure supplement 1E-H)**, suggesting that it is feasible to use the ABC-expression/KO platform for rapid and efficient somatic genetics analysis of sleep regulatory genes.

Figure 1. with 1 supplement

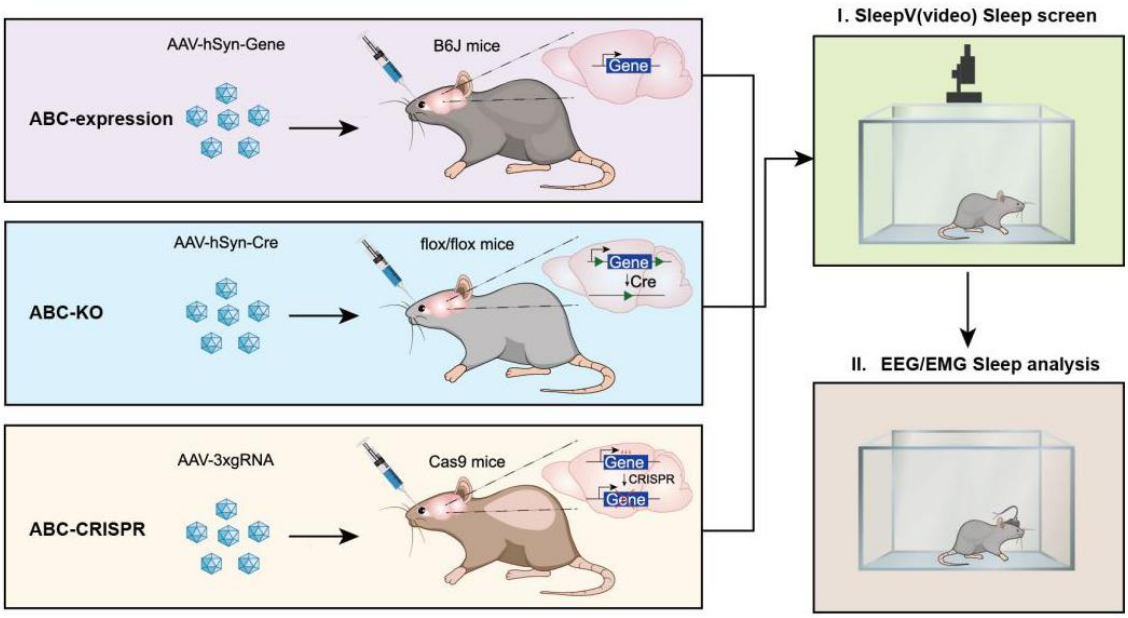

Adult brain chimeric (ABC) platform for somatic genetics analysis of sleep genes in adult mice.
ABC-expression in C57BL/6J adult mice by retro-orbital injection of AAV-PHP.eB to deliver systemic gene expression from the human synapsin (hSyn) promoter in the adult brain neurons. ABC-KO of target gene in conditional flox/flox adult mice by retroorbital injection of AAV-PHP.eB expressing Cre recombinase. Multiplex ABC-CRISPR of target genes by retroorbital injection of AAV-3xsgRNA expressing a set of triple sgRNAs targeting different exons of the same gene. The ABC-expression/KO/CRISPR mice are subjected to high-throughput sleep analysis by SleepV (video) system followed (or directly) by EEG/EMG recording.

Figure 1-figure supplement 1.

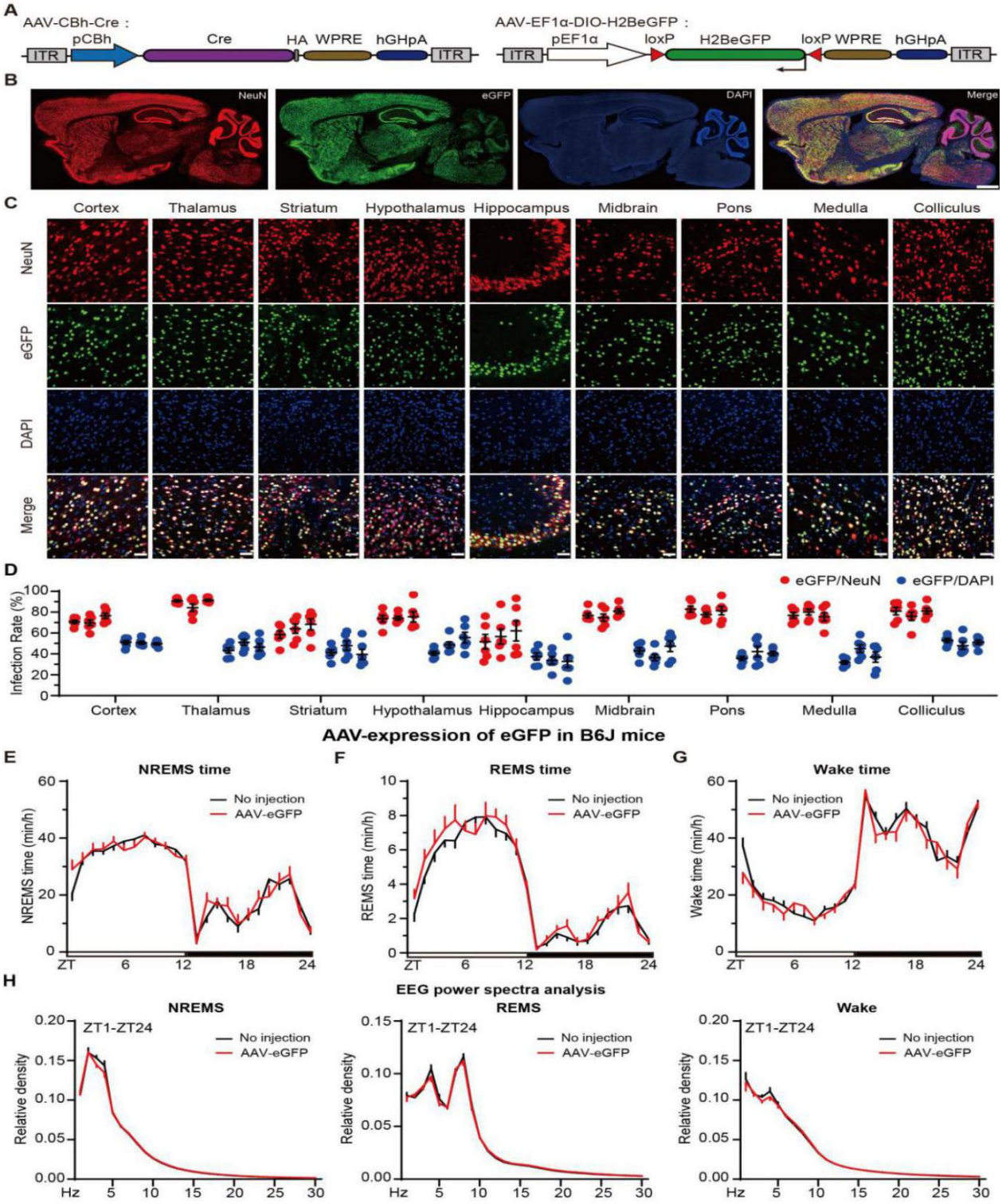

Development of ABC platform for somatic genetics analysis of sleep genes.
(A) Schematic of the AAV-CBh:Cre and AAV-pEF1α:DIO-H2B-eGFP constructs. **(B)** Representative images showing co-immunostaining of eGFP and NeuN in the sagittal brain sections of AAV-CBh-Cre and AAV-EF1α-DIO-eGFP co-injected mice. **(C)** Representative images of NeuN$^+$ (red) neurons or DAPI$^+$ (blue) cells that also express eGFP in nine different brain regions. **(D)** Quantification of the viral transduction rates, which is calculated by the percentage of NeuN$^+$ neurons (red) and DAPI$^+$ (blue) cells that express eGFP, in nine brain regions shown in (C). **(E-H)** Hourly plots of NREMS (E), REMS (F) or Wake (G) time and EEG power spectra analysis of NREMS, REMS and Wake states (H) of no virus (n=19) or AAV-hSyn-eGFP (n=9) injected mice. Data are mean ± s.e.m. (E-H) Two-way ANOVA with Dunn's multiple comparisons test. n.s. not significant.

150

151 **A highly accurate SleepV (video) system expedites mouse sleep screening**

152 The EEG/EMG recording is the "Gold Standard" method for sleep/wake analysis in mammals
153 (Lo et al., 2004; Weiergraber et al., 2005). Based on the different patterns of electrical signals, each
154 short (4 to 20-s) epoch of EEG/EMG data is classified into one of three states: wakefulness (Wake),
155 rapid eye movement sleep (REMS) or non-rapid eye movement sleep (NREMS). NREMS, which
156 occupies ~90% of total sleep time, is characterized by high percentage of the delta (1-4 Hz) power
157 of EEG spectrum. The delta power of NREMS measures sleep quality or depth, which is often
158 regarded as a good index of homeostatic sleep need (Franken et al., 2001).

159 However, this EEG/EMG method is not optimal for high-throughput mouse sleep screening
160 because it requires labor-intensive and invasive surgery to implant electrodes into the skull and
161 muscle and extensive recovery time from surgery before EEG/EMG recording. Moreover, the
162 semi-automated sleep staging software only has ~90% accuracy and requires intensive efforts to
163 manually correct the annotation of several days of EEG/EMG data per mouse. On the other hand, a
164 number of non-invasive sleep monitoring systems have been developed and utilized for mouse
165 sleep analysis, including the infrared video recording system (Banks et al., 2020; Fisher et al., 2012;
166 Pack et al., 2007), the piezoelectric system tracking mouse movement (Flores et al., 2007;
167 Yaghouby et al., 2016) and the plethysmography system monitoring the respiration of mouse
168 (Sunagawa et al., 2016).

169 Here, we developed an artificial intelligence (AI)-augmented video-based sleep monitoring
170 system that we named SleepV, which used a novel pattern recognition algorithm for sleep/wake
171 staging based on inactivity/activity of the mouse **(Figures 2A and Figure 2-figure supplement**
172 **1A-B)**. First, SleepV algorithm uses Gaussian filtering, adaptive and global thresholding to extract
173 from every image frame (25 frames/sec) the suspected regions of interest (ROIs), which are then
174 judged to be a mouse or not by a pre-trained deep neural network. Secondly, to determine whether

175 the mouse is active or not, the algorithm calculates a high confidence difference score for the
176 mouse between “t” and “t+m” frames by integrating the network prediction score (predict), the
177 mouse mask area (Intersection of Union, IoU), the center of mass of the mask (activity), and the
178 gray information (color) within the detected mask. Finally, SleepV defines the sleep state as ⩾ 40-
179 s of continuous immobility similar to previously reported video-based sleep monitoring systems
180 (Banks et al., 2020; Fisher et al., 2012; Pack et al., 2007).

181 We performed silmultaneous infrared video recording and EEG/EMG recording on six
182 C57BL/6J adult mice to examine the accuracy of sleep/wake staging by fully automated SleepV
183 analysis. **(Video S1)**. As compared to semi-automated EEG/EMG analysis with manual corrections,
184 SleepV showed suboptimal accuracy (average 88.2%) by overestimating the number of sleep bouts
185 owning to misjudging small mouse movements during sleep as waking **(Figure 2-figure**
186 **supplement 1C and F)**. To improve the performance of SleepV, we systematically tested a series
187 of thresholds of 0, 5, 10, 15, 20, 25, 30-s to filter subtle mouse movements during sleep, and
188 compared the number of sleep bouts as well as the accuracy, sensitivity and specificity of
189 sleep/wake staging **(Figure 2-figure supplement 1C-F and Video S2)**. Notably, we found that the
190 best performance of SleepV was achieved with a 15-s threshold, that is, by annotating ⩽ 15-s of
191 activity between two sleep bouts as sleep.

192 With this improvement, the accuracy of sleep/wake staging by SleepV was now comparable to
193 that of semi-automatic EEG/EMG analysis with human corrections **(Figure 2B)**. Although SleepV
194 could not distinguish between NREMS and REMS, there was a remarkable 95-99% epoch-by-
195 epoch agreement between the two methods, with ~96% in sensitivity, specificity and accuracy of
196 sleep/wake staging by SleepV **(Figure 2C and 2D)**. The mean accuracy (96.4%) of SleepV is
197 significantly higher than that (92-94%) of previous reported video-based sleep monitoring systems
198 (Banks et al., 2020; Fisher et al., 2012; Pack et al., 2007).

199

Figure 2. with 3 supplements

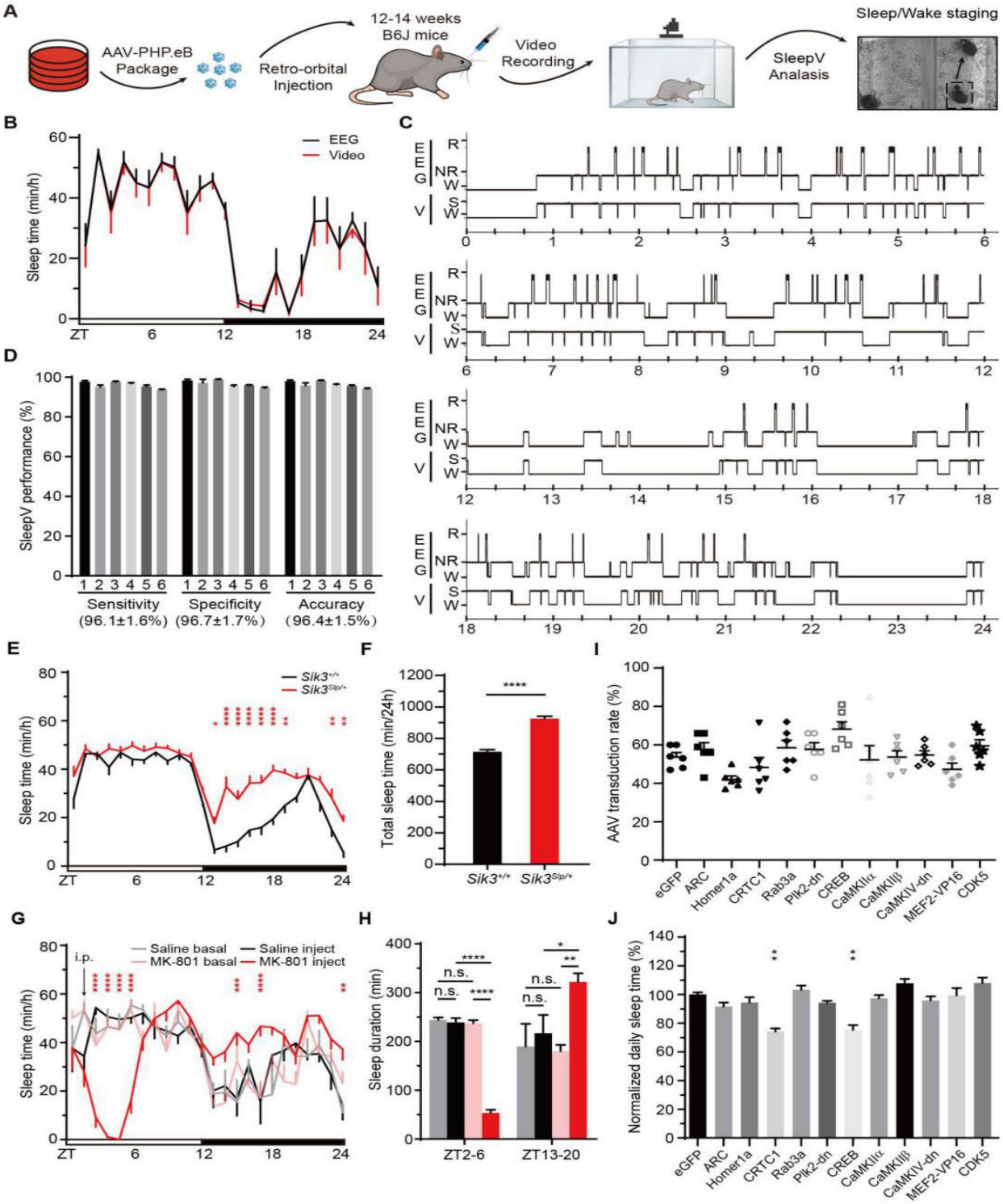

Development of a SleepV(video)-based high-throughput ABC sleep screening platform.
(A) Schematic of video-based ABC-expression sleep screening platform. **(B)** Hourly plot of sleep time of six C57BL/6J mice by simultaneous SleepV(video) and EEG/EMG analysis. **(C)** Epoch-by-epoch comparison of sleep/wake staging of the same mouse by simultaneous SleepV and EEG/EMG analysis. **(D)** Quantitative analysis of the sensitivity, specificity and accuracy of sleep/wake staging of six mice by SleepV (total 77760 epochs, 20s/epoch). **(E)** Hourly plot of sleep time of *Sik3*$^{+/+}$ (n=11) and *Sik3*$^{Slp/+}$ (n=11) mice analyzed by SleepV. **(F)** Quantification of daily sleep time in *Sik3*$^{+/+}$ (n=11) and *Sik3*$^{Slp/+}$ (n=11) mice. **(G)** Hourly plot of sleep time of baseline condition or after i.p. injection of saline (black, n=4) or 2mg/kg MK-801 (red, n=4) at ZT2 in C57BL/6J mice. **(H)** Quantification of sleep time during ZT2-6 and ZT13-20 after saline or MK-801 injection. **(I)** Graph showing viral transduction rates of cortical neurons in

AAV-hSyn-GeneX injected mice. **(J)** Graph showing daily sleep time of ABC-GeneX mice (n ≥ 5) normalized to ABC-eGFP mice. Data are mean ± s.e.m. (B, E, G, H) Two-way ANOVA with Dunn's multiple comparisons test. (F) Unpaired t test. (J) One-way ANOVA with Dunn's multiple comparisons test. n.s. not significant; * $p < 0.05$; ** $p < 0.01$; **** $p < 0.0001$.

Figure 2-figure supplement 1.

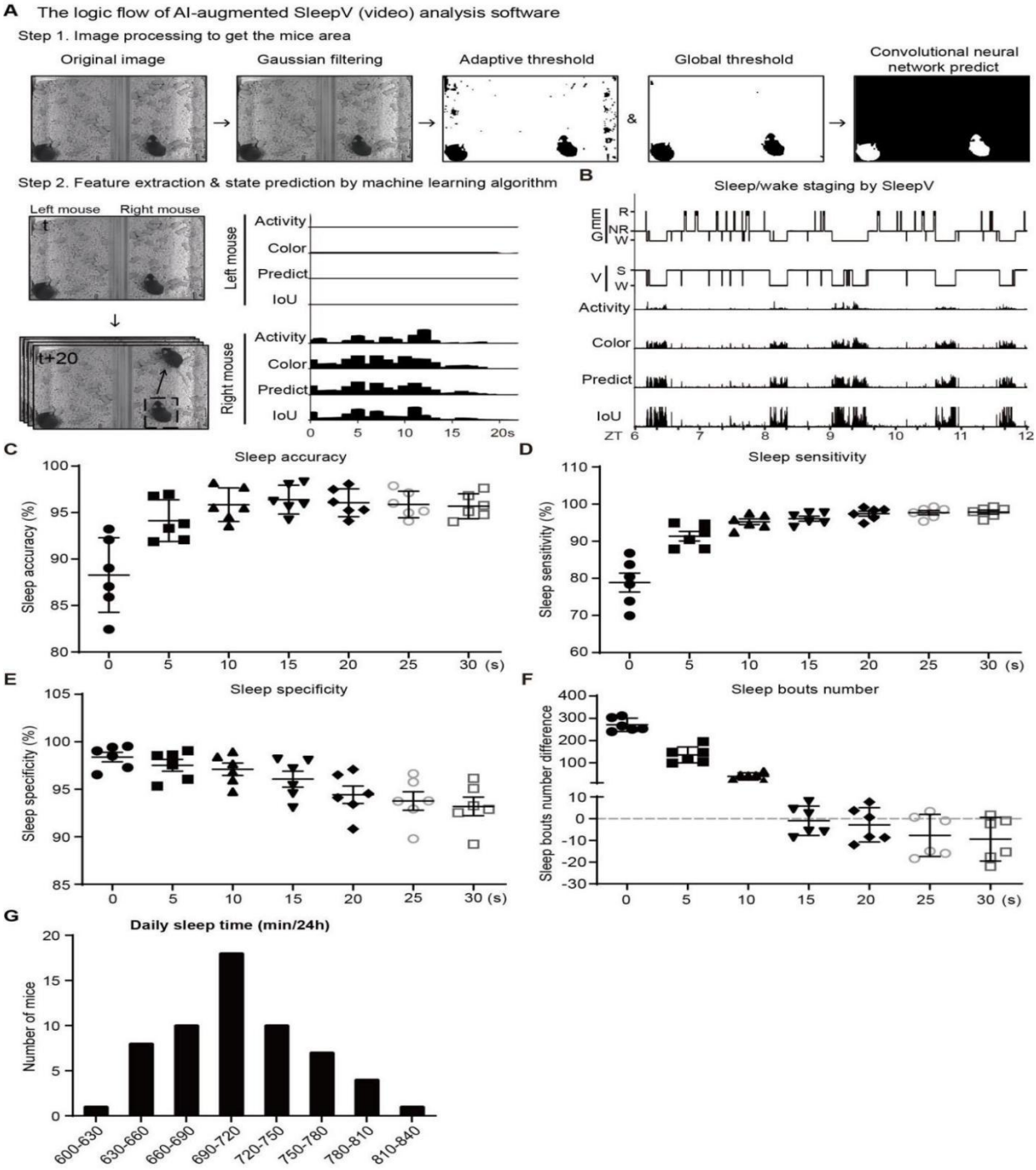

Development of a highly accurate SleepV system for high-throughout mouse sleep screening.
(A) The logic flow of sleep/wake staging of video recording by SleepV software. **(B)** Epoch-by-epoch comparison of sleep/wake staging of the same mouse by simultaneous SleepV and EEG/EMG recording and analysis. **(C-F)** Graphs showing the accuracy, sensitivity, specificity and sleep bout number of sleep-wake staging by SleepV after filtering 0, 5, 10, 15, 20, 25 or 30s of small movements during sleep. **(G)** Distribution of daily sleep time in fifty-nine C57BL/6J mice analyzed by SleepV.

224 **Figure 2-Video S1.**
225 **SleepV can easily detect sleep/wake state transition.**
226 Shown are EEG/EMG characterized behavior states, SleepV characterized behavior states, and real time color&activity
227 changes. NREM (N)-Wake (W)-NREM transitions were observed on the left mouse. REM (R)-Wake (W) transition
228 was observed on the right mouse. The video is shown at 3x the original speed. S, sleep.
229
230 **Figure 2-Video S2.**
231 **SleepV can filter small movement during sleep.**
232 Shown are EEG/EMG characterized behavior state, SleepV characterized behavior state, and real time color&activity
233 changes. Both the left and right mice showed small movement during NREM sleep, which could be filtered by SleepV.
234 The video is shown at 3x the original speed.
235

236 Next, we used SleepV to record the sleep/wake cycles of fifty-nine C57BL/6J adult mice for
237 three consecutive days. The distribution of daily sleep time measured by SleepV in these mice was
238 comparable to that of EEG/EMG analysis in previous studies **(Figure 2-figure supplement 1G**)
239 (Funato et al., 2016; Wang et al., 2018). Moreover, SleepV could easily distinguish the
240 hypersomnia phenotype of *Sleepy* (*Sik3*$^{Slp/+}$) mice, which showed on average ~210 min increase in
241 daily sleep time relative to wild-type littermates **(Figure 2E and 2F)**. To test whether SleepV could
242 detect dynamic changes in sleep/wake behavior, we intraperitoneally (i.p.) injected C57BL/6J mice
243 with 2mg/kg MK-801–a specific inhibitor of NMDA receptor–at zeitgeber time 2 (ZT2) (Sunagawa
244 et al., 2016; Tatsuki et al., 2016; Wang et al., 2018). As compared to the baseline and saline
245 injection controls, MK-801 treatment rapidly decreased sleep time during ZT2-6, which was
246 followed by rebound sleep during ZT13-20 **(Figure 2G and 2H)**. Collectively, these results
247 demonstrate that SleepV is a highly accurate, non-invasive and fully automatic sleep monitoring
248 system that is suitable for high-throughput mouse sleep screening.

249

250 **A pilot ABC-expression sleep screen of synaptic plasticity regulators**

251 Accumulating studies suggest a close link between synaptic plasticity and sleep need
252 regulation (Donlea et al., 2009; Ganguly-Fitzgerald et al., 2006; Huber et al., 2006; Huber et al.,
253 2004). To test our hypothesis that changing synaptic plasticity could lead to changes in sleep need,
254 we used SleepV system to conduct a pilot ABC-expression sleep screen of eleven known regulators

255 of synaptic plasticity **(Figure 2I)**. These included the immediate early gene products ARC and
256 Homer1a (Diering et al., 2017; Hu et al., 2010; Plath et al., 2006; Rial Verde et al., 2006; Shepherd
257 et al., 2006), cyclin-dependent kinase 5 (CDK5) (Bibb, 2003), Rab3a (Kapfhamer et al., 2002),
258 dominant negative form of polo-like kinase 2 (Plk2-dn) (Seeburg et al., 2008), Ca^{2+}/calmodulin-
259 dependent protein kinase II (CaMKIIα/β) and IV (CaMKIV) (Ibata et al., 2008; Lisman et al.,
260 2012), activity-dependent transcriptional factors cyclic AMP-response element binding protein
261 (CREB) and CREB regulated transcriptional coactivator 1 (CRTC1), and constitutively active
262 $MEF2^{VP16}$–a fusion protein between the DNA binding domain of MEF2 and VP16 transactivation
263 domain (Benito and Barco, 2010; Ch'ng et al., 2012; Flavell et al., 2006; Kandel, 2012; Nonaka et
264 al., 2014). As shown by co-immunostaining of HA-tag and NeuN, intravenous administration of
265 AAV-PHP.eB consistently resulted in systemic expression of target genes in 40-80% of neurons
266 across the adult mouse brains **(Figure 2I)**. While ABC-expression of most genes had little effect on
267 the sleep/wake cycle, this pilot screen identified two potential hits, CREB and CRTC1, which
268 significantly reduced daily sleep amount **(Figure 2J)**.

269 CREB is a well-known transcriptional activator that binds as a dimer to the cAMP response
270 elements (CRE), which contain a palindromic (TGACGTCA) or half-site (TGACG or CGTCA)
271 sequence, in the promoter or enhancer regions of target genes (Comb et al., 1986; Montminy et al.,
272 1986; Short et al., 1986). The *Creb1* gene encodes multiple CREB isoforms by alternative splicing,
273 of which the α and Δ isoforms, but not the β isoform, show high affinity for CRE sites (Ruppert et
274 al., 1992). Phosphorylation of $CREB_{\alpha}$ at serine 133 (or $CREB_{\Delta}$ at serine 119) by cAMP-dependent
275 protein kinase (PKA) promotes the recruitment of coactivators, including histone acetyl
276 transferases CBP/p300, and transcriptional activation of certain target genes (Chrivia et al., 1993;
277 Gonzalez and Montminy, 1989; Shaywitz and Greenberg, 1999). Alternatively, CREB functions in
278 tandem with CRTCs, also known as transducers of regulated CREB activity coactivators (TORCs),

279 to activate the transcription of a specific subset of target genes (Conkright et al., 2003; Iourgenko et
280 al., 2003).
281
282 **ABC-expression of CREB and/or CRTC1 reduces NREMS amount and delta power**
283 We performed EEG/EMG recording to further characterize the sleep phenotypes caused by
284 ABC-expression of $CREB_{\Delta}$. It has been shown that serine 133 to alanine (S133A) phosphor-
285 mutation of $CREB_{\alpha}$ prevents transcriptional activation of specific target genes (Chrivia et al., 1993;
286 Gonzalez and Montminy, 1989). Thus, we compared the sleep phenotypes as a result of ABC-
287 expression of wild-type or S119A phosphor-mutant $CREB_{\Delta}$ in C57BL/6J adult mice. Co-
288 immunostaining revealed that intravenous administration of AAV-hSyn-$CREB_{\Delta}$ or AAV-hSyn-
289 $CREB_{\Delta}^{S119A}$ resulted in efficient transduction of the majority of cortical and thalamic neurons
290 **(Figure 3A and 3B)**. Both ABC-$CREB_{\Delta}$ and ABC-$CREB_{\Delta}^{S119A}$ mice, relative to ABC-eGFP mice,
291 exhibited on average ~120 min decrease in daily NREMS amount accompanied by reduced
292 NREMS delta power, which occurred mostly during the dark phase **(Figure 3C-E and Figure 3-**
293 **figure supplement 1A-E)**. These results suggest that ABC-expression of $CREB_{\Delta}$ reduces NREMS
294 amount and NREMS delta power in a manner independent of S119 phosphorylation.
295 Next, we asked whether ABC-coexpression of $CREB_{\Delta}$ and CRTC1 could result in additive
296 sleep phenotypes as compared to ABC-expression of either $CREB_{\Delta}$ or CRTC1 alone. In contrast to
297 nuclear localization of $CREB_{\Delta}$, CRTC1 was predominantly localized in the cytoplasm **(Figure 3A)**.
298 Relative to ABC-eGFP mice, ABC-CRTC1 mice exhibited ~47 min decrease in daily NREMS time
299 and reduced NREMS delta power during the dark phase **(Figure 3F-H and Figure 3-figure**
300 **supplement 1F-J)**. It should be noted that SleepV overestimated the reduction of sleep time in
301 ABC-CRTC1 mice by misjudging excessive muscle twitching during sleep as waking in these mice
302 **(Figure 3-figure supplement 1K-L and Video S3)**. Importantly, ABC-coexpression of $CREB_{\Delta}$
303 and CRTC1 resulted in enhanced sleep phenotypes: ~150 min decrease in daily NREMS time

304 accompanied by lower NREMS delta power during the dark phase **(Figure 3F-H)**. These results
305 suggest that the function of CREB in sleep regulation is probably facilitated by a CRTC-dependent
306 mechanism. Furthermore, this pilot screen demonstrates the proof-of-principle that the combination
307 of ABC platform and SleepV system can facilitate high-throughput screening of sleep genes in
308 mice.

309

310 **Figure 3.** with 2 supplements

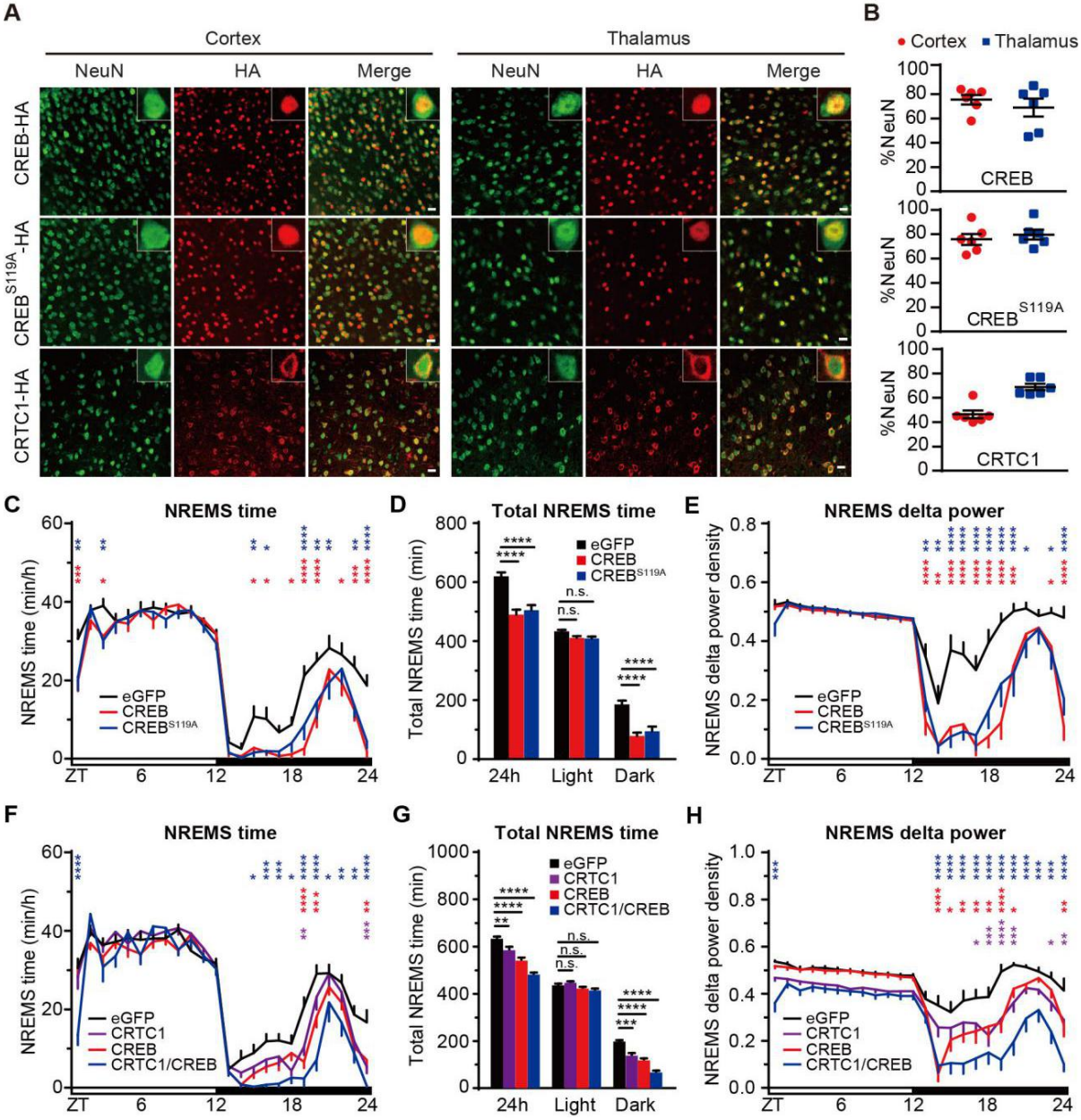

311

312 **ABC-expression of CREB and/or CRTC1 reduces NREMS amount and delta power.**
313 **(A)** Co-immunostaining of HA^{+} (red) and NeuN^{+} (green) neurons in the cortex and thalamus of AAV-hSyn-CREB
314 (ABC-CREB), AAV-hSyn-CREB^{S119A} (ABC-CREB^{S119A}) and AAV-hSyn-CRTC1 (ABC-CRTC1)-injected mice. **(B)**

Quantification of the viral transduction rates, which is calculated by the percentage of NeuN^{+} neurons that express HA-tagged proteins, in the cortical and thalamic neurons of ABC-CREB, ABC-CREB^{S119A} and ABC-CRTC1 mice. **(C-E)** Hourly plot of NREMS time (C), quantification of total NREMS time (D) and hourly plot of NREMS delta power (E) in the ABC-eGFP (n=11), ABC-CREB (n=12) and ABC-CREB^{S119A} (n=11) mice. Shown above are the statistical analysis for comparison between ABC-CREB (red*) or ABC-CREB^{S119A} (blue*) mice and control ABC-eGFP mice. **(F-H)** Hourly plot of NREMS time (F), quantification of total NREMS time (G) and hourly plot of NREMS delta power (H) in the ABC-eGFP, (n=12), ABC-CRTC1 (n=15), ABC-CREB (n=15) and ABC-CRTC1/CREB (n=12) mice. Shown above are statistical analysis for comparison between ABC-CRTC1 (purple*), ABC-CREB (red*), or ABC-CRTC1/CREB (blue*) mice and control ABC-eGFP mice. Data are mean ± s.e.m. (C-H) Two-way ANOVA with Dunn's multiple comparisons test. n.s. not significant; * $p < 0.05$; ** $p < 0.01$; *** $p < 0.001$; **** $p < 0.0001$.

Figure 3-figure supplement 1

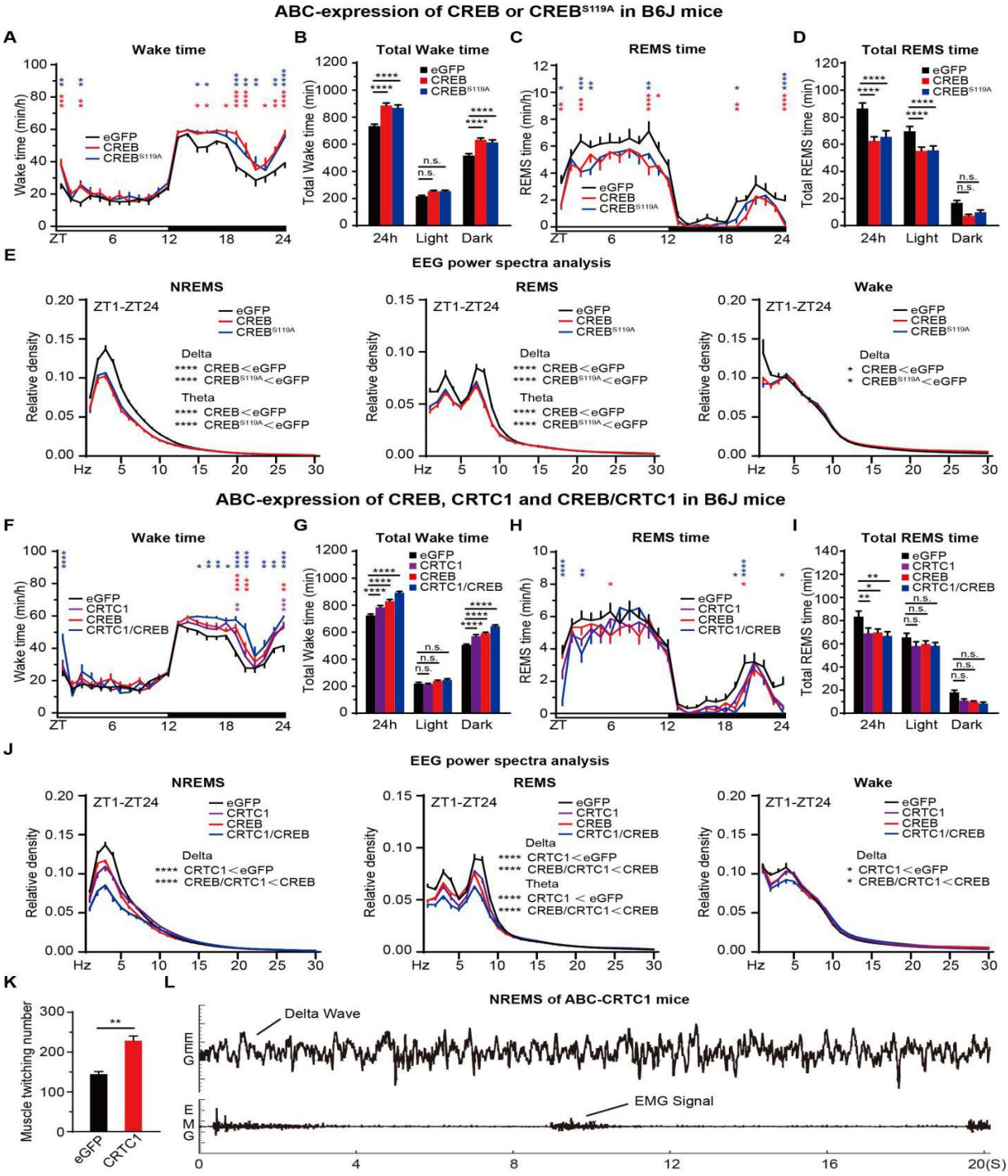

ABC-expression of CREB and/or CRTC1 reduces NREMS amount and delta power.
(A-E) Hourly plots of Wake (A) or REMS (C) time, quantification of total Wake (B) or REMS (D) time and EEG power spectra analysis of NREMS, REMS and Wake states (E) in the ABC-eGFP (n=11), ABC-CREB$_{\Delta}$ (n=12) and ABC-CREB$_{\Delta}^{S119A}$ (n=11) mice. Shown above is statistical analysis for comparison between ABC-CREB (red*) or ABC-CREB^{S119A} (blue*) mice and control ABC-eGFP mice. **(F-J)** Hourly plots of Wake (F) or REMS (H) time, quantification of total Wake (G) or REMS (I) time and EEG power spectra analysis of NREMS, REMS and Wake states (J) in ABC-eGFP (n=12), ABC-CRTC1 (n=15), ABC-CREB$_{\Delta}$ (n=15) and ABC-CRTC1/CREB$_{\Delta}$ (n=12) mice. Shown above is the statistical analysis for comparison between ABC-CRTC1 (purple*), ABC-CREB$_{\Delta}$ (red*), or ABC-CRTC1/CREB$_{\Delta}$ (blue*) mice and control ABC-eGFP mice. **(K)** Quantification of muscle twitching episodes of ABC-eGFP and ABC-CRTC1 mice during NREMS. **(L)** Representative EEG/EMG hypnogram depicting frequent muscle twitching during NREMS in the ABC-CRTC1 mice. Data are mean ± s.e.m. (A-J) Two-way ANOVA with Dunn's multiple comparisons test. (K) Unpaired t test. n.s. not significant;* $p < 0.05$; ** $p < 0.01$; *** $p < 0.001$; **** $p < 0.0001$.

Figure 3-Video S3.
ABC-CRTC1 mouse shows frequent muscle twitching during sleep.

Inducible ABC-expression of CREB^{VP16} and/or CRTC1^{CA} causes strong sleep phenotypes

ABC-expression of constitutively active CREB^{VP16}, a fusion protein between the DNA-binding domain of CREB and VP16 transactivation domain (Barco et al., 2002), or constitutively active CRTC1^{CA} containing two (S151A and S245A) phosphor-mutations (Sonntag et al., 2017), resulted in lethality one week after AAV injection in C57BL/6J adult mice. To study the immediate sleep phenotypes resulted from ABC-expression of CREB^{VP16} or CRTC1^{CA}, we used a Tet-on inducible system to express CREB^{VP16} or CRTC1^{CA} in the adult mouse brains by co-injection of two AAV-PHP.eB viruses expressing rtTA from the EF1α promoter and CREB^{VP16} or CRTC1^{CA} from the TRE promoter, respectively **(Figure 4A)**. There was no difference in the baseline sleep-wake architecture among the inducible (i)ABC-eGFP, iABC-CREB^{VP16} and iABC-CRTC1^{CA} mice when transcription from the TRE promoter was inactive in the absence of Doxycycline (Dox) (data not shown). On the other hand, the expression of GFP, CREB^{VP16} or CRTC1^{CA} was rapidly induced in the brain cells of these mice within three days after drinking Dox-containing water **(Figure 4B, C and Figure 4-figure supplement 1A, B)**. Interestingly, a slight circadian shift of the sleep/wake cycle was observed at the light/dark transition among all mice possibly due to the effects of Dox

Figure 4. with 1 supplement.

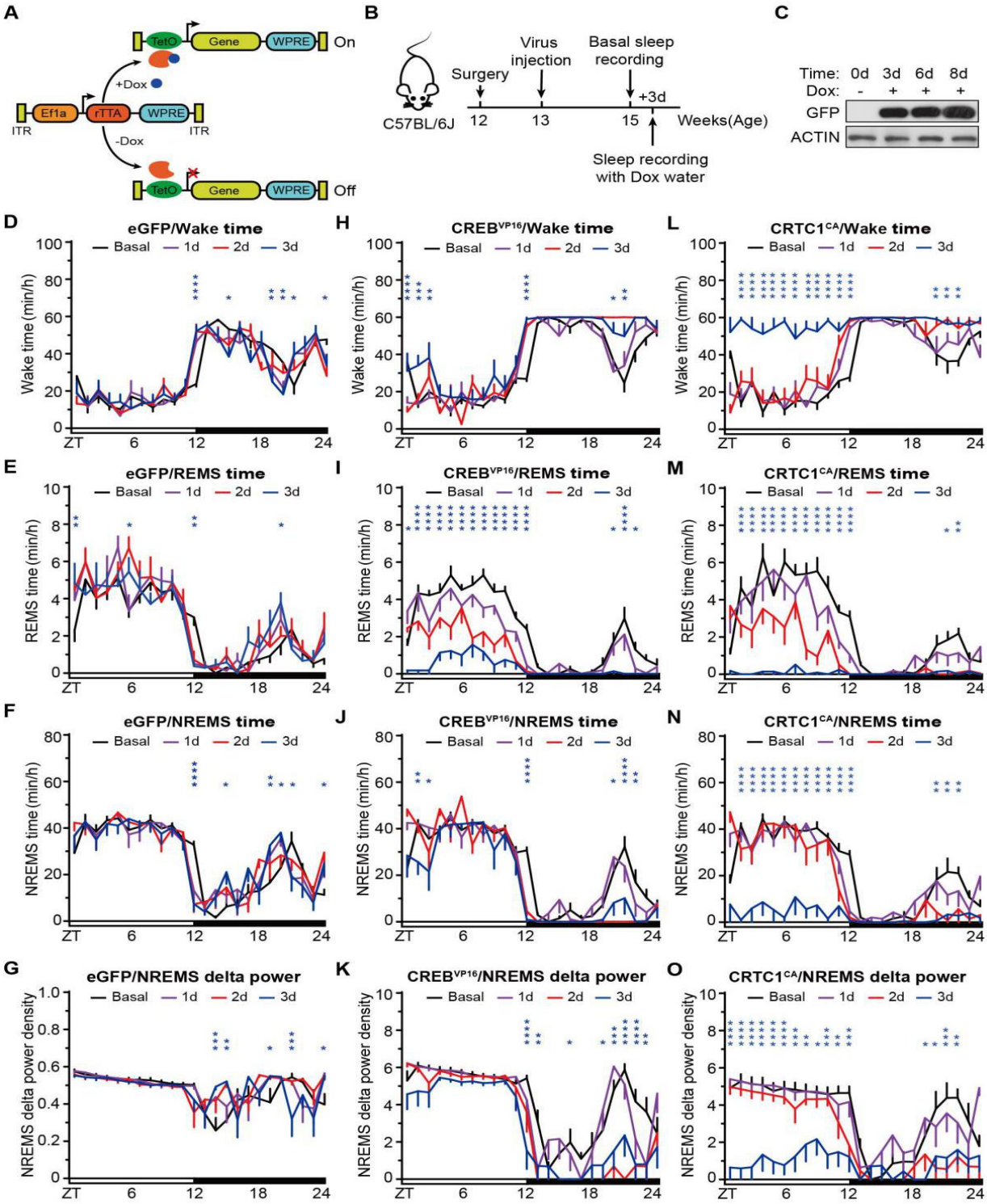

Inducible ABC-expression of CREB^{VP16} or CRTC1^{CA} causes significant sleep phenotypes.
(A) Schematic of Tet-on inducible (i)ABC-expression system with or without Doxcycline (Dox). **(B)** A flow chart of the iABC-expression and EEG/EMG sleep recording experiment. **(C)** Immunoblotting of whole brain lysates from iABC-eGFP mice before and after Dox treatment with anti-GFP and anti-ACTIN antibodies. **(D-G)** Hourly plots of Wake time (D), REMS time (E), NREMS time (F) and NREMS delta power (G) of the iABC-eGFP mice (n=8). **(H-K)** Hourly plots of Wake time (H), REMS time (I), NREMS time (J) and NREMS delta power (K) in the iABC-CREB^{VP16} mice (n=7). **(L-O)** Hourly plots of Wake time (L), REMS time (M), NREMS time (N) and NREMS delta power (O) in the iABC-CRTC1^{CA} mice (n=7). Data are mean ± s.e.m. (D-O) Two-way ANOVA with Dunn's multiple comparisons test. n.s. not significant; * $p < 0.05$; ** $p < 0.01$; *** $p < 0.001$; **** $p < 0.0001$.

Figure 4-figure supplement 1.

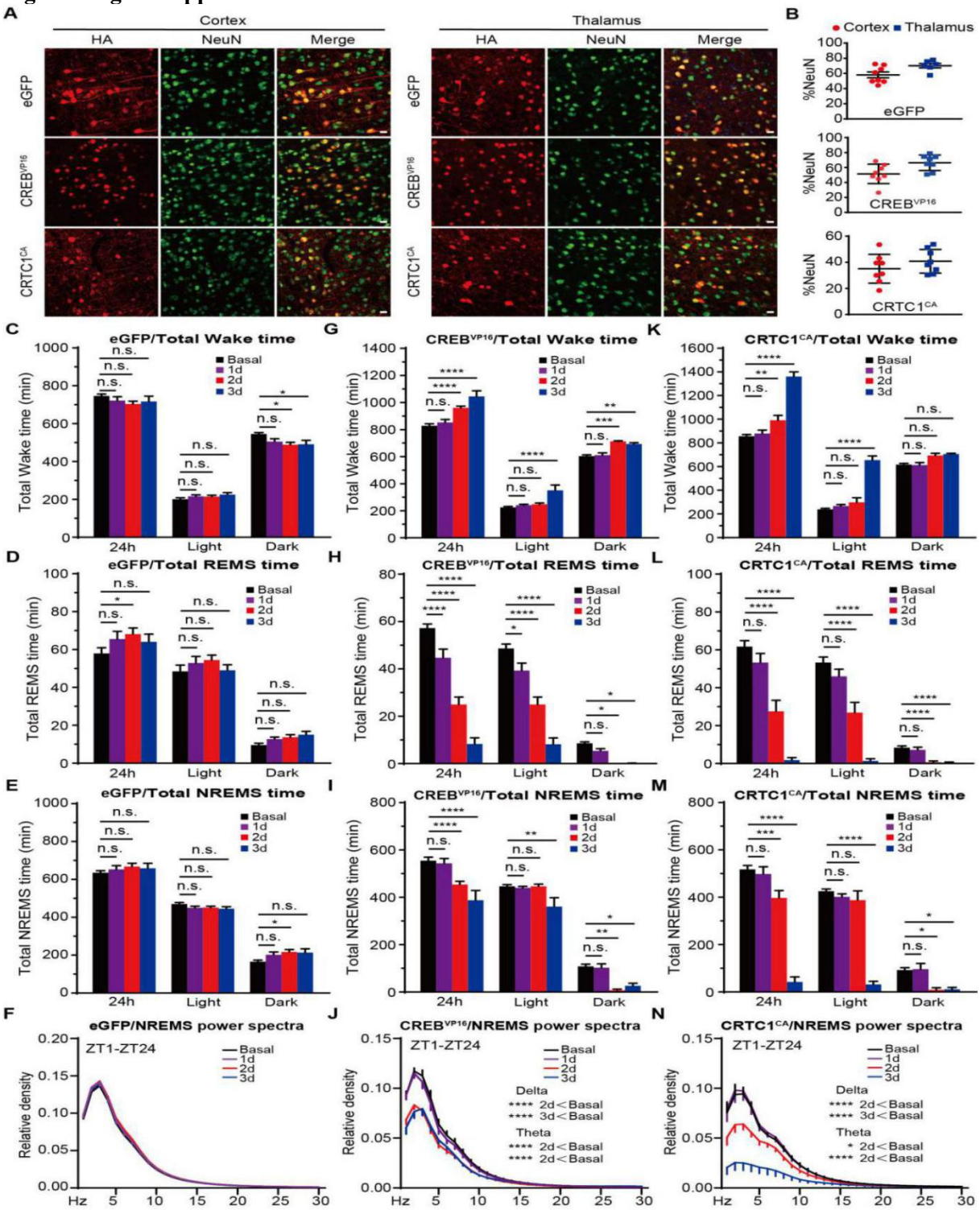

Inducible ABC-expression of CREB^{VP16} or CRTC1^{CA} causes significant sleep phenotypes.
(A) Co-immunostaining of HA^{+} (red) and NeuN^{+} (green) neurons in the cortex and thalamus of the the inducible (i) ABC-eGFP, ABC-CREB^{VP16} and ABC-CRTC1^{CA} mice. Quantification of the viral transduction rates, which is calculated by the percentage of NeuN^{+} neurons that express HA-tagged proteins, in the cortical and thalamic neurons showed in (A). **(C-F)** Quantification of total Wake time (C), REMS time (D), or NREMS time (E) and EEG power spectra analysis of NREMS (F) in the iABC-eGFP mice (n=8). **(G-J)** Quantification of total Wake time (G), REMS time (H), or NREMS time (I) and EEG power spectra analysis of NREMS (J) in the iABC-CREB^{VP16} mice (n=7). **(K-N)** Quantification of total Wake time (K), REMS time (L), or NREMS time (M) and EEG power spectra analysis of NREMS (N) in the iABC-CRTC1^{CA} mice (n=7). Data are mean ± s.e.m. (C-N) Two-way ANOVA with Dunn's multiple comparisons test. n.s. not significant; * p <0.05; ** p < 0.01; *** p < 0.001; **** p < 0.0001.

384 **(Figure 4D-O)**. While ABC-induction of GFP did not affect total sleep/wake time, ABC-induction
385 of $CREB^{VP16}$ or $CRTC1^{CA}$ caused progressive decrease in daily amounts of NREMS and REMS
386 accompanied by corresponding increase in total wake time during three days of Dox treatment
387 **(Figure 4D-O and Figure 4-figure supplement 1C-N)**. Remarkably, ABC-$CRTC1^{CA}$ mice were
388 almost constantly awake on day 3 of Dox treatment as shown by 91.8% and 97.1% reduction in
389 NREMS and REMS, respectively **(Figure 4L-O and Figure 4-figure supplement 1K-N)**. These
390 results suggest that iABC-expression system can be used to study the immediate sleep phenotypes
391 of target genes of which constitutive expression causes rapid lethality in adult mice.
392
393 **ABC-KO of *Creb1* by Cre/loxP recombination increases daily NREMS amount**
394 *Creb1* is an essential gene of which complete ablation results in perinatal lethality in mice
395 (Bleckmann et al., 2002). A partial *Creb1* knockout strain, in which the α and Δ isoforms of CREB
396 are deleted, is homozygous viable and exhibits ~100 min increase of daily NREMS time
397 (Graves et al., 2003). Moreover, forebrain-specific knockout of *Creb1* in the excitatory neurons
398 similarly increases daily NREMS amount (Wimmer et al., 2021). To generate ABC-$Creb1^{KO}$ mice,
399 we retro-orbitally injected $Creb1^{flox/flox}$ mice with AAV-PHP.eB expressing mCherry or Cre
400 recombinase from the pan-neuronal hSyn promoter, respectively. Immunoblotting revealed that the
401 level of CREB expression was reduced by ~50% in whole brain lysates of AAV-hSyn-Cre injected
402 mice relative to AAV-hSyn-mCherry injected mice **(Figure 5A-C)**. The efficiency of ABC-
403 $Creb1^{KO}$ might be underestimated because CREB was also expressed in the astrocytes that could
404 not be targeted by neuron-specific Cre expression (Pardo et al., 2017). Consistent with previous
405 studies (Graves et al., 2003; Wimmer et al., 2021), ABC-$Creb1^{KO}$ mice exhibited ~100 min
406 increase in daily NREMS amount, with no significant change in NREMS delta power **(Figure 5D-
407 F and Figure 5-figure supplement 1A-E)**. These results suggest that ABC-KO of *Creb1* can result
408

Figure 5. with 1 supplement

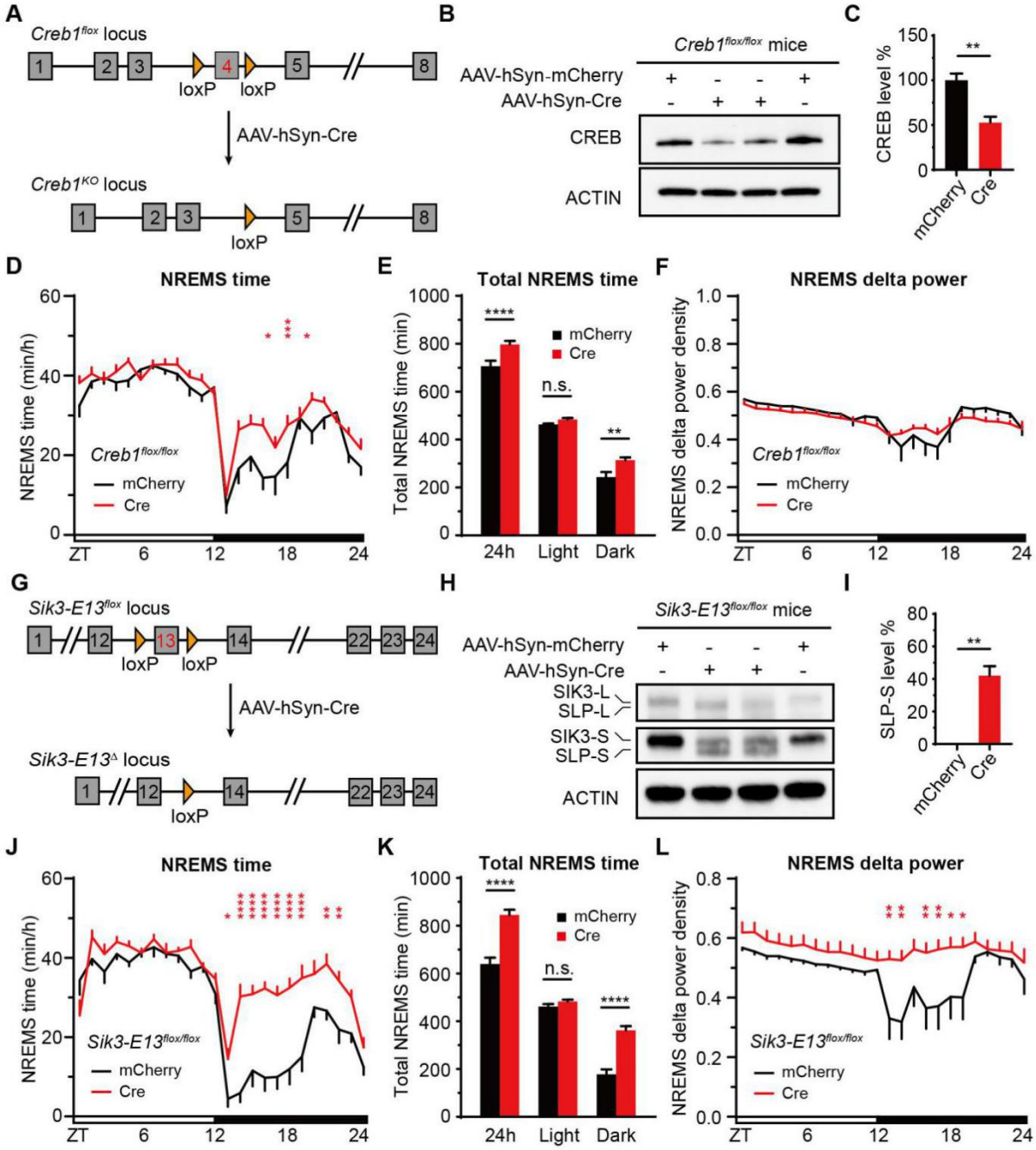

ABC-KO of *Creb1* or exon 13 of *Sik3* by Cre-loxP recombination causes hypersomnia.
(A) Schematic of ABC-KO of *Creb1* by AAV-hSyn-Cre injection of *Creb1*$^{flox/flox}$ mice. **(B)** Immunoblotting of brain lysates from AAV-hSyn-mCherry or AAV-hSyn-Cre injected *Creb1*$^{flox/flox}$ mice with anti-CREB and anti-ACTIN antibodies. **(C)** Quantification of CREB expression in (B) (n=4). **(D-F)** Hourly plot of NREMS time (D), quantification of total NREMS time (E) and hourly plot of NREMS delta power (F) in the AAV-hSyn-mCherry (n=9) or AAV-hSyn-Cre (n=14) injected *Creb1*$^{flox/flox}$ mice. **(G)** Schematic of ABC-KO of exon 13 of *Sik3* by AAV-hSyn-Cre injection of *Sik3-E13*$^{flox/flox}$ mice. **(H)** Immunoblotting of brain lysates from AAV-hSyn-mCherry or AAV-hSyn-Cre injected *Sik3-E13*$^{flox/flox}$ mice with anti-SIK3 and anti-ACTIN antibodies. **(I)** Quantification of SLP-S expression in (H) (n=4), which is calculated by the percentage of SLP-S/(SIK3-S+SLP-S). **(J-L)** Hourly plot of NREMS time (J), quantification of total NREMS time (K) and hourly plot of NREMS delta power (L) in the AAV-hSyn-mCherry (n=8) or AAV-hSyn-Cre (n=8) injected *Sik3-E13*$^{flox/flox}$ mice. Data are mean ± s.e.m. (C and I) Unpaired t test. (D-F) and (J-L) Two-way ANOVA with Dunn's multiple comparisons test. n.s. not significant; * $p < 0.05$; ** $p < 0.01$; *** $p < 0.001$; **** $p < 0.0001$.

Figure 5-figure supplement 1.

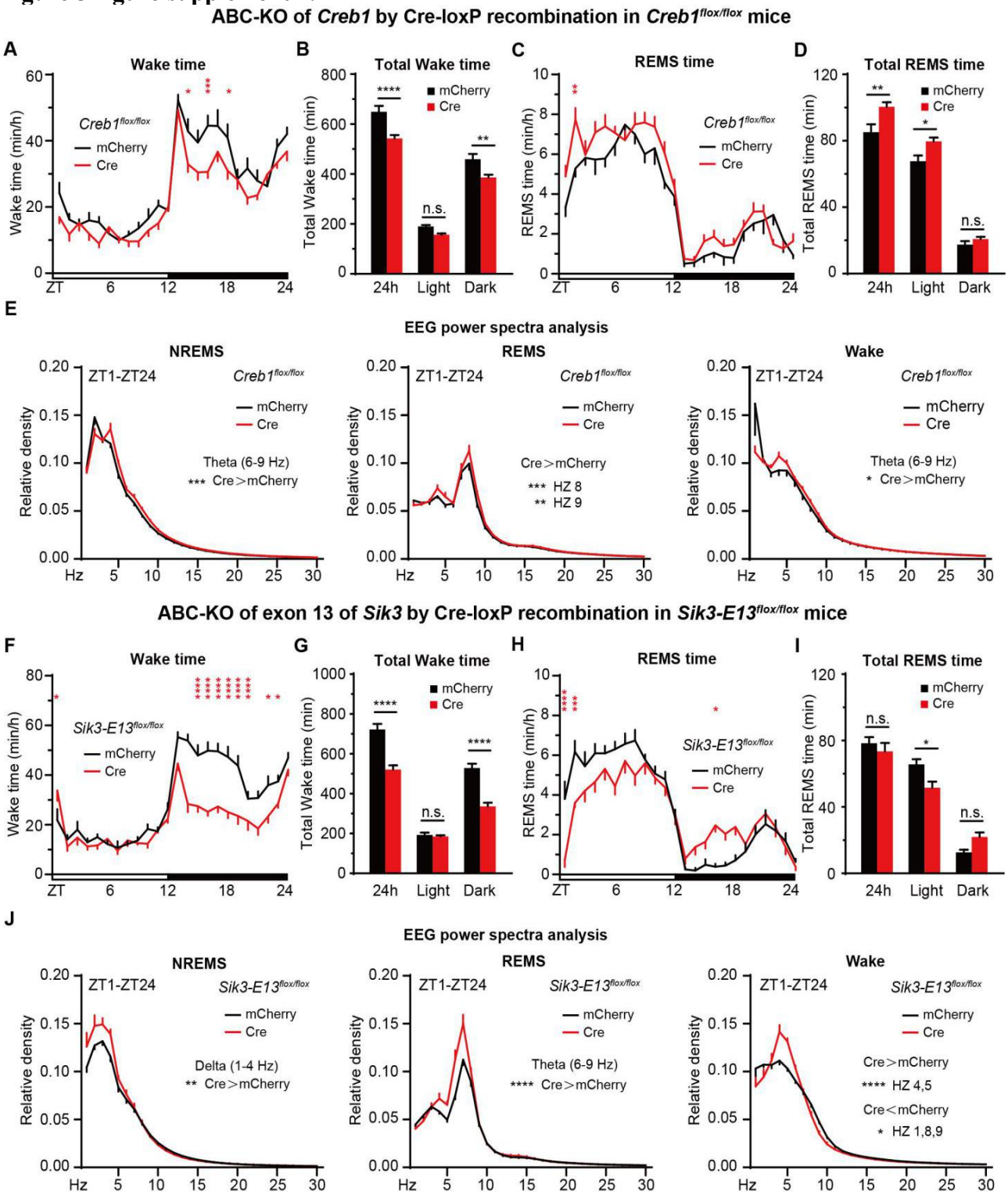

ABC-KO of *Creb1* or exon 13 of *Sik3* by AAV-mediated Cre-loxP recombination causes hypersomnia.
(A-E) Hourly plots of Wake (A) or REMS (C) time, quantification of total Wake (B) or REMS (D) time and EEG power spectra analysis of NREMS, REMS and Wake states (E) in the AAV-hSyn-mCherry (n=9) or AAV-hSyn-Cre (n=14) injected *Creb1*$^{flox/flox}$ mice. **(F-J)** Hourly plots of Wake (F) or REMS (H) time, quantification of total Wake (G) or REMS (I) time and EEG power spectra analysis of NREMS, REMS and Wake states (J) in the AAV-hSyn-mCherry (n=8) or AAV-hSyn-Cre (n=8) injected *Sik3-E13*$^{flox/flox}$ adult mice. Data are mean ± s.e.m. (A-J) Two-way ANOVA with Dunn's multiple comparisons test. n.s. not significant; * p <0.05; ** p < 0.01; *** p < 0.001; **** p < 0.0001.

433 in a significant sleep phenotype comparable to that of germline *Creb1* mutant mice (Graves et al.,
434 2003; Wimmer et al., 2021).
435
436 **ABC-KO of exon 13 of *Sik3* phenocopies *Sleepy* mice**
437 Forward genetic screening identified a *Sleepy* (*Sik3*$^{Slp/+}$) mouse strain, in which a gain-of-
438 function splicing mutation causes the skipping of exon 13 from *Sik3* transcripts and in-frame
439 deletion of 52 amino acids from SIK3 proteins, an AMP-activated protein kinase (AMPK)-related
440 protein kinase (Funato et al., 2016). The *Sik3*$^{Slp/+}$ mice exhibit ~250 min increase in daily NREMS
441 time with constitutively elevated NREMS delta power (Funato et al., 2016) as well as other
442 phenotypes, such as obesity and reproductive defects (Funato and Yanagisawa, personal
443 communications). Moreover, *Sik3* is an essential gene that is broadly expressed in mouse brain
444 neurons (Funato et al., 2016). Thus, it remains unclear whether the hypersomnia of *Sik3*$^{Slp/+}$ mice is
445 the primary phenotype owing to direct effects of SLP kinases in sleep regulation, or secondary
446 phenotype resulted from the developmental defects of the brain or dysfunctions of peripheral
447 organs.
448 To distinguish among these possibilities, we performed retro-orbital injection of AAV-
449 hSyn-Cre into *Sik3-E13*$^{flox/flox}$ adult mice, such that Cre/loxP-mediated recombination would
450 convert *Sik3-E13*^{flox} into a functionally equivalent *Slp* (*Sik3-E13*$^{\Delta}$) allele **(Figure 5G)**.
451 Immunoblotting estimated that mutant SLP proteins were expressed in at least 40% of the adult
452 brain neurons following AAV-hSyn-Cre injection **(Figure 5H and 5I)**. Accordingly, ABC-KO of
453 exon 13 of *Sik3* induced marked hypersomnia–200 to 300 min increase in daily NREMS time
454 accompanied by constitutively elevated NREMS delta power–similar to that of *Sleepy* mice
455 carrying the germline *Slp* mutation **(Figure 5J-L and Figure5-figure supplement 1F-J)**. These
456 results suggest that the hypersomnia of *Sleepy* mice is the primary phenotype as a result of direct
457 effects of mutant SLP kinases on the sleep regulatory machinery in the adult brain neurons.

458 **ABC-KO of genes by triple-target CRISPR in Cas9 mice**

459 We reasoned that it would be more direct and faster to generate ABC-KO mice with the use
460 of CRISPR/Cas9 technology. In this system, Cas9 nuclease is directed by single-guide (sg)RNA to
461 introduce site-specific DNA break in the target gene, which is repaired by the error-prone non-
462 homologous end-joining pathways, resulting in indel mutations (e.g., short deletions or insertions)
463 (Hsu et al., 2014; Jinek et al., 2012; Wang et al., 2013). However, these Cas9-mediated indel
464 mutations occur at a moderate frequency and not all mutations can ablate target gene function.
465 Because the vast majority of adult brain neurons are non-dividing, terminally differentiated cells,
466 the efficiency of ABC-KO by CRISPR needs to be nearly 100%, such that both alleles of the target
467 gene are disrupted in almost all AAV-transduced brain cells. Although it was recently reported that
468 intravenous injection of AAV-PHP.eB expressing single sgRNA can efficiently disrupt target gene
469 in the majority of adult brain neurons (Xiao et al., 2021), this strategy often required extensive
470 screening of sgRNAs and was not suitable for high-throughput analysis.

471 Multiplexing strategies using several sgRNAs targeting the same gene have been utilized to
472 improve the efficiency of KO by CRISPR in various model organisms (Port et al., 2020; Xie et al.,
473 2015; Yin et al., 2015). Notably, triple-target CRISPR in zygotes can produce whole-body biallelic
474 knockout mice with 96-100% efficiency in a single generation (Sunagawa et al., 2016; Tatsuki et
475 al., 2016). Thus, we compared the efficiency of ABC-KO by CRISPR by injecting *Rosa26*$^{LSL\text{-}Cas9}$
476 mice with AAV-PHP.eB expressing HA-tagged Cre recombinase from the hSyn promoter as well
477 as one, two or three U6:sgRNA cistrons targeting *NeuN*, a ubiquitously expressed gene in the adult
478 brain neurons **(Figure 6-figure supplement 1A and B)**. The efficiency of ABC-KO of *NeuN* was
479 significantly higher with triple sgRNAs than with single or double sgRNAs **(Figure 6-figure**
480 **supplement 1C)**. Moreover, the efficiency of ABC-*NeuN*^{KO} increased in a viral dose-dependent
481 manner and peaked at three weeks after AAV injection **(Figure 6-figure supplement 1D and E)**.
482 Whole genome sequencing of ABC-*NeuN*^{KO} mouse brain revealed on-target indel mutations and

483 large inter-exon deletions, but rarely off-target mutations **(Figure 6-figure supplement 1F and G)**.
484 Accordingly, immunoblotting showed that the level of NeuN expression was specifically reduced
485 by ~70%, whereas another pan-neuronal protein Tublin J remain unchanged in the ABC-*NeuN*^{KO}
486 brain lysates **(Figure 6-figure supplement 1H and I)**. Co-immunostaining of NeuN and Cre
487 indicated that the expression of NeuN disappeared, indicative of biallelic KO of *NeuN*, in the
488 majority of the adult brain neurons expressing both Cre and 3xsgRNA^{NeuN} **(Figure 6-figure**
489 **supplement 1J)**.
490

491 **ABC-CRISPR of *Slp/Sik3* rescues hypersomnia of *Sik3*$^{Slp/+}$ mice**

492 Because ABC-KO of exon 13 of *Sik3* could induce hypersomnia in adult mice **(Figure 5J-L)**,
493 we hypothesized that ABC-KO of *Slp/Sik3* by triple-target CRISPR should rescue hypersomnia of
494 *Sik3*$^{Slp/+}$ mice. To test our hypothesis, we performed ABC-CRISPR of *Slp/Sik3* alleles by injecting
495 constitutively Cas9-expressing *Sik3*$^{Slp/+}$;*Rosa26*$^{Cas9/+}$ adult mice with AAV-3xsgRNA^{Sik3} expressing
496 triple sgRNAs targeting different exons of *Sik3* gene **(Figure 6A)**. Whole genome sequencing and
497 genomic PCR revealed both on-target indel mutations and large inter-exon deletions between
498 distinct sgRNA target sites, but rarely off-target mutations, in the AAV-3xsgRNA^{Sik3} injected
499 mouse brains **(Figure 6B and 6C)**. As shown by non-linear enhanced chemilumilescent (ECL)
500 Western blotting, the levels of SIK3/SLP proteins were estimated to reduce by ~75% in the ABC-
501 *Sik3*^{KO} brain lysates **(Figure 6D and 6E)**. By contrast, linear Western blotting, with the use of
502 alkaline phosphatase (AP)-conjugated secondary antibodies, indicated that the levels of SIK3/SLP
503 proteins were actually reduced by ~50% in the ABC-*Sik3*^{KO} brain lysates **(Figure6-figure**
504 **supplement 2A-D)**. Importantly, ABC-CRISPR of *Slp/Sik3* resulted in ~150 min reduction in daily
505 NREMS time accompanied by constitutively reduced NREMS delta power in *Sik3*$^{Slp/+}$;*Rosa26*$^{Cas9/+}$
506 male mice **(Figure 6F-H and Figure 6-figure supplement 2E-I)**. Likewise, ABC-CRISPR of
507

Figure 6. with 2 supplements

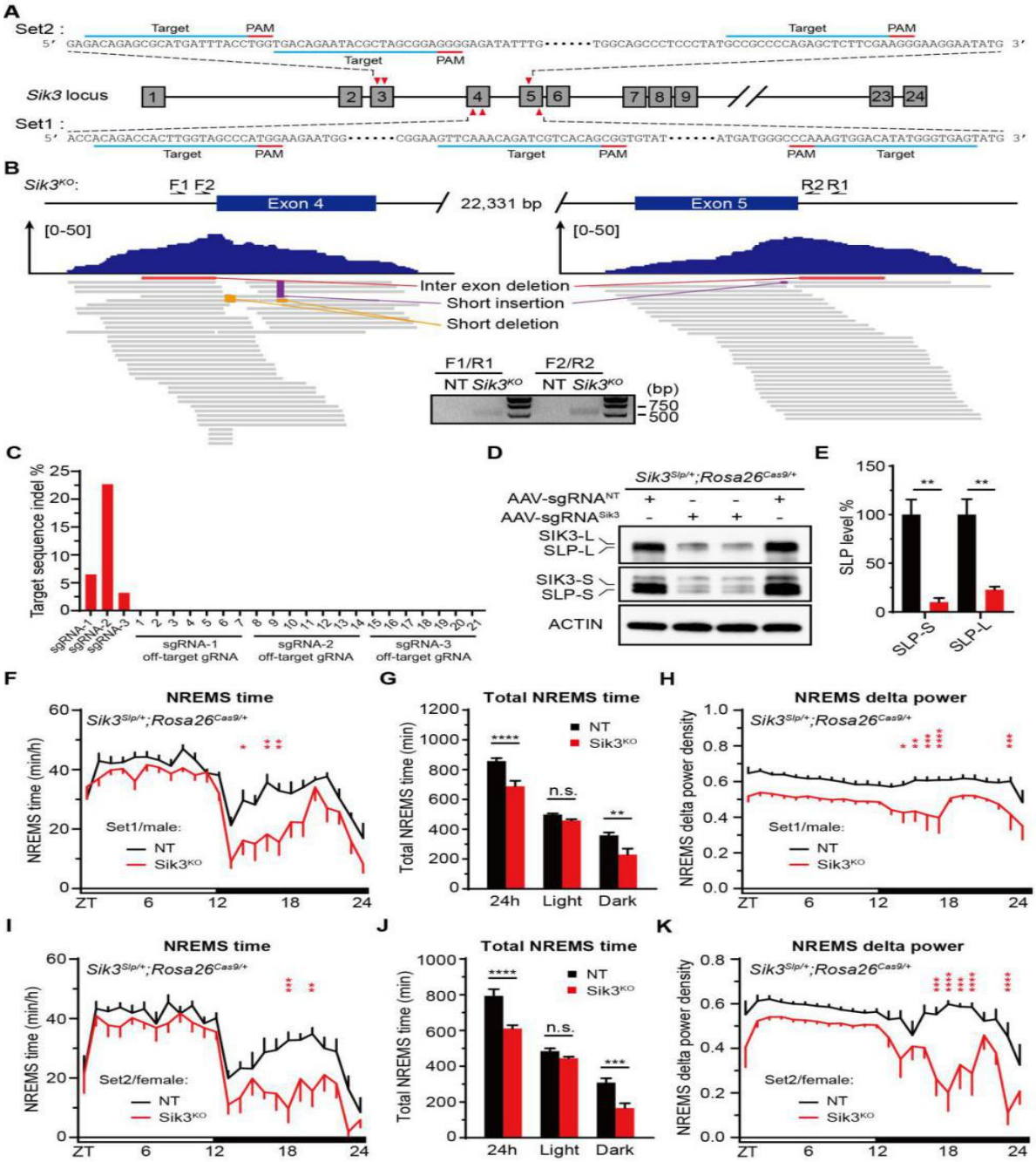

ABC-CRISPR of *Slp/Sik3* rescues hypersomnia of *Sik3*$^{Slp/+}$;*Rosa26*$^{Cas9/+}$ mice.
(A) Schematic showing two sets of triple sgRNA target sites within exons 3, 4 and 5 of *Sik3* gene. **(B)** Genomic alignments of whole genome sequencing reads of ABC-*Sik3*^{KO} mouse brain around the sgRNA target sites within exons 4 and 5 of *Sik3* gene. Different types of mutations are highlighted based on the whole genome sequencing data. Inset shows genomic PCR result with two primer pairs to detect the large inter-exon deletions. **(C)** Quantitative analysis of indel mutations at the sgRNA target sites and twenty-one predicted off-target sites for the three sgRNAs (set 1) targeting *Sik3* gene. **(D)** Immunoblotting of whole brain lysates from AAV-sgRNA^{NT} and AAV-sgRNA^{Sik3} (set 1) injected *Sik3*$^{Slp/+}$; *Rosa26*$^{Cas9/+}$ male mice with anti-SIK3 and anti-ACTIN antibodies. **(E)** Quantification of the levels of SIK3-L/SLP-L and SIK3-S/SLP-S proteins shown in (D) (n=3). **(F-H)** Hourly plot of NREMS time (F), quantification of total NREMS time (G) and hourly plot of NREMS delta power (H) in the AAV-sgRNA^{NT} (n=7) or AAV-sgRNA^{Sik3} (set 1, n=7) injected *Sik3*$^{Slp/+}$; *Rosa26*$^{Cas9/+}$ male mice. **(I-K)** Hourly plot of NREMS time (I), quantification of total NREMS time (J) and hourly plot of NREMS delta power (K) in the AAV-sgRNA^{NT} (n=7) or AAV-gRNA^{Sik3} (set 2, n=7) injected *Sik3*$^{Slp/+}$; *Rosa26*$^{Cas9/+}$ female mice. Data are mean ± s.e.m. (E) Unpaired t test. (F-K) Two-way ANOVA with Dunn's multiple comparisons test. n.s. not significant; * $p < 0.05$; ** $p < 0.01$; *** $p < 0.001$; **** $p < 0.0001$.

Figure 6-figure supplement 1.

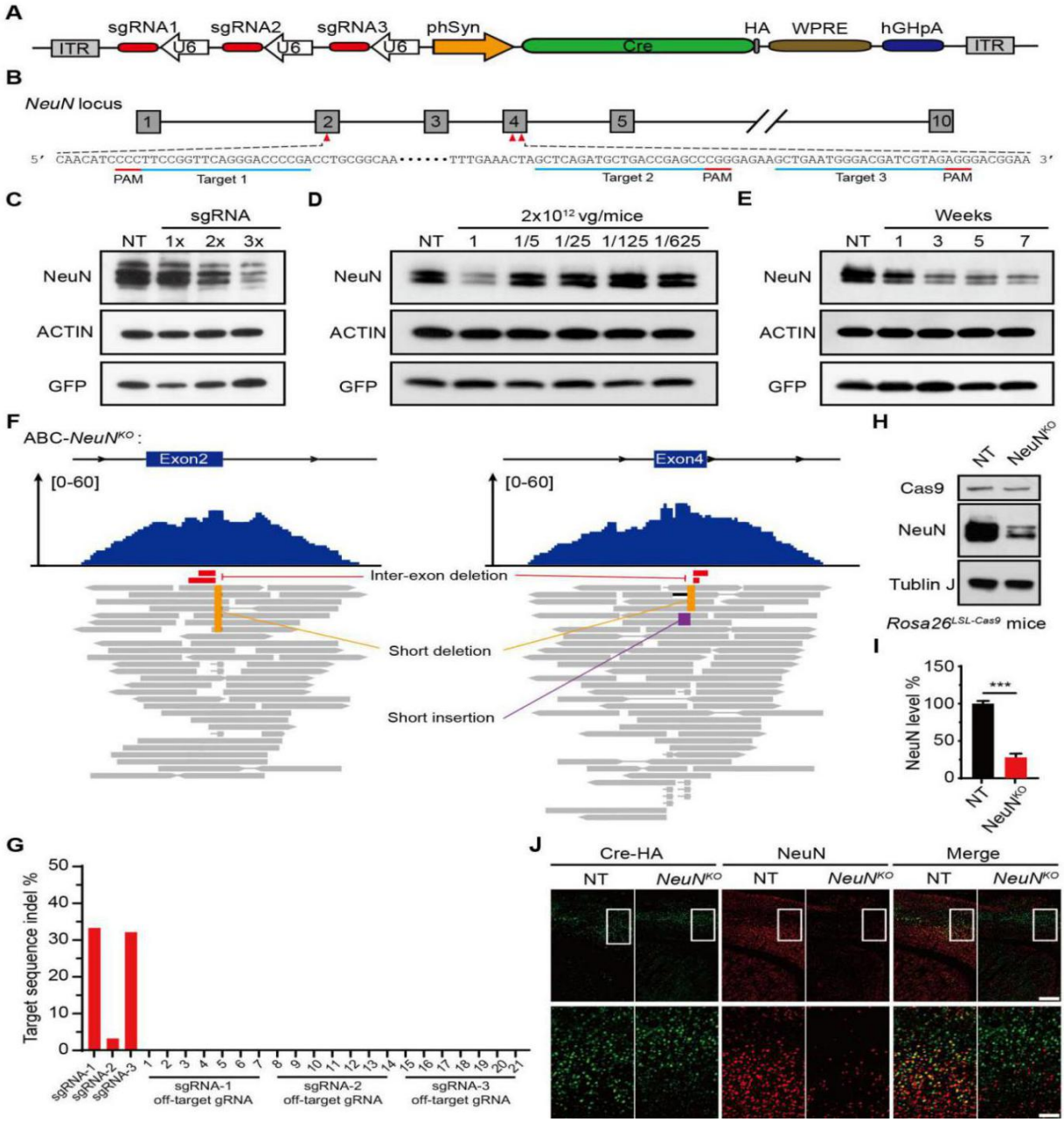

ABC-KO of target genes by triple-target CRISPR in Cas9 mice.
(A) Schematic of AAV-3xsgRNA^{NeuN} that expresses HA-Cre recombinase from hSyn promoter and three U6:sgRNA cistrons. **(B)** Schematic of target site sequences within exons 2 and 4 of *NeuN* gene. Immunoblotting of NeuN proteins in brain lysates from AAV-3xsgRNA^{NT}, AAV-1xsgRNA^{NeuN}, AAV-2xsgRNA^{NeuN}, AAV-3xsgRNA^{NeuN} (10^{12} vg/mice) injected *Rosa26*$^{LSL\text{-}Cas9}$ mice. **(D)** Immunoblotting of NeuN proteins in brain lysates from Cas9 mice injected with different doses of AAV-3xsgRNA^{NeuN}. **(E)** Immunoblotting of NeuN proteins in brain lysates from AAV-3xsgRNA^{NeuN} injected Cas9 mice at one, three, five or seven weeks after (10^{12} vg/mice) virus injection. AAV-3xsgRNA^{NT} injected mouse brains were collected at three weeks after virus injection. **(F)** Genomic alignments of whole genome sequencing reads of ABC-*NeuN*^{KO} mouse brain DNA at the target sites within exons 2 and 4 of *NeuN* gene. The top and bottom panels show read coverage and read alignments, respectively, with different types of mutations highlighted. **(G)** Quantitation of indel mutations at the three target sites and twenty-one predicted off-target sites for the three sgRNAs targeting *NeuN* gene based on the whole genome sequencing data. **(H)** Immunoblotting of whole brain lysates from AAV-3xsgRNA^{NT} and AAV-3xsgRNA^{NeuN} injected *Rosa26*$^{LSL\text{-}Cas9}$ mice with the corresponding antibodies. **(I)** Quantification of the level of NeuN expression in (H) (n=4). **(J)** Co-immunostaining of HA-Cre and NeuN in the prefrontal cortex sections of AAV-3xsgRNA^{NT} and AAV-3xsgRNA^{NeuN} injected mice. The bottom row shows magnified images of the corresponding boxed regions in the top row. Scale bars, 400 μm (top) and 100 μm (bottom). Data are mean±s.e.m. (I) Unpaired t test. n.s. not significant; * $p<0.05$; ** $p<0.01$; *** $p<0.001$; **** $p<0.0001$.

Figure 6-figure supplement 2.

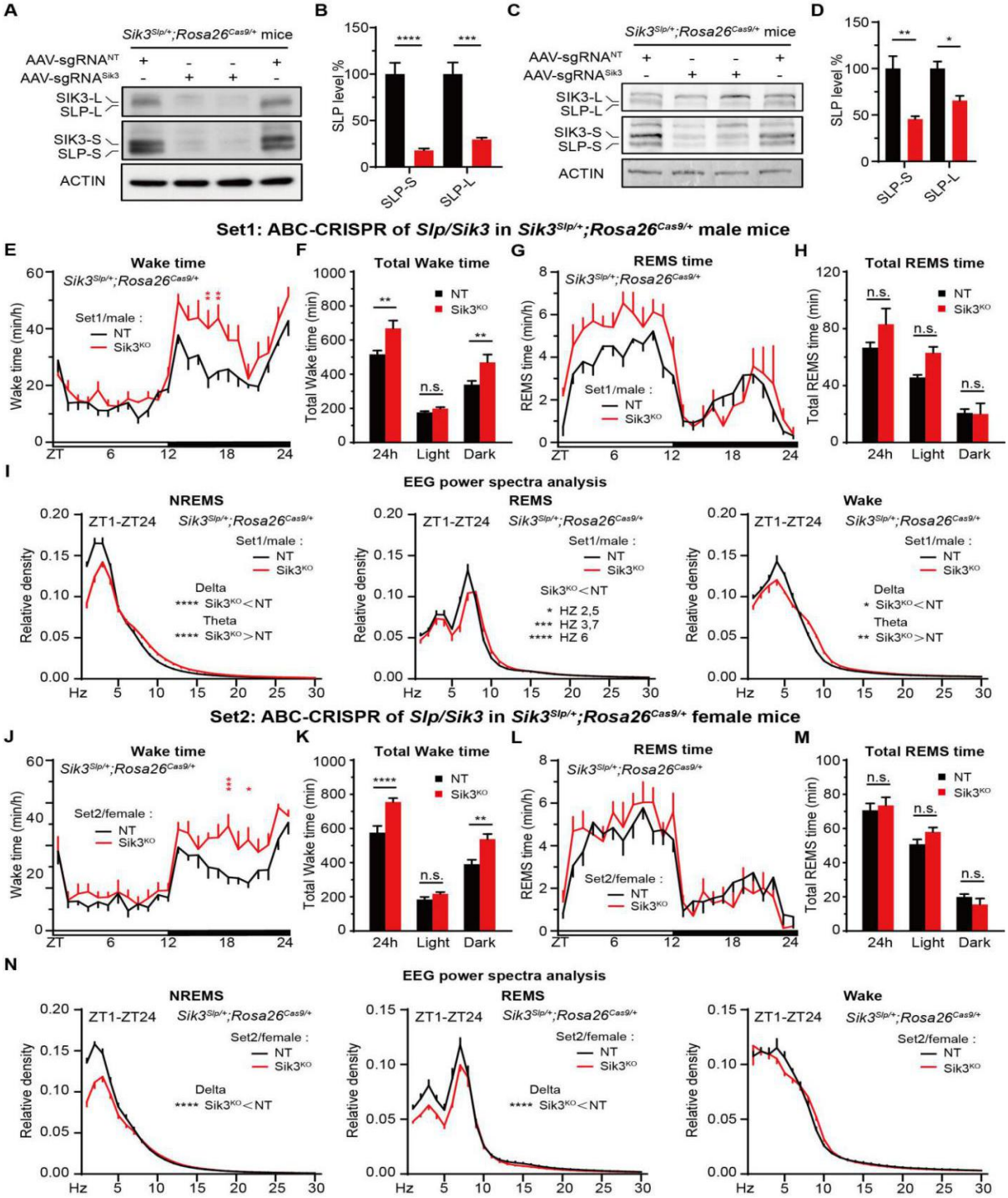

ABC-CRISPR of *Slp/Sik3* rescues hypersomnia of *Sik3*$^{Slp/+}$;*Rosa26*$^{Cas9/+}$ mice.

(A) Western blotting (ECL) of whole brain lysates from AAV-sgRNA^{NT} and AAV-sgRNA^{Sik3} (set 2) injected *Sik3*$^{Slp/+}$;*Rosa26*$^{Cas9/+}$ female mice with anti-SIK3 and anti-ACTIN antibodies. **(B)** Quantification of the levels of SIK3-L/SLP-L and SIK3-S/SLP-S proteins shown in (A) (n=4). **(C)** Alkaline phosphatase-based linear Western blotting of the same membrane used in (A) with anti-SIK3 and anti-ACTIN antibodies. **(D)** Quantification of the levels of SIK3-L/SLP-L and SIK3-S/SLP-S proteins shown in (C) (n=4). **(E-I)** Hourly plots of Wake (E) or REMS (G) time, quantification of total Wake (F) or REMS (H) time and EEG power spectra analysis of NREMS, REMS and Wake states (I) in the AAV-sgRNA^{NT} (n=7) or AAV-sgRNA^{Sik3} (set 1, n=7) injected *Sik3*$^{Slp/+}$; *Rosa26*$^{Cas9/+}$ male mice. **(J-N)** Hourly plots of Wake (J) or REMS (L) time, quantification of total Wake (K) or REMS (M) time and EEG power spectra analysis of NREMS, REMS and Wake states (N) in the AAV-sgRNA^{NT} (n=6) or AAV-sgRNA^{Sik3} (set 2, n=7) injected *Sik3*$^{Slp/+}$;*Rosa26*$^{Cas9/+}$ female mice. Data are mean ± s.e.m. (B and D) Unpaired t test. (E-N) Two-way ANOVA with Dunn's multiple comparisons test. n.s. not significant; * $p < 0.05$; ** $p < 0.01$; *** $p < 0.001$; **** $p < 0.0001$.

557 *Slp/Sik3* using a second set of sgRNAs caused ~180 min reduction in daily NREMS time with
558 diminished NREMS delta power in *Sik3*$^{Slp/+}$;*Rosa26*$^{Cas9/+}$ female mice **(Figure 6I-K and Figure 6-**
559 **figure supplement 2J-N)**. These results suggest that the hypersomnia of *Sleepy* mice requires
560 continuous expression of mutant SLP kinases in the adult brain neurons.
561
562 **Multiplex ABC-CRISPR of orexin/hypocretin receptors causes narcolepsy-like episodes**
563 The deficiency of neuropeptide orexin/hypocretin or its receptors, OX1R/HCRTR1 and
564 OX2R/HCRTR2 (hereafter OX1R and OX2R for simplicity) results in narcolepsy-like phenotypes,
565 such as abnormal wake to REMS transition and cataplexy, in mice (Chemelli et al., 1999;
566 Kalogiannis et al., 2010; Kohlmeier et al., 2013). For double ABC-CRISPR of OX1R and OX2R,
567 we co-injected Cas9-expressing mice with two AAV-PHP.eB viruses expressing separate sets of
568 triple sgRNAs targeting either *Ox1r* or *Ox2r* gene, respectively **(Figure 7A)**. As shown by reverse
569 transcription (RT)-quantitative (q)PCR, the levels of *Ox1r* and *Ox2r* transcripts were reduced by
570 ~75% and ~60%, respectively, in the AAV-sgRNA$^{Ox1r/Ox2r}$ injected (ABC-*Ox1r/Ox2r*^{DKO}) relative
571 to AAV-sgRNA^{NT} injected (ABC-NT) mouse brains **(Figure 7B)**. At first, all of the ABC-
572 *Ox1r/Ox2r*^{DKO} mice exhibited no sleep abnormality as compared to the ABC-NT control mice.
573 After feeding with chocolates–a known stimulant of narcolepsy (Oishi et al., 2013), three out of
574 eight ABC-*Ox1r/Ox2r*^{DKO} mice exhibited frequent narcolepsy-like episodes, which was
575 characterized by the abnormal transitions from wake to REMS during EEG/EMG recording
576 **(Figure 7C-E)**. However, we did not observe cataplexy during the narcolepsy episodes through
577 simultaneous video/EEG recording and manual inspection. This partial narcoleptic phenotype was
578 probably due to incomplete knockout of OX1R and OX2R in the adult brain neurons. These results
579 suggest that multiplex ABC-CRISPR can enable one-step analysis of the sleep phenotypes of
580 redundant genes in adult mice.
581

582 **Figure 7.**

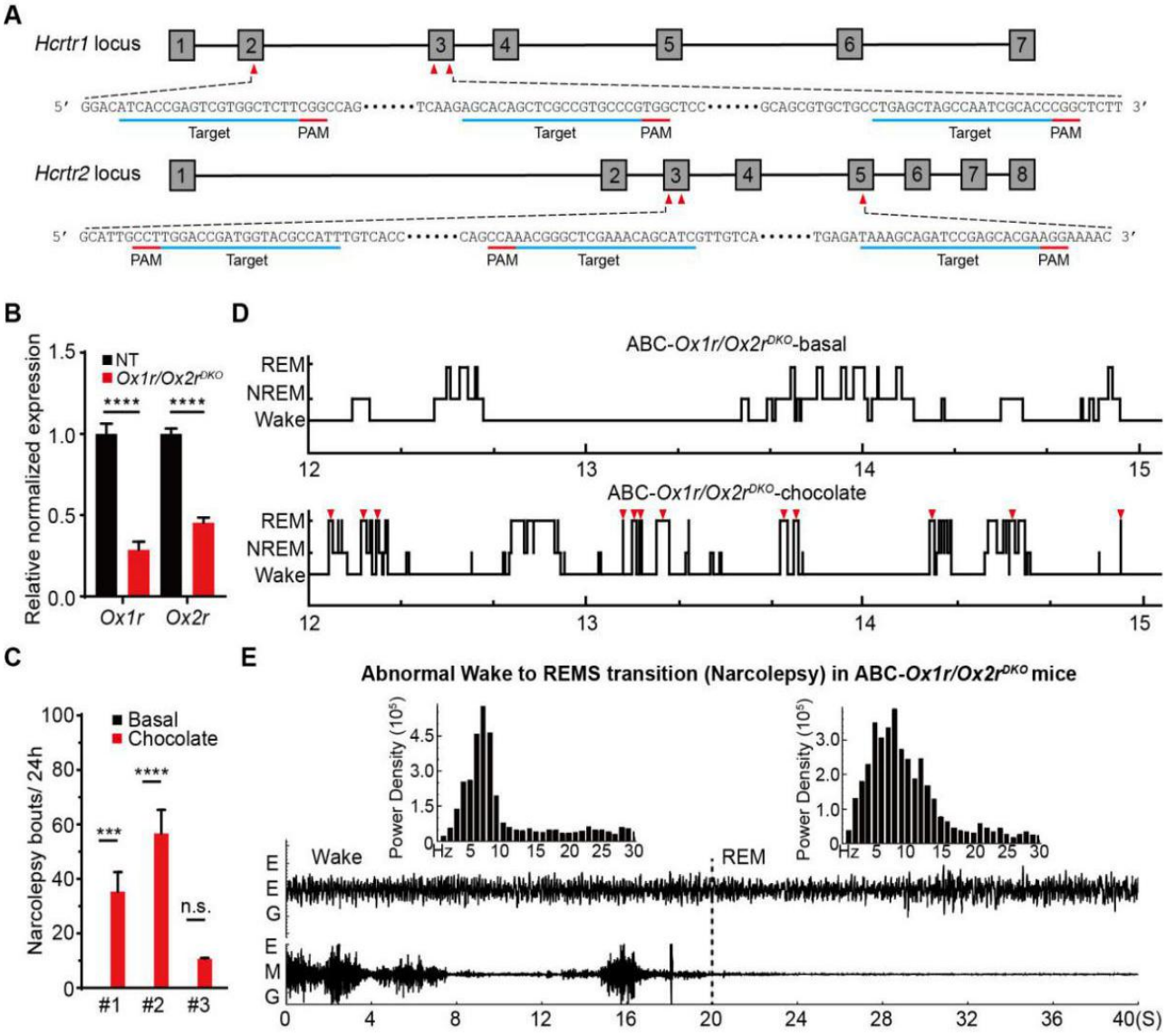

583

584 **Multiplex ABC-CRISPR of *Ox1r* and *Ox2r* causes chocolate-induced narcolepsy episodes.**
585 **(A)** Schematic showing the two sets of sgRNA target sites within exons 2 and 3 of *Ox1r* gene and exons 3 and 5 of *Ox2r* gene. **(B)**
586 Quantification of *Ox1r* and *Ox2r* transcript levels in the ABC-NT and ABC-*Ox1r/Ox2r*^{DKO} mouse brains by real-time reverse-
587 transcription (RT)-quantitative PCR. **(C)** Quantification of the number of narcolepsy episodes in three ABC-*Ox1r/Ox2r*^{DKO} mice
588 before and after chocolate feeding for three days. **(D)** Representative hypnograms (ZT12-15) of ABC-*Ox1r/Ox2r*^{DKO} mice before
589 and after chocolate feeding. Red triangles mark abnormal wake to REM transitions during narcolepsy-like episodes. **(E)**
590 Representative EEG/EMG signals depicting the abnormal Wake to REM transition during one narcoleptic episode in the ABC-
591 *Ox1r/Ox2r*^{DKO} mice. Data are mean ± s.e.m. (B and C) Unpaired t test. n.s. not significant; * $p < 0.05$; ** $p < 0.01$; *** $p < 0.001$;
592 **** $p < 0.0001$.
593

594 **ABC-expression/KO screens identify Ankrd63 and NR1 as potentially new sleep regulators**

595 We recently investigated the molecular substrates of homeostatic sleep need by comparing
596 whole brain phosphoproteomes of *Sleepy* mutant and sleep-deprived wild-type mice (Wang et al.,

597 2018). We identified 80 sleep need index phosphoproteins (SNIPPs), whose phosphorylation states
598 change in relation to sleep need in these two opposite models of high sleep need. The majority of
599 SNIPPs are annotated synaptic proteins, implicating a potential mechanistic link between synaptic
600 phosphoproteome and sleep need regulation. Furthermore, mutant SLP kinase preferentially
601 associates with SNIPPs, suggesting that they may function as downstream substrates of SLP kinase
602 and effectors of homeostatic sleep regulation.

603 To identify new sleep regulators, we performed ABC-expression screening of eight
604 candidate SNIPPs, including Abl-interactor-1(Abi1) (Rial Verde et al., 2006), Ankyrin repeat and
605 sterile alpha motif domain-containing protein 1B (Anks1b) (Tindi et al., 2015), ADP-ribosylation
606 factor-GTPase-activating proteins 2 (Arfgap2) (Saitoh et al., 2009), ADP-ribosylation factor-
607 GTPase-activating proteins 3 (Arfgap3) (Dembla et al., 2014), Ankyrin repeat domain-containing
608 protein 63 (Ankrd63), Synaptopodin (Synpo) (Zhang et al., 2013), DEAD-Box Helicase 3 Y-linked
609 (Ddx3y) (Vakilian et al., 2015), Pyruvate dehydrogenase E1 subunit alpha 1 (Pdha1) (Jakkamsetti
610 et al., 2019), and followed by EEG/EMG-based sleep analysis. As shown by immunoblotting
611 **(Figure 8A)**, seven of eight SNIPPs were expressed at substantial levels in the adult mouse brains
612 following intravenous AAV injection. Among these, only ABC-expression of Ankrd63 resulted in
613 significant sleep phenotypes relative to ABC-eGFP and other ABC-SNIPP mice **(Figure 8B)**.
614 Specifically, ABC-Ankrd63 mice showed reduction in NREMS time and NREMS delta power,
615 increase of wake time and no change in REMS time **(Figure 8C-E and Figure 8-figure**
616 **supplement 1A-E)**.

617 Previously, Ueda and colleagues have reported that *Nr3a* KO mice exhibit a short sleep
618 phenotype by using triple-target CRISPR to generate whole-body biallelic KO mice for members of
619 the N-methyl-D-aspartic (NMDA) receptor family (Sunagawa et al., 2016). However, the sleep
620 functions of essential genes *Nr1* and *Nr2b* could not be analyzed owning to embryonic lethality of
621 KO mice. Here, we performed ABC-KO of *Nr1* by injection of AAV-hSyn-Cre into $Nr1^{flox/flox}$ adult

Figure 8. with 1 supplement

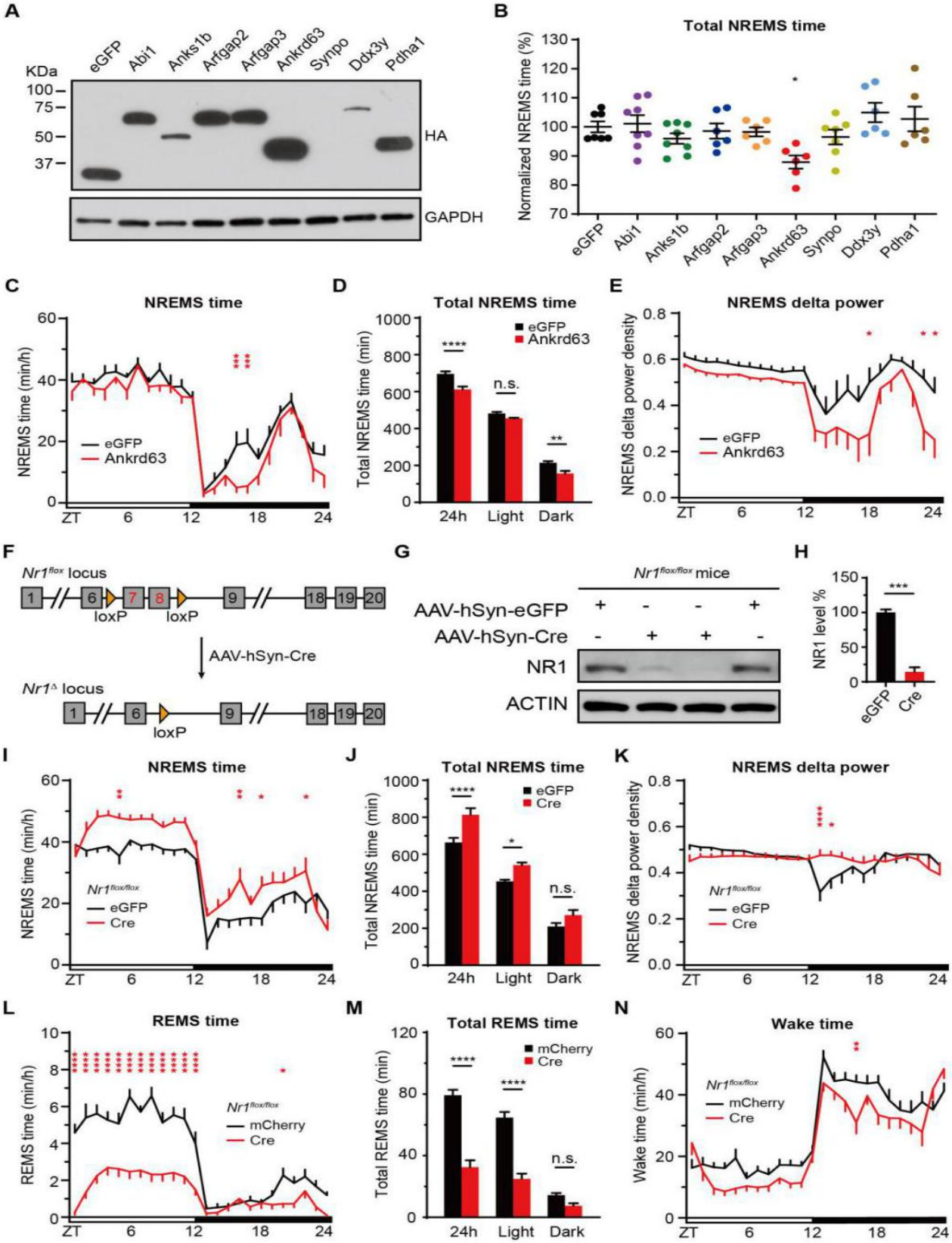

ABC-expression/KO screen identifies Ankrd63 and NR1 as two new sleep regulators.
(A) Immunoblotting of whole brain lysates from AAV-hSyn-SNIPPs injected C57BL/6J adult mice with anti-HA and anti-GAPDH antibodies. **(B)** Daily NREMS time of ABC-SNIPPs mice (n ≥ 5) normalized to that of ABC-eGFP mice.

627 **(C-E)** Hourly plots of NREMS time (C), quantification of total NREMS time (D) and hourly plot of NREMS delta
628 power (E) in the ABC-eGFP (n=7) or ABC-Ankrd63 (n=6) mice. **(F)** Schematic of ABC-KO of *Nr1* by intravenous
629 injection of AAV-hSyn-Cre in *Nr1*$^{flox/flox}$ mice. **(G)** Immunoblotting of brain lysates from AAV-hSyn-eGFP or AAV-
630 hSyn-Cre injected *Nr1*$^{flox/flox}$ mice with anti-NR1 and anti-ACTIN antibodies. **(H)** Quantification of the level of NR1
631 proteins in (G) (n=3). **(I-N)** Hourly plots of NREMS (I), REMS (L) or Wake (N) time, quantification of total NREMS
632 (J) or REMS (M) time and hourly plot of NREMS delta power (K) in the AAV-hSyn-eGFP (n=15) or AAV-hSyn-Cre
633 (n=15) injected *Nr1*$^{flox/flox}$ mice. Data are mean ± s.e.m. (B) One-way ANOVA with Dunn's multiple comparisons test.
634 (C-E and I-N) Two-way ANOVA with Dunn's multiple comparisons test. (H) Unpaired t test. n.s. not significant; * $p <$
635 0.05; ** $p < 0.01$; **** $p < 0.0001$.
636

637 **Figure 8-figure supplement 1.**

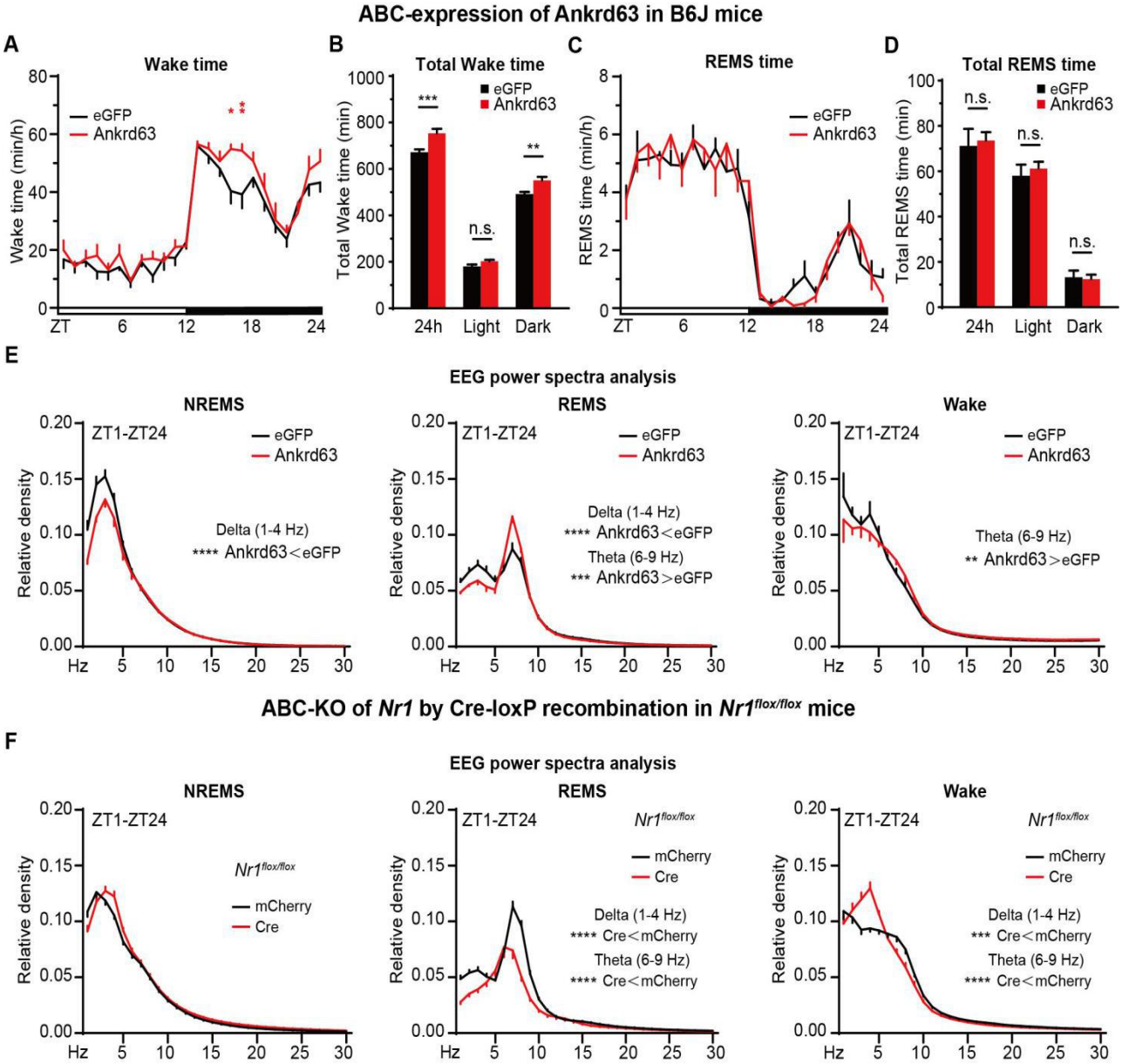

638

639 **ABC-expression/KO screen identifies Ankrd63 and NR1 as two new sleep regulators.**
640 **(A-E)** Hourly plots of Wake (A) or REMS (C) time, quantification of total Wake (B) or REMS (D) time and EEG
641 power spectra analysis of NREMS, REMS and Wake states (E) in the ABC-eGFP (n=7) or ABC-Ankrd63 (n=6)
642 injected mice. **(F)** EEG power spectra analysis of NREMS, REMS and Wake states in the AAV-hSyn-eGFP (n=15) or
643 AAV-hSyn-Cre (n=15) injected *Nr1*$^{flox/flox}$ mice. Data are mean ± s.e.m. (A-F) Two-way ANOVA with Dunn's multiple
644 comparisons test. n.s. not significant; * $p < 0.05$; ** $p < 0.01$; *** $p < 0.001$; **** $p < 0.0001$.

645 mice, in which exons 7 and 8 of *Nr1* gene were flanked by two loxP sites **(Figure 8F)**.
646 Immunoblotting confirmed efficient KO of NR1 expression in the majority of adult brain neurons
647 **(Figure 8G and 8H)**. Accordingly, ABC-KO of *Nr1* caused on average ~150 min increase in daily
648 NREMS amount, ~47 min (~60%) decrease in daily REMS amount, and ~100 min decrease in total
649 wake time **(Figure 8I-N and Figure 8-figure supplement 1F)**. It is worth noting that $Nr3a^{KO}$ and
650 ABC-$Nr1^{KO}$ mice showed opposite changes in NREMS amount, suggest a complex role of NMDA
651 receptor in the regulation of daily sleep time. Taken together, this candidate ABC-expression/KO
652 screen identified Ankrd63 and NR1 as two potentially new sleep regulators.
653

654 **DISCUSSION**

655 **Rapid and efficient somatic genetics analysis of sleep in adult mice**

656 The molecular mechansims of mammalian sleep regulation remain largely unknown.
657 Forward genetics screening of randomly mutagenized mice is a powerful and hypothesis-free
658 approach to identify key sleep regulatory genes in mammals (Banks et al., 2020; Funato et al., 2016;
659 Kapfhamer et al., 2002; Takahashi et al., 1994). On the other hand, reverse genetics, through the
660 making of transgenic, knock-in, KO and conditional KO mice for specific genes of interest,
661 represents a hypothesis-driven approach to identify and characterize new sleep regulatory genes
662 (Graves et al., 2003; Hellman et al., 2010; Honda et al., 2018; Mikhail et al., 2017; Takahashi et al.,
663 1994). This latter approach is greatly accelerated by next generation gene-editing technologies,
664 such as the CRISPR/Cas9 system (Hsu et al., 2014; Sunagawa et al., 2016; Tatsuki et al., 2016;
665 Wang et al., 2013). However, classical forward and reverse genetics approaches involve germline
666 mutations, therefore, are unwieldy to study the essential genes (owning to early lethality) or
667 redundant genes (owning to lack of phenotype) **(Table 1)**. In some but not all cases, forward or
668 reversed genetics may identify viable gain-of-function or partial loss-of-function mutations that can
669 uncover the sleep phenotypes of essential genes (Funato et al., 2016; Graves et al., 2003).

Table 1. Comparison between forward/reverse genetics and somatic genetics approaches in mouse sleep study.

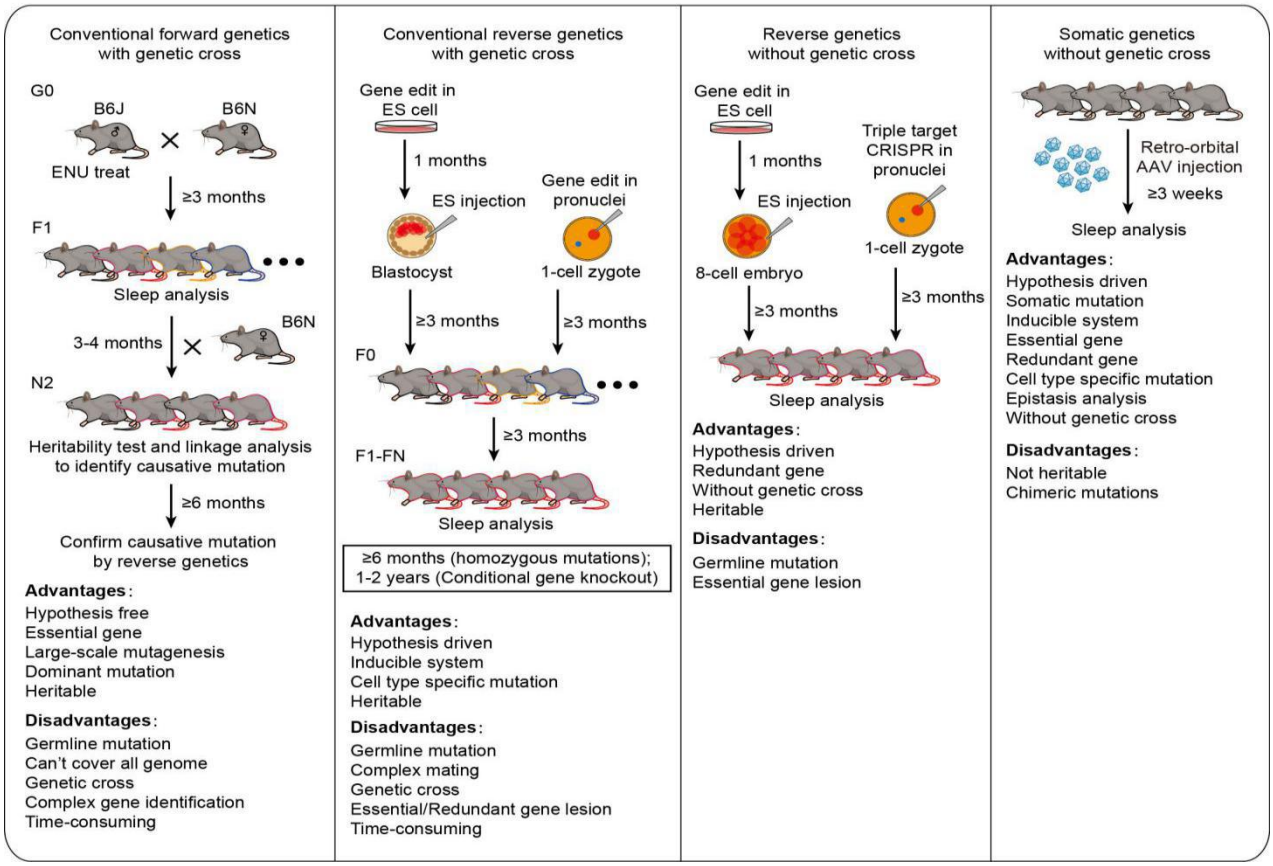

In this study, we applied the AAV-based ABC-expression/KO platform for somatic genetics analysis of sleep in adult mice **(Table 1)**. We conducted two pilot ABC sleep screens that identified CREB and three potentially new sleep regulators: CRTC1, Ankrd63 and NR1. Moreover, both constitutive and Tet-inducible expression of CREB and CRTC1 significantly reduced daily NREMS amount and NREMS delta power. There are two well-known mechanisms for the activation of CREB activity: a) phosphorylation of S133 of CREB; b) CRTCs function as co-activators for CREB. Our results suggest that the ability of CREB to regulate sleep quantity/quality is probably independent of S133 phosphorylation, but can be enhanced by CRTC1. These results demonstrate the proof-of-principle that this somatic genetics approach should facilitate rapid identification of new sleep regulatory genes, especially from essential genes, in adult mice by skipping the mouse development.

Moreover, the ABC-expression/KO platform is a highly efficient approach to conduct sophisticated genetic experiments in adult mice without genetic crosses. For example, when ABC-

684 expression or KO of two different genes produce opposite sleep phenotypes, epistasis analysis can
685 be rapidly carried out to determine whether the two genes operate in the same or parallel pathways
686 and map the order of these genes if they are in the same pathway. For structural and functional
687 analysis of key sleep regulators, ABC-expression of wild-type and mutant proteins can be
688 conducted to rescue the sleep phenotypes of ABC-KO of endogenous proteins. Furthermore, a
689 suppressor screen can be easily conducted to identify the downstream effectors of SLP/SIK3
690 kinases in sleep regulation by ABC-expression of candidate proteins in *Sik3*$^{Slp/+}$ mice, or by ABC-
691 CRISPR of target genes in *Sik3*$^{Slp/+}$;*Rosa26*$^{Cas9/+}$ mice. Similarly, the ABC-expression/KO platform
692 can be used for enhancer screens to uncover the redundant pathways of sleep regulation. Thus, this
693 somatic genetics approach should also facilitate efficient characterization of the molecular
694 pathways of sleep regulation in mice.
695
696 **ABC-KO by AAV-Cre injection facilitates systematic screening of conditional flox mice**
697 To bypass embryonic lethality, conditional flox mice are sometimes crossed with
698 CaMKIIα-Cre transgenic mice, which begin to express Cre recombinase during the third postnatal
699 week (Tsien et al., 1996). Alternatively, conditional flox mice can be crossed with transgenic mice
700 expressing from a pan-neuronal promoter the Cre^{ERT2} fusion proein between Cre and mutant
701 estrogen receptor, which only becomes activated and translocates to the nucleus upon binding of
702 synthetic 4-hydroxytamoxifen (Feil et al., 1996). In theory, the sleep phenotypes could be evaluated
703 in adult mice after tamoxifen injection to induce Cre-dependent KO of target gene in the adult brain
704 neurons. However, both methods have significant drawbacks: 1) CaMKIIα-Cre mice express Cre
705 only in excitatory neurons of the forebrain and Cre expression begins days after birth; 2) Cre^{ERT2}-
706 mediated loxP recombination is inefficient after tamoxifen injection in adult mice (Iwasaki et al.,
707 2021).

708 We showed that intravenous injection of *Creb1*$^{flox/flox}$ adult mice with AAV-hSyn-Cre could
709 efficiently knockout CREB expression in the adult brain neurons and significantly increase daily
710 NREMS amount. On the other hand, AAV-hSyn-Cre injection efficiently excised exon 13 of *Sik3*
711 in the adult brain neurons of *Sik3-E13*$^{flox/flox}$ mice, which phenocopied germline *Sleepy* mutant mice.
712 Thus, ABC-KO by AAV-mediated Cre/loxP recombination can create either loss- or gain-of-
713 function mutations of target gene for sleep phenotype analysis in the adult mice. It is important to
714 highlight that this simple ABC-KO method is more efficient than traditional method of breeding
715 *synapsin 1-Cre*^{ERT2}*;Sik3-E13*$^{flox/+}$ mice, which exhibit little or no sleep phenotype after tamoxifen
716 injection in adult mice (Iwasaki et al., 2021).
717 A significant recent development for mouse genetics is the availability of a large repertoire
718 of conditional flox strains for most mouse genes from the International Knockout Mouse
719 Consortium (IKMC) and commercial sources. Therefore, we envision that ABC-KO by AAV-Cre
720 injection will facilitate systematic screening of conditional flox mice for sleep and other brain-
721 related phenotypes. Moreover, AAV-delivered Cre expression from various cell type-specific
722 promoters, such as hSyn (neurons), CaMKII (excitatory neurons), mDlx (inhibitory neurons) and
723 etc. (de Leeuw et al., 2016; Dimidschstein et al., 2016; Graybuck et al., 2021; Mich et al., 2021;
724 Tsien et al., 1996), represents a simpler and more efficient method to investigate cell type-specific
725 functions of the target gene in the mouse brain without crossing the flox mice with various Cre-
726 transgenic mice.
727
728 **How to distinguish between primary vs. secondary sleep phenotypes?**
729 A large number of genes play important roles in the development of mouse brain. Thus, it is
730 often uncertain whether the sleep phenotype of a mutant mouse strain is the primary phenotype or
731 secondary phenotype owning to developmental abnormalities of the brain. The ABC-
732 expression/knockout platform can be used to effectively address this challenging question by

733 skipping mouse development and directly assessing the sleep phenotypes of somatic mutations in
734 the adult brain neurons. For example, ABC-KO of exon 13 of *Sik3* induced hypersomnia in *Sik3-*
735 *E13*$^{flox/flox}$ mice, whereas ABC-CRISPR of *Slp/Sik3* largely reversed hypersomnia in *Sleepy*
736 (*Sik3*$^{Slp/+}$) mice. These results strongly suggest that the hypersomnia of *Sleepy* mice is the primary
737 phenotype owing to a direct role of mutant SLP kinase in sleep regulation in the adult brain
738 neurons. Thus, this type of somatic genetics analysis can serve as an effective tool to distinguish
739 between the primary and secondary sleep phenotypes for genes that are also important for mouse
740 brain development.
741
742 **Multiplex ABC-CRISPR enables one-step analysis of redundant sleep genes**
743 To analyze the phenotypes of redundant genes, it is time-consuming (≥ 2 years) to generate
744 double or triple knockout mice through classical germline genetic approaches (Sunagawa et al.,
745 2016). A combination of triple-target CRISPR and modified embryonic stem cell technologies
746 allows for biallelic knockout of multiple genes in a single generation, however, this strategy only
747 works for non-essential genes (Sunagawa et al., 2016). Here, we successfully used multiplex ABC-
748 CRISPR technology to disrupt both *Ox1r* and *Ox2r* genes in adult mice, resulting in chocolate-
749 induced narcolepsy episodes. It should be noted that the efficiency of multiplex ABC-CRISPR can
750 be further improved by optimizing the sgRNA structure or pre-screening of sgRNAs, and by
751 potentially developing other CRISPR/Cas systems. For example, unlike CRISPR/Cas9 that requires
752 three U6:sgRNA cistrons to target the same gene, CRISPR/Cpf1 (Cas12a) and CRISPR/Cas13d
753 (targeting RNA) can process a polycistronic transcript into multiple gRNAs targeting the same or
754 different genes (Konermann et al., 2018; Zetsche et al., 2017; Zhong et al., 2017). Thus, multiplex
755 ABC-CRISPR will enable one-step analysis of redundant sleep genes in adult mice, which is also
756 applicable for essential genes and can be achieved in one month rather than 1-2 years.
757

758 **Concluding statement**

759 We believe that this somatic genetics approach could potentially be useful for studies of
760 many brain-related patho/physiological and behavioral processes. First, it skips embryonic
761 development and directly assess the functions of genes in adult mice without genetic crosses, which
762 is especially useful for studying essential genes or redundant pathways. Second, it allows non-
763 neuroscientists and neuroscientists alike to easily express or ablate target genes in adult moue
764 brains without strong skills in stereotactic injection or prior knowledge of where the genes may
765 function in the mouse brain; Third, it facilitates complex mouse genetic experiments, such as
766 epistasis analysis and enhancer/suppressor screens, with an unprecedented speed that is simply
767 impossible with existing tools. Furthermore, similar strategies can be developed for somatic
768 genetics studies of mouse genes in other peripheral organs by using AAV variants engineered to
769 efficiently transduce the muscle, heart, kidney, intestine, lung, skin, testis and ovary (Chan et al.,
770 2017; Gradinaru, 2020; Pulicherla et al., 2011; Tabebordbar et al., 2021).

771

772

ACKNOWLEDGEMENTS

We are thankful for Drs. M. Luo and F. Shao for sharing reagents; K. Wu, Z. Li, W. Min, Y. Zhuang, H. Huang, and Y. Yin for technical assistance; Drs. X. Wang, F. Shao, R. Xi, and N. Tang for discussion and comments on the manuscript; B. Wu for developing the EEG/EMG analysis software; M. Shi for graphical abstract design. This work was supported by the Natural Science Foundation of China (61772526 to Z.C.), the Beijing Municipal Science and Technology Commission (Z181100001318004 to Q.L.) and the National Key Research and Development Program of China.

AUTHOR CONTRIBUTIONS

Q.L., G.W., Q.L., J.X., S.Z., R.Z. designed and executed the experiments with help from F.W., Z.C.; G.W. Q.L., J.X., R.Z. developed the ABC-expression/KO platform and performed molecular genetics experiments with help from Z.C., W.J.; S.Z., Q.L., Z.C. developed the SleepV (video) system; X.G., S.Z., Z.C., C.M., L.C., B.S. performed EEG/EMG recording and analysis; F.W., R.Z. generated multiple mouse strains; Q.S., Y.G. performed AAV packaging and purification; H.W., X.W., H.L. helped mouse husbandry. G.W., Q.L., J.X., S.Z., R.Z.prepared the figures and Q.L., wrote the manuscript with help from G.W., Q.L.

COMPETING INTERESTS

We declare no competing interests.

794 # Materials and methods

795 ## Key resources table

Reagent type(species) or resource	Source or reference	Designation	Identifiers	Additional information
Gene (Mus musculus)	*Abi1*	Origene	Cat# MR206165	
Gene (Mus musculus)	*Anks1b*	Origene	Cat# MR219888	
Gene (Mus musculus)	*Arfgap2*	Origene	Cat# MR208335	
Gene (Mus musculus)	*Arfgap3*	Origene	Cat# MR208404	
Gene (Mus musculus)	*Ankrd63*	Origene	Cat# MR213874	
Gene (Mus musculus)	*Synpo*	Origene	Cat# MR215248	
Gene (Mus musculus)	*Ddx3y*	Origene	Cat# MR209824	
Gene (Mus musculus)	Pdha1	Origene	Cat# MR206079	
Gene (Mus musculus)	*Arc*	CCDS DB	CCDS37102.1	
Gene (Mus musculus)	*Homer1a*	CCDS DB	CCDS26687.1	
Gene (Mus musculus)	*Rab3a*	CCDS DB	CCDS22379.1	
Gene (Mus musculus)	*Plk2*	CCDS DB	CCDS26767.1	
Gene (Mus musculus)	*CamkIIα*	CCDS DB	CCDS29276.1	
Gene (Mus musculus)	*CamkIIβ*	CCDS DB	CCDS24411.1	
Gene (Mus musculus)	*CamkIV*	CCDS DB	CCDS29122.1	
Gene (Mus musculus)	*Cdk5*	CCDS DB	CCDS51434.1	
Gene (Mus musculus)	*Creb1*	CCDS DB	CCDS15005.1	
Gene (Mus musculus)	*Crtc1*	CCDS DB	CCDS40372.1	
Genetic reagent (Mus musculus)	C57BL/6J mice	Jackson Laboratory	Cat# 000664	

Genetic reagent (Mus musculus)	Rosa26-Cas9 knock-in mice	Jackson Laboratory	Cat# JAX:026179	
Genetic reagent (Mus musculus)	Rosa26-LSL-Cas9 knock-in mice	Jackson Laboratory	Cat# JAX:026175	
Genetic reagent (Mus musculus)	Creb1 flox mice	N/A	N/A	Gift from Dr. Fengchao Wang
Genetic reagent (Mus musculus)	Sik3-E13 flox mice	This paper	N/A	
Genetic reagent (Mus musculus)	Nr1 flox mice	This paper	N/A	
Antibody	Rabbit monoclonal anti-CREB	Cell Signaling	Cat# 9197	Western (1:1000); IF (1:500)
Antibody	Rabbit polyclonal anti-NeuN	Millipore	Cat# ABN78	Western (1:1000); IF (1:500)
Antibody	Mouse monoclonal anti-Actin	Beyotime	Cat# AF0003	Western (1:2000)
Antibody	Rabbit monoclonal anti-3-Tubulin	Cell Signaling	Cat# 5568	Western (1:1000)
Antibody	Rabbit polyclonal anti-GFP	Beyotime	Cat# AG279	Western (1:1000)
Antibody	Rabbit polyclonal to anti-CRISPR-Cas9	Abcam	Cat# ab204448	Western (1:500)
Antibody	Mouse monoclonal anti-HA	Sigma-Aldrich	Cat# H6533	Western (1:10000)
Antibody	Mouse monoclonal anti-NR1	Millipore	Cat# 05-432	Western (1:1000)
Antibody	HRP-labeled goat anti-rabbit IgG (H+L)	Beyotime	Cat# A0208	Western (1:10000)
Antibody	Mouse monoclonal anti-GAPDH	EarthOx	Cat# E021010-01	Western (1:2000)
Antibody	HRP-labeled goat anti-mouse IgG (H+L)	Beyotime	Cat# A0216	Western (1:10000)
Antibody	AP-labeled goat anti-rabbit IgG (H+L))	Beyotime	Cat# A0239	Western (1:10000)
Antibody	AP-labeled goat anti-mouse IgG(H+L)	Beyotime	Cat# A0258	Western (1:10000)
Antibody	Rat monoclonal anti-HA	Roche	Cat# 11867423001	IF(1:500)
Antibody	Chicken polyclonal anti-GFP	Abcam	Cat# ab13970	IF(1:2000)

Antibody	Alexa Fluor 555 conjugated goat-anti-rat IgG (H+L)	Cell Signaling	Cat# 4417	IF(1:500)
Antibody	Alexa Fluor 488 conjugated goat anti-rabbit IgG (H+L)	Jackson ImmunoResearch Labs	Cat# 111-545-003	IF(1:500)
Antibody	Alexa Fluor 488 conjugated goat anti-chicken IgY (H+L)	Abcam	Cat# ab150169	IF(1:500)
Antibody	Rabbit polyclonal anti-SIK3	Abcam	N/A	Western (2.5ug/ml)
Chemical compound, drug	TRIzol	Invitrogen	Cat #15596026	
Chemical compound, drug	DAPI solution	Solarbio	Cat #C0060	(100 ng/ml)
Chemical compound, drug	Isoflurane (Rodent use)	RWD Life Science	Cat #RWD-R510-22	(4% for induction, 2% for maintenance)
Chemical compound, drug	OptiPrep Density Gradient Medium	Sigma-Aldrich	Cat #D1556-250ML	(15%, 25%, 40% and 58%)
Chemical compound, drug	PEI MAX-Transfection Grade Linear Polyethylenimine Hydrochloride (MW 40,000)	Polysciences, Inc.	Cat #24765-1	(1ug/ul)
Chemical compound, drug	Difco Skim Milk	BD Life Sciences.	Cat #232100	(5%)
Chemical compound, drug	Bovine Serum Albumin	Sigma-Aldrich	Cat #V900933	(3%)
Chemical compound, drug	Triton X-100	Sigma-Aldrich	Cat #X100-100ML	(0.3%)
Chemical compound, drug	Phosphate buffered saline	Amresco	Cat #0780-10KG	1x
Chemical compound, drug	Chloroform	Beijing chem works	N/A	
Chemical compound, drug	Etanol	Beijing chem works	N/A	
Chemical compound, drug	Isopropyl alcohol	Beijing chem works	N/A	
Chemical compound, drug	Tween 20	Aladdin	N/A	(0.1%)
Chemical compound, drug	Diethyl pyrocarbonate	Sangon Biotech	Cat #A100174-0025	(0.1%)
Chemical compound, drug	Doxorubicin hydrochloride	Sangon Biotech	Cat #A603456	(2mg/ml)
Chemical compound, drug	MK-801	Sigma-Aldrich	Cat #M107-50MG	(2mg/kg)
Commercial assay or kit	BeyoECL Plus Kit	Beyotime	Cat# P0018M	
Commercial assay or kit	BCIP/NBT Alkaline Phosphatase Color Development Kit	Beyotime	Cat# C3206	
Commercial assay or kit	QuantScript RT Kit	TIANGEN Biotech	Cat# KR103	

Commercial assay or kit	EndoFree Maxi Plasmid Kit	TIANGEN Biotech	Cat# DP117	
Commercial assay or kit	TIANamp Genomic DNA Kit	TIANGEN Biotech	Cat# DP304	
Commercial assay or kit	NEBNext Ultra II DNA Library Prep Kit	New England Biolabs	Cat# E7645L	
Commercial assay or kit	Quick Ligation Kit	New England Biolabs	Cat# M2200L	
Deposited data	WGS data	This paper	https://bigd.big.ac.cn/gsa/browse/CRA005128	
Deposited data	Deposited code	This paper	https://github.com/wochiguodong/SleepV.git	
Cell line (*H. sapiens*)	AAVpro	Takara	https://www.takarabio.com/search-results?term=632273&tab=product; Cat# 632273	
Recombinant DNA reagent	pUCmini-iCAP-PHP.eB	Addgene	http://n2t.net/addgene:103005	
Recombinant DNA reagent	pAdDeltaF6	Addgene	http://n2t.net/addgene:112867	
Recombinant DNA reagent	pAAV: EF1α-DIO-H2B-eGFP	N/A	N/A	Gift from Dr. Minmin Luo
Recombinant DNA reagent	pAAV-U6-sgRNA(backbone)-CBh-Cre	Addgene	http://n2t.net/addgene:60229	
Recombinant DNA reagent	pAAV-U6-sgRNA(backbone)-hSyn-Cre-2A-EGFP-KASH	Addgene	http://n2t.net/addgene:60231	
Recombinant DNA reagent	pAAV-hSyn-eGFP	Addgene	http://n2t.net/addgene:105539	
Recombinant DNA reagent	pAAV-CBh-Cre	This paper	N/A	See Materials and Methods: Generation of AAV vectors.
Recombinant DNA reagent	pAAV-hSyn-Cre	This paper	N/A	See Materials and Methods: Generation of AAV vectors.
Recombinant DNA reagent	pAAV-hSyn-Abi1	This paper	N/A	See Materials and Methods: Generation of AAV vectors.
Recombinant DNA reagent	pAAV-hSyn-Anks1b	This paper	N/A	See Materials and Methods: Generation of AAV vectors.

Recombinant DNA reagent	pAAV-hSyn-Arfgap2	This paper	N/A	See Materials and Methods: Generation of AAV vectors.
Recombinant DNA reagent	pAAV-hSyn-Arfgap3	This paper	N/A	See Materials and Methods: Generation of AAV vectors.
Recombinant DNA reagent	pAAV-hSyn-Ankrd63	This paper	N/A	See Materials and Methods: Generation of AAV vectors.
Recombinant DNA reagent	pAAV-hSyn-Synpo	This paper	N/A	See Materials and Methods: Generation of AAV vectors.
Recombinant DNA reagent	pAAV-hSyn-Ddx3y	This paper	N/A	See Materials and Methods: Generation of AAV vectors.
Recombinant DNA reagent	pAAV-hSyn-Pdha1	This paper	N/A	See Materials and Methods: Generation of AAV vectors.
Recombinant DNA reagent	pAAV-Tre-eGFP	This paper	N/A	See Materials and Methods: Generation of AAV vectors.
Recombinant DNA reagent	pAAV-Tre-CREB-VP16	This paper	N/A	See Materials and Methods: Generation of AAV vectors.
Recombinant DNA reagent	pAAV-Tre-CRTC1-CA	This paper	N/A	See Materials and Methods: Generation of AAV vectors.
Recombinant DNA reagent	pAAV-hSyn-Arc	This paper	N/A	See Materials and Methods: Generation of AAV vectors.
Recombinant DNA reagent	pAAV-hSyn-Homer1a	This paper	N/A	See Materials and Methods: Generation of AAV vectors.
Recombinant DNA reagent	pAAV-hSyn-Rab3a	This paper	N/A	See Materials and Methods: Generation of AAV vectors.
Recombinant DNA reagent	pAAV-hSyn-Plk2-dn	This paper	N/A	See Materials and Methods: Generation of AAV vectors.
Recombinant DNA reagent	pAAV-hSyn-CamKIIa	This paper	N/A	See Materials and Methods: Generation of AAV vectors.
Recombinant DNA reagent	pAAV-hSyn-CamKIIb	This paper	N/A	See Materials and Methods: Generation of AAV vectors.
Recombinant DNA reagent	pAAV-hSyn-CaMKIV-dn	This paper	N/A	See Materials and Methods: Generation of AAV vectors.
Recombinant DNA reagent	pAAV-hSyn-CDK5	This paper	N/A	See Materials and Methods: Generation of AAV vectors.
Recombinant DNA reagent	pAAV-hSyn-CREB	This paper	N/A	See Materials and

				Methods: Generation of AAV vectors.
Recombinant DNA reagent	pAAV-hSyn-CRTC1	This paper	N/A	See Materials and Methods: Generation of AAV vectors.
Recombinant DNA reagent	pAAV-hSyn-MEF2-VP16	This paper	N/A	See Materials and Methods: Generation of AAV vectors.
Recombinant DNA reagent	pAAV-U6:NeuN-hsyn-Cre	This paper	N/A	See Materials and Methods: Generation of AAV vectors.
Recombinant DNA reagent	pAAV-2xU6:NeuN-hsyn-Cre	This paper	N/A	See Materials and Methods: Generation of AAV vectors.
Recombinant DNA reagent	pAAV-3xU6:NeuN-hsyn-Cre	This paper	N/A	See Materials and Methods: Generation of AAV vectors.
Recombinant DNA reagent	pAAV-3xU6:Sik3-1-hsyn-eGFP	This paper	N/A	See Materials and Methods: Generation of AAV vectors.
Recombinant DNA reagent	pAAV-3xU6:Sik3-2-hsyn-eGFP	This paper	N/A	See Materials and Methods: Generation of AAV vectors.
Recombinant DNA reagent	pAAV-3xU6:Oxr1-hsyn-eGFP	This paper	N/A	See Materials and Methods: Generation of AAV vectors.
Recombinant DNA reagent	pAAV-3xU6:Oxr2-hsyn-eGFP	This paper	N/A	See Materials and Methods: Generation of AAV vectors.
Sequence-based reagent	CBh-Cre_F	This paper	PCR primers	CGACGCGTACCCGTTACATAACTTACGGTAAATGGC
Sequence-based reagent	CBh-Cre_R	This paper	PCR primers	CCCAAGCTTGATATCGAATTCTTAAGCGTAATCTG
Sequence-based reagent	*Arc_F*	This paper	PCR primers	ATCTGATACCGGTGCCACCATGGAGCTGGACCATATGACCAC
Sequence-based reagent	*Arc_R*	This paper	PCR primers	ATCTGATGGATCCTTCAGGCTGGGTCCTGTCACTG
Sequence-based reagent	*Homer1a_F*	This paper	PCR primers	ATCTGATACCGGTGCCACCATGGGGGAGCAACCTATCTTCAGC
Sequence-based reagent	*Homer1a_R*	This paper	PCR primers	ATCTGATGGATCCACGCGTCTTAATC

				ATGATTGCTGAATTGAATGTGTACC
Sequence-based reagent	*Crtc1*_F	This paper	PCR primers	ATCTGATACCGGTGCCACCATGGCGACTTCGAACAATCC
Sequence-based reagent	*Crtc1*_R	This paper	PCR primers	ATCTGATGGATCCCAGGCGGTCCATTCGGAAGG
Sequence-based reagent	*Crtc1*-S151A_F	This paper	PCR primers	GGAGGACCAACGCTGACTCTGC
Sequence-based reagent	*Crtc1*-S151A_R	This paper	PCR primers	GCAGAGTCAGCGTTGGTCCTCC
Sequence-based reagent	*Crtc1*-S245A_F	This paper	PCR primers	CACAGGGGGCGCCCTTCCTGAC
Sequence-based reagent	*Crtc1*-S245A_R	This paper	PCR primers	GTCAGGAAGGGCGCCCCCTGTG
Sequence-based reagent	*Creb1*_F	This paper	PCR primers	AGCTACCGGTGCCACCATGACCATGGAATCTGGAGCAG
Sequence-based reagent	*Creb1*_R	This paper	PCR primers	CGCGGATCCATCTGATTTGTGGCAGTAAAGGTCC
Sequence-based reagent	*Creb1*-S119A_F	This paper	PCR primers	GGAGGCCTGCCTACAGGAAAATTTTGAATGAC
Sequence-based reagent	*Creb1*-S119A_R	This paper	PCR primers	CTGTAGGCAGGCCTCCTTGAAAGGATTTCC
Sequence-based reagent	*Rab3a*_F	This paper	PCR primers	ATCTGATACCGGTGCCACCATGGCTTCCGCCACAGACTC
Sequence-based reagent	*Rab3a*_R	This paper	PCR primers	ATCTGATGGATCCGCAGGCACAATCCTGATGAG
Sequence-based reagent	*Plk2*-dn_F	This paper	PCR primers	ATCTGATACCGGTGCCACCATGCTGCAGGGTTTCACTCCGGAC
Sequence-based reagent	*Plk2*-dn_R	This paper	PCR primers	ATCTGATGGATCCGTTACATCTCTGTAAGAGCATGTTC

Sequence-based reagent	*CamkIIα*_F	This paper	PCR primers	ATCTGATACCGGTGCCACCATGGCTACCATCACCTGCACC
Sequence-based reagent	*CamkIIα*_R	This paper	PCR primers	ATCTGATGGATCCATGCGGCAGGACGGAGGGCG
Sequence-based reagent	*CamkIIβ*_F	This paper	PCR primers	ATCTGATACCGGTGCCACCATGGCCACCACGGTGACCTG
Sequence-based reagent	*CamkIIβ*_R	This paper	PCR primers	ATCTGATGGATCCCTGCAGCGGGGCCACTGGAG
Sequence-based reagent	*CamkIV*_F	This paper	PCR primers	ATCTGATACCGGTGCCACCATGCTCAAAGTCACGGTGCCCTC
Sequence-based reagent	*CamkIV*_R	This paper	PCR primers	ATCTGATACGCGTGTACTCTGGCTGAATCGCATCC
Sequence-based reagent	*CamkIV*-dn_F	This paper	PCR primers	CAAAGTGTTAAAGGAAACAGTGGACAAG
Sequence-based reagent	*CamkIV*-dn_R	This paper	PCR primers	CTTGTCCACTGTTTCCTTTAACACTTTG
Sequence-based reagent	*Mef2c*_F	This paper	PCR primers	ATCTGATACCGGTGCCACCATGGGGAGAAAAAAGATTCAGATTACG
Sequence-based reagent	*Mef2c*_R	This paper	PCR primers	ATCTGATGGATCCTGTTGCCCATCCTTCAGAGAGTC
Sequence-based reagent	*Cdk5*_F	This paper	PCR primers	ATCTGATACCGGTGCCACCATGCAGAAATACGAGAAACTGGAG
Sequence-based reagent	*Cdk5*_R	This paper	PCR primers	ATCTGATGGATCCTGGGGGACAGAAGTCAGAGAAG
Sequence-based reagent	Tre_F	This paper	PCR primers	GCAGGGCCCGAGTTTACTCCCTATCAGTGATAGAGAACGTATGAAGAGT

Sequence-based reagent	Tre_R	This paper	PCR primers	GCAACCGGTTTTACGAGGGTAGGAAGTGGTACGGAAAGTTGGT
Sequence-based reagent	rTTA_F	This paper	PCR primers	ACCGGATCCGCCACCATGTCTAGACTGGACAAGAGCAAAGTCATAAACTCTGCTC
Sequence-based reagent	rTTA_R	This paper	PCR primers	CTTGATATCGAATTTACCCGGGGAGCATGTCAAGGTCAAAAT
Sequence-based reagent	non-target sgRNAs control_sgRNA1-F	This paper	PCR primers	ACCACGTGTAAGGCGAACGCCTT
Sequence-based reagent	non-target sgRNAs control_sgRNA1-R	This paper	PCR primers	AACAAGGCGTTCGCCTTACACGT
Sequence-based reagent	non-target sgRNAs control_sgRNA2-F	This paper	PCR primers	ACCGACTCCGGGTACTAAATGTC
Sequence-based reagent	non-target sgRNAs control_sgRNA2-R	This paper	PCR primers	AACGACATTTAGTACCCGGAGTC
Sequence-based reagent	non-target sgRNAs control_sgRNA3-F	This paper	PCR primers	ACCCCGCGCCGTTAGGGAACGAG
Sequence-based reagent	non-target sgRNAs control_sgRNA3-R	This paper	PCR primers	AACCTCGTTCCCTAACGGCGCGG
Sequence-based reagent	non-target sgRNAs control_sgRNA1-F	This paper	PCR primers	ACCGCGAGGTATTCGGCTCCGCG
Sequence-based reagent	non-target sgRNAs control_sgRNA1-R	This paper	PCR primers	AACCGCGGAGCCGAATACCTCGC
Sequence-based reagent	non-target sgRNAs control_sgRNA2-F	This paper	PCR primers	ACCGCTTTCACGGAGGTTCGACG
Sequence-based reagent	non-target sgRNAs control_sgRNA2-R	This paper	PCR primers	AACCGTCGAACCTCCGTGAAAGC
Sequence-based reagent	non-target sgRNAs control_sgRNA3-F	This paper	PCR primers	ACCATGTTGCAGTTCGGCTCGAT
Sequence-based reagent	non-target sgRNAs control_sgRNA3-R	This paper	PCR primers	AACATCGAGCCGAACTGCAACAT

Sequence-based reagent	*Neun*_sgRNA1-F	This paper	PCR primers	ACCTCGGGGTCCCTGAACCGGAA
Sequence-based reagent	*Neun*_sgRNA1-R	This paper	PCR primers	AACTTCCGGTTCAGGGACCCCGA
Sequence-based reagent	*Neun*_sgRNA2-F	This paper	PCR primers	ACCGCTCAGATGCTGACCGAGCC
Sequence-based reagent	*Neun*_sgRNA2-R	This paper	PCR primers	AACGGCTCGGTCAGCATCTGAGC
Sequence-based reagent	*Neun*_sgRNA3-F	This paper	PCR primers	ACCGCTGAATGGGACGATCGTAG
Sequence-based reagent	*Neun*_sgRNA3-R	This paper	PCR primers	AACCTACGATCGTCCCATTCAGC
Sequence-based reagent	Set1 *Sik3*_sgRNA1-F	This paper	PCR primers	ACCACAGACCACTTGGTAGCCCA
Sequence-based reagent	Set1 *Sik3*_sgRNA1-R	This paper	PCR primers	AACTGGGCTACCAAGTGGTCTGT
Sequence-based reagent	Set1 *Sik3*_sgRNA2-F	This paper	PCR primers	ACCACTCACCCATATGTCCACTT
Sequence-based reagent	Set1 *Sik3*_sgRNA2-R	This paper	PCR primers	AACAAGTGGACATATGGGTGAGT
Sequence-based reagent	Set1 *Sik3*_sgRNA3-F	This paper	PCR primers	ACCGTTCAAACAGATCGTCACAG
Sequence-based reagent	Set1 *Sik3*_sgRNA3-R	This paper	PCR primers	AACCTGTGACGATCTGTTTGAAC
Sequence-based reagent	Set2 *Sik3*_sgRNA1-F	This paper	PCR primers	ACCTGACAGAATACGCTAGCGGA
Sequence-based reagent	Set2 *Sik3*_sgRNA1-R	This paper	PCR primers	AACTCCGCTAGCGTATTCTGTCA
Sequence-based reagent	Set2 *Sik3*_sgRNA2-F	This paper	PCR primers	ACCGCCGCCCCAGAGCTCTTCGA
Sequence-based reagent	Set2 *Sik3*_sgRNA2-R	This paper	PCR primers	AACTCGAAGAGCTCTGGGGCGGC
Sequence-based reagent	Set2 *Sik3*_sgRNA3-F	This paper	PCR primers	ACCGACAGAGCGCATGATTTACC
Sequence-based reagent	Set2 *Sik3*_sgRNA3-	This paper	PCR primers	AACGGTAAATCAT

	R			GCGCTCTGTC
Sequence-based reagent	*Oxr1*_sgRNA1-F	This paper	PCR primers	ACCATCACCGAGTCGTGGCTCTT
Sequence-based reagent	*Oxr1*_sgRNA1-R	This paper	PCR primers	AACAAGAGCCACGACTCGGTGAT
Sequence-based reagent	*Oxr1*_sgRNA2-F	This paper	PCR primers	ACCCTGAGCTAGCCAATCGCACC
Sequence-based reagent	*Oxr1*_sgRNA2-R	This paper	PCR primers	AACGGTGCGATTGGCTAGCTCAG
Sequence-based reagent	*Oxr1*_sgRNA3-F	This paper	PCR primers	ACCAGCACAGCTCGCCGTGCCCG
Sequence-based reagent	*Oxr1*_sgRNA3-R	This paper	PCR primers	AACCGGGCACGGCGAGCTGTGCT
Sequence-based reagent	*Oxr2*_sgRNA1-F	This paper	PCR primers	ACCTAAAGCAGATCCGAGCACGA
Sequence-based reagent	*Oxr2*_sgRNA1-R	This paper	PCR primers	AACTCGTGCTCGGATCTGCTTTA
Sequence-based reagent	*Oxr2*_sgRNA2-F	This paper	PCR primers	ACCGATGCTGTTTCGAGCCCGTT
Sequence-based reagent	*Oxr2*_sgRNA2-R	This paper	PCR primers	AACAACGGGCTCGAAACAGCATC
Sequence-based reagent	*Oxr2*_sgRNA3-F	This paper	PCR primers	ACCAATGGCGTACCATCGGTCCA
Sequence-based reagent	*Oxr2*_sgRNA3-R	This paper	PCR primers	AACTGGACCGATGGTACGCCATT
Sequence-based reagent	3xsgRNA-MCS_F	This paper	PCR primers	CGCGGGTACCCTCGAGTCTAGATTAATTAAGGCGCGCCGGATCCACGCGTGGCC
Sequence-based reagent	3xsgRNA-MCS_R	This paper	PCR primers	ACGCGTGGATCCGGCGCGCCTTAATTAATCTAGACTCGAGGGTACC
Sequence-based reagent	sgRNA1_F	This paper	PCR primers	ATCGACGCGTGAGGGCCTATTTCC

Sequence-based reagent	sgRNA1_R	This paper	PCR primers	CGCGGATCCACGCGCTACGGACTAGC
Sequence-based reagent	sgRNA2_F	This paper	PCR primers	CGGGATCCGAGGGCCTATTTCCCATGATTCC
Sequence-based reagent	sgRNA2_R	This paper	PCR primers	GCTCTAGACACGCGCTACGGACTAGC
Sequence-based reagent	sgRNA3_F	This paper	PCR primers	GCTCTAGAGAGGGCCTATTTCCCATGATTCC
Sequence-based reagent	sgRNA3_R	This paper	PCR primers	GGGGTACCCACGCGCTACGGACTAGC
Sequence-based reagent	qRT-PCR for *Oxr1* mRNA_F	This paper	PCR primers	ATTCCGGGAGCAGTTCAAGG
Sequence-based reagent	qRT-PCR for *Oxr1* mRNA_R	This paper	PCR primers	GCTCTGCAAGGACAAGGACT
Sequence-based reagent	qRT-PCR for *Oxr2* mRNA_F	This paper	PCR primers	CCACGGACTATGACGACGAG
Sequence-based reagent	qRT-PCR for *Oxr2* mRNA_R	This paper	PCR primers	TTCCCGATGAGAGCCACAAC
Sequence-based reagent	F1/R1 for ABC-*CRISPR of Sik3* _F	This paper	PCR primers	CTGTTCAGGCTTTGTTGGTTCAT
Sequence-based reagent	F1/R1 for ABC-*CRISPR of Sik3* _R	This paper	PCR primers	TCTGTTGTTGCCACAGCCAT
Sequence-based reagent	F2/R2 for ABC-CRISPR of *Sik3*_F	This paper	PCR primers	TGTTCAGGCTTTGTTGGTTCA
Sequence-based reagent	F2/R2 for ABC-CRISPR of *Sik3*_R	This paper	PCR primers	TGCAGGTGCAAAGGGAGTAG
Sequence-based reagent	ITR_F	(Aurnhammer et al., 2012)	PCR primers	GGAACCCCTAGTGATGGAGTT
Sequence-based reagent	ITR_R	(Aurnhammer et al., 2012)	PCR primers	CGGCCTCAGTGAGCGA
Sequence-based reagent	Genotype identification for *Rosa26*^{Cas9} mice _21306	(Platt et al., 2014)	JAX stock #026179	CTGGCTTCTGAGGACCG

Sequence-based reagent	Genotype identification for *Rosa26*^{Cas9} mice _24493	(Platt et al., 2014)	JAX stock #026179	AGCCTGCCCAGAAGACTCC
Sequence-based reagent	Genotype identification for *Rosa26*^{Cas9} mice _26932	(Platt et al., 2014)	JAX stock #026179	CTCCGTCGTGGTCCTTATAGT
Sequence-based reagent	Genotype identification for *Rosa26*^{Cas9} mice _oIMR5984	(Platt et al., 2014)	JAX stock #026179	GCTAACCATGTTCATGCCTTC
Sequence-based reagent	Genotype identification for *Rosa26*$^{LSL\text{-}Cas9}$ mice_31277	(Platt et al., 2014)	JAX stock #026175	ACACCAGCACCAAAGAGGTG
Sequence-based reagent	Genotype identification for *Rosa26*$^{LSL\text{-}Cas9}$ mice_8469	(Platt et al., 2014)	JAX stock #026175	GTAGGTCAGGGTGGTCACGA
Sequence-based reagent	Genotype identification for *Rosa26*$^{LSL\text{-}Cas9}$ mice_oIMR9020	(Platt et al., 2014)	JAX stock #026175	AAGGGAGCTGCAGTGGAGTA
Sequence-based reagent	Genotype identification for *Rosa26*$^{LSL\text{-}Cas9}$ mice_oIMR9021	(Platt et al., 2014)	JAX stock #026175	CCGAAAATCTGTGGGAAGTC
Sequence-based reagent	Genotype identification for *Sik3-E13*^{flox} mice_F	This paper	PCR primers	GGGGCTGGACTTGGCTGAAATACCC
Sequence-based reagent	Genotype identification for *Sik3-E13*^{flox} mice_R	This paper	PCR primers	ACGAATGCACTGAAGCACGTGTGC
Sequence-based reagent	Genotype identification for *Creb1*^{flox} mice_F	This paper	PCR primers	ACTCATAACTCATGTCGGAATCCTT
Sequence-based reagent	Genotype identification for *Creb1*^{flox} mice_R	This paper	PCR primers	TTGGGAATCAGTTACACTATCCACAG
Sequence-based reagent	Genotype identification for	This paper	PCR primers	GATAGAGGAGGTGGAGGCTGTGCCAG

	Nr1^{flox} mice_F			
Sequence-based reagent	Genotype identification for *Nr1*^{flox} mice_R	This paper	PCR primers	GAAGACAGCTTAAGAAGGGGTTCCTGGG
Software, algorithm	ImageJ	Schindelin et al., 2012	https://imagej.net/	
Software, algorithm	OlyVIA	Olympus	https://www.olympus-lifescience.com/en/support/downloads/#!dlOpen=%23detail847249644	
Software, algorithm	Zen Microscope software	Zeiss	https://www.zeiss.com/microscopy/int/products/microscope-software/zen.html	
Software, algorithm	Trimmomatic	Bolger, A. M et al., 2014	http://www.usadellab.org/cms/index.php?page=trimmomatic	
Software, algorithm	Burrows–Wheeler Aligner	Li H et al., 2009	http://bio-bwa.sourceforge.net/	
Software, algorithm	Genome Analysis Toolkit	Broad Institute	https://software.broadinstitute.org/gatk/	
Software, algorithm	Adobe Illustrator	Adobe	http://www.adobe.com/products/illustrator.html	
Software, algorithm	Prism	GraphPad	https://www.graphpad.com/scientific-software/prism/	
Software, algorithm	CFX Manager	Bio-Rad	http://www.bio-rad.com/en-eh/product/cfx-manager-software	
Other	RIPA Lysis Buffer	Beyotime	Cat# P0013B	
Other	Benzonase Nuclease	Sigma-Aldrich	Cat# E1014-25KU	
Other	Tris base	Amresco	Cat# 0497-5KG	
Other	cOmplete Protease Inhibitor Cocktail Tablets	Roche	Cat# 11836145001	
Other	PhosSTOP Phosphatase	Roche	Cat# 4906837001	

	Inhibitor Cocktail Tablet			
Other	Pluronic F-68	Gibco	Cat# 24040032	
Other	iTaq Universal SYBR Green Supermix	Bio-Rad	Cat# 1725125	
Other	Primary Antibody Dilution Buffer	Beyotime	Cat #P0023A	
Other	PrimeSTAR HS DNA Polymerase (premix)	Takara	Cat #R040A	
Other	TaKaRa Taq DNA Polymerase	Takara	Cat #R001A	
Other	Amicon Ultra-4 Centrifugal Filter Unit	Millipore	Cat #UFC801024	
Other	Optima L-100XP Ultracentrifuge	Beckman	N/A	
Other	TurboMix	Scientific Industries	Cat #SI-0564	
Other	Ultra-Clear Tube	Beckman	Cat #344059	
Other	Cell Scrapers	Biologix	Cat #70-2180	

796

797 **Mice**

798 All animal experiments were performed according to procedures approved by the institutional
799 Animal Care and Use Committee of National Institute of Biological Sciences, Beijing (NIBS). All
800 mice were provided food and water *ad libitum* and were housed under humidity and temperature
801 controlled conditions (22-24°C) on a 12-h light: 12-h dark cycle. *Rosa26*^{Cas9} (JAX, 026179) and
802 *Rosa26*$^{LSL\text{-}Cas9}$ (JAX, 026175) were purchased from the Jackson laboratory. The *Creb1*^{flox}, *Sik3-*
803 *E13*^{flox} and *Nr1*^{flox} mice were generated by flanking exon 4 of *creb1*, exon13 of *Sik3* or exons 7 and
804 8 of *Nr1* with two loxP sites, respectively, in the transgenic animal facility at NIBS. All strains
805 were bred to generate the appropriate genotypes for this study. Littermates were used wherever
806 possible for experiments. Most experiments used male mice except *Sik3-E13*^{flox}*;Rosa26*^{Cas9} female
807 mice which were specific indicated in the study. For each experiment, the age of the animals is
808 ranged from 11 to 18 weeks.

809

810 **Generation of AAV vectors**

811 The pAAV: EF1α-DIO-H2B-eGFP plasmid was a gift from Dr. Minmin Luo's lab (NIBS).
812 pAAV-CBh-Cre was constructed by cloning the CBh-Cre cassette from pAAV-U6-
813 sgRNA(backbone)-CBh-Cre (Addgene, 60229) into MluI-HF (R3198L, NEB) and HindIII-HF
814 (R3104S, NEB) digested pAAV-hSyn-eGFP (Addgene, 105539). pAAV-hSyn-Cre and pAAV-
815 hSyn-SNIPPs were subcloned with AsiSI (R0630L, NEB) and MluI-HF (R3198L, NEB) restricted
816 endonuclease from pAAV-hSyn-eGFP by replacing eGFP with Cre or Abi1 (Origene, MR206165),
817 Anks1b (Origene, MR219888), Arfgap2 (Origene, MR208335), Arfgap3 (Origene, MR208404),
818 Ankrd63 (Origene, MR213874), Synpo (Origene, MR215248), Ddx3y (Origene, MR209824),
819 Pdha1 (Origene, MR206079) coding sequence.

820 The cDNAs of Arc (CCDS37102.1), Homer1a (CCDS26687.1), Rab3a (CCDS22379.1), Plk2-
821 dn (CCDS26767.1, 332-682aa) , CamKIIα (CCDS29276.1), CamKIIβ (CCDS24411.1), CaMKIV
822 (CCDS29122.1), CDK5 (CCDS51434.1), CREB (CCDS15005.1) and CRTC1 (CCDS40372.1)
823 were amplified from mouse brain cDNA library by primers contain AgeI-HF (R3552L, NEB) and
824 BamHI-HF (R3136L, NEB) digested site. CaMKIV-dn and $CRTC1^{CA}$ were constructed from
825 CaMKIV or CRTC1 by site-directed mutagenesis using specific primers that contain K75E or
826 S151A/S245A mutations. $MEF2^{VP16}$ and $CREB^{VP16}$ were constructed by fusing MEF2C
827 (CCDS84042.1, 1-117aa) and CREB (CCDS15004.1, 88-341aa) with C-terminal VP16-3xHA and
828 N-terminal VP16 by Gibson assembly. All these cDNAs were inserted into pAAV-hSyn-eGFP by
829 replacing eGFP with individual cDNA.

830 The pAAV-Tre-eGFP, pAAV-Tre-$CREB^{VP16}$ and pAAV-Tre-$CRTC1^{CA}$ were constructed by
831 subcloing Tre promoter to pAAV-hSyn-eGFP, pAAV-hSyn-$CREB^{VP16}$ and pAAV-hSyn-$CRTC1^{CA}$.
832 Reverse tetracycline-controlled transactivator (rtTA) expression was driven by the EF1α promoter.
833 Tre promoter and rtTA sequences were obtained from Dr. Feng Shao's lab (NIBS).

834 The sgRNA sequences were designed based on the Mouse GeCKO v2 Library (Sanjana et al., 2014;
835 Sunagawa et al., 2016). Annealed oligos for individual sgRNA were first inserted into the SapI
836 (R0569S, NEB) digested pAAV-U6-sgRNA(backbone)-hSyn-Cre-2A-EGFP-KASH (Addgene,
837 60231) vector. To better construct the double and triple sgRNA vectors, we had inserted an
838 multiple cloning site (MCS) sequence before the hSyn promoter of pAAV-hSyn-eGFP and pAAV-
839 hSyn-Cre. Then, these modified pAAV-hSyn-eGFP or pAAV-hSyn-Cre plasmids contain double or
840 triple U6:sgRNA cistrons were constructed through PCR amplification two or three different
841 sgRNAs that target the same gene by two or three pair primers, Restriction endonuclease of MluI-
842 HF (R3198L, NEB), BamHI-HF (R3136L, NEB), XbaI (R0145S, NEB) and KpnI-HF (R3142S,
843 NEB) were used for the vectors and fragments digestion, Quick Ligation Kit (M2200L, NEB) was
844 used for the ligation of these appropriate clone. All these plasmids were saved and amplified in
845 NEB Stable Competent *E. coli* (C3040I, NEB).

846 **Virus generation**

847 AAV-PHP.eBs were packaged in AAVpro 293T cells (Clontech, 632273). Cells were
848 harvested by cell lifter (Biologix, 70-2180) 72-h after co-transfection with PHP.eB (Addgene,
849 103005), pAdDeltaF6 (Addgene, 112867) and transfer plasmids using polyethylenimine MAX
850 (Polysciences, 24765). The cell pellets were suspended in 1X Gradient Buffer (10mM Tris-HCl
851 pH=7.6, 150mM NaCl, 10mM $MgCl_2$). Cells were lysed by five repeated cycles of liquid nitrogen
852 freezing, 37°C water bath thawing and vortex. Then the cell lysate was mixed with ≥50 U/mL of
853 Benzonase nuclease (Milipore, E1014) and incubated at 37°C for 30 min. Centrifuge the cell lysate
854 at 21,130g for 30 min at 4°C and transfer the supernatant to a pre-build iodixanol (Optiprep, D1556)
855 step gradients (15%, 25%, 40% and 58%) for ultracentrifugation purification. Vacuum centrifuge at
856 41000rpm, 4°C for 4-h, the virus particles were in the layer of 40% iodixanol gradient. Accurately
857 insert the needle ~1-2 mm below the interface between the 40% and 58% gradient and extract all
858 the 40% virus containing layer. Purified AAV-PHP.eB were concentrated using Amicon filters

859 (EMD, UFC801096) and formulated in sterile phosphate-buffered saline (PBS) supplemented with
860 0.01% Pluronic F68 (Gibco, 24040032). Virus titers were determined by qPCR using a linearized
861 AAV plasmid as a standard.
862
863 **Video-based sleep recording and screening**
864 For video-based sleep screening, 9-11 weeks old C57BL/6J male mice were retro-orbitally
865 injected with 10^{12} AAV-PHP.eB viruses expressing different cDNAs from the hSyn promoter. Two
866 weeks after virus injection, mice were individually housed in Ancare cages with food and water
867 provided *ad libitum* on a 12-h light: 12-h dark cycle. The sleep/wake behaviors of the mice were
868 recorded by an infrared camera (704 x 576 resolution) at 25 frames/s. Infrared LED lights were
869 placed above the cages for videotaping mouse behaviors during the dark phase. For all mice, 3 days
870 of video data were continuously recorded to calculate average daily sleep time for each mouse.
871
872 **Automatic sleep/wake staging by SleepV software**
873 The automatic sleep/wake staging of video data consists of two stages: 1) an AI-augmented
874 video analysis algorithm was developed to extract various information of test mouse from each
875 sampled frame. 2) the state of test mouse (active or inactive) at the video clip level was obtained by
876 grouping the frame-level information within a time window.
877 (1) Video analysis stage:
878 The suspected regions of interest (ROIs) are first extracted from each sample frame using
879 traditional image processing techniques, such as Gaussian filtering, adaptive and global threshold.
880 More than one ROIs are allowed to be detected because of the complication of food, water gel and
881 shadows caused by environmental light. This multi-detection strategy ensures that the true mouse
882 region is not missed. A deep neural network is then used to make a binary classification of each
883 ROI as a mouse or not. Our neural network backbone was based on Resnet18 architecture (He et al.,

2016). We trained the Resnet18 model using 7,200 positive images and 9,000 negative images with manual labeling. All image frames for training were randomly chosen from six mice, which covered both light and dark conditions, and as many mouse postures as possible. All the experiments were carried out on a workstation with a NVIDIA Titan XP GPU, Intel Core i7-7000 CPU.

During the training process, labeled frames data were randomly split into two parts: 80% for training and 20% for validation. We chose cross entropy as the binary classification loss function, and Stochastic Gradient Descent (SGD) as the optimizer with a fixed learning rate 0.001. The training process lasted 50 epochs, as a result, the model accuracy was 99.3% on training dataset and about 96.1% on validation dataset. The ROI with the highest confidence score is designated as the mouse region, while the others were classified as the background noise.

According to the size of ROI and position coordinate, we extracted several descriptive features, i.e., the network prediction score (predict), the detected mouse mask area (IoU), the center of mass of the mask (activity), and the gray information (color) within the detected mask. Similarly, the frame-level features within a time window centered on that frame were also extracted. Denote f_{t} as the current frame, $\{f_{t-m}, f_{t-m+1}, \ldots f_{t+m}\}$ refer to the frames within this time window, where m is a hyperparameter. The differences between f_{t} and f_{t+i}, including predict score difference P_i (predict), mask difference M_i (IoU), center of mass difference of the mouse body A_i (activity), and gray pixel difference G_i (color), were calculated and normalized. We defined $P_i > 0.1$, or $G_i > 3$, or $A_i > 5$, or the normalized value $(G_i + M_i + P_i)/3 > 0.5$ as the threshold to judge the mouse was active at frame t.

(2) Sleep/wake state determination stage:

According to the frame-level preliminary judgment, SleepV defines the sleep state as ≥ 40-s of continuous immobility as previously developed video-based sleep analysis softwares (Fisher et al., 2012; Pack et al., 2007). To further improve the performance of SleepV, we used a series of 0,

909 5, 10, 15, 20, 25, 30s thresholds to filter subtle mouse movements during sleep and compared the
910 sensitivity, specificity, accuracy, and sleep bouts number of SleepV with EEG/EMG analysis. We
911 found that annotating ≤ 15-s of mouse movements in between two sleep states as sleep achieve the
912 best performance of automatic sleep/wake staging by SleepV, which is comparable to that of semi-
913 automatic sleep/wake staging by EEG/EMG analysis software with manual corrections.
914

915 **Tet-on inducible system**

916 For Tet-on inducible sleep recording, EEG/EMG surgeries were carried out on 12-weeks old
917 mice. The mice were recovered for one week and AAV-Tre-eGFP, AAV-Tre-CREB^{VP16} or AAV-
918 Tre-CRTC1^{CA} was co-injected with AAV-EF1α-rtTA through retro-orbital injection. After two
919 weeks virus expression, baseline sleep recording was performed for 3 days without Doxycycline.
920 Then the water was changed with 2mg/mL Doxycycline containing water and subjected to
921 EEG/EMG recording for another 3 days.
922

923 **Genomic DNA Extraction and Captured Illumina Sequencing**

924 Genomic DNA was extracted from mouse brain using TIANamp Genomic DNA Kit
925 (TIANGEN, DP304) following the recommended protocol. Genomic DNA (1-1.5 g) was sheared to
926 300 to 400-bp by Covaris S220 (Covaris, Woburn, MA, USA) and purified with 1X magnetic
927 beads (Ampure XP; Beckman Coulter). Sheared DNA fragments was Subjected to Illumina paired-
928 end DNA library using NEBNext ultra II DNA Library Prep Kit (E7645L, NEB).
929 Preparation and PCR-amplified for three cycles and libraries size were selected with 0.55-1X
930 magnetic beads (Ampure XP, Beckman). Amplified libraries were sequenced using the HiSeq X
931 ten Platform (Illumina) as paired-end 150 base reads according to the manufacturer's protocol.
932 Illumina raw sequencing reads were processed through a standard pipeline consisting of low-
933 quality read filtering through Trimmomatic (version 0.36), alignment to mouse genome GRCm38

934 (mm10) using the Burrows–Wheeler Aligner (BWA, version 0.7.17-r1188) algorithm. The aligned
935 BAM files were processed using the Genome Analysis Toolkit (GATK, version 4.1.4), including
936 mark PCR duplicates and correction for realignments and mapping quality score recalibrations.
937 Haplotype Caller was used for variant calling.
938 Twenty-one potential off-target sites for the three sgRNAs targeting *Sik3* and *NeuN* genes listed
939 below were identified using Cas-OFFinder (http://www.rgenome.net/cas-offinder/).
940 *Sik3* sgRNA-1(ACAGACCACTTGGTAGCCCA):
941 1. AagGACCACTTGtTAGCCCAAGG chr2:87098654
942 2. ACAaAgCACTTGGTAGCCtAAGG chr4:46756223
943 3. ACAGACCACgTGtTAGaCCAAGG chr4:57954753
944 4. gCAGAaCACTGTGGTAGCCCAGGG chr4:126131919
945 5. AtA-ACCACTTGGTAGgCCAGGGAGG chr17:86795878
946 6. ACAGACCAaTctGT-GCCCAGGGTGG chr8:122648253
947 7. ACAGACCACaTGG-AGCtCAAGaAGG chr15:5662796
948
949 *Sik3* sgRNA-2(ACTCACCCATATGTCCACTT):
950 8. ACTCAgCCATtTGTCCAtTTGGG chr7:123562465
951 9. ACTCACtCATATGTgCACTgGGG chr2:25603475
952 10. ACTCACCCtTAgGgCCACTTGGG chr12:17052697
953 11. ACaCAgCCAgATGTCCACTTGGG chr17:60959507
954 12. ACTCACaaATATG-CCAgTTTGGTGG chr15:16585273
955 13. tCTCAgCCATATGTCCACTTC-cAGG chr5:136277718
956 14. A-TCACCCtTATGTgCtCTTTGGTGG chr7:66324551
957
958 *Sik3* sgRNA-3(GTTCAAACAGATCGTCACAG):

959 15. GTTCAAACAGATCGaaACgGAGG chr5:52797383

960 16. GTTCAcACAGtTaGTCACAGTGG chr5:144210416

961 17. GTTCtAACAaATtGTCACAGGGG chr1:49457652

962 18. GcTCAAACAtATtGTCACAGGGG chr4:17192911

963 19. GTCTCAAACAcATCGgCACAGGGG chr8:4772824

964 20. GTCTCAAACAcATCGaCACAGGGG chr1:163033701

965 21. GaTCAAACAGATaGT-ACAGAGG chr15:77931180

966

967 *NeuN* sgRNA-1(TCGGGGTCCCTGAACCGGAA):

968 1. TCtGGaTCCCgGAACCGGAAAGG chr16:7277126

969 2. TCGGGGTCCCTGAACCactAAGG chr7:30375662

970 3. TaGGGGTCCCTGAAaCaGAATGG chr7:45640152

971 4. TgGGGtTCCCTGAACCccAAAGG chrX:11971373

972 5. TCTGGGGTCCCTGAACCtGcAAGG chr17:48361361

973 6. TCGGGGTCCCaGCAACCaGAAGGG chr5:99874083

974 7. TCGGGGaCCCgGAACCTGGAAGGG chr5:109528520

975

976 *NeuN* sgRNA-2(GCTCAGATGCTGACCGAGCC):

977 8. GCTCAGATGCTGACaGAcCtGGG chr16:25376832

978 9. GCTgAGATGCaGACtGAGCCTGG chr16:30614345

979 10. GCTCAGcTGCTGgCCcAGCCTGG chr15:82930003

980 11. GCTtAGATGCTGAtgGAGCCTGG chr7:101383685

981 12. GCTCAGATGCTGgCCTGtGCCAGG chr9:120120623

982 13. GCTCAGATGtTGtCCAGAGCCAGG chr5:66096471

983 14. GCTCAGGcTGCTGACaGAGCtGGG chrX:11232414

984

985 *NeuN* sgRNA-3(GCTGAATGGGACGATCGTAG):

986 15. GCTGttTGGGAgGATCGTAGAGG chr13:48330995

987 16. GCTGtATGGtAgGATCGTAGGGG chr4:22110214

988 17. GCTGAATGGGAgGATCaTcaGGG chrX:98480354

989 18. GCTGAATGGagCGATgGgAGAGG chr15:10917958

990 19. GCTGGAATGtGAgGATaGTAGTGG chrX:164503183

991 20. GCTGAATGAGGAaGATaGTgGTGG chr5:35422881

992 21. GCTGgATGGGACGATgGTACtTGG chr8:28174078

993

994 **EEG/EMG surgery**

995 All EEG/EMG surgeries were performed by experienced technicians. 11 to 13-weeks old male
996 or female mice (all experiments were conducted with male mice if not indicated otherwise) were
997 anesthetized by isoflurane (4% for induction, 2% for maintenance) and surgical tools were
998 sterilized by ethanol just before use. After confirming the mice lack of pain, the head region was
999 shaved, cleaned with ethanol and the skull was exposed. The exposed skull was cleaned by cotton
1000 swabs to improve binding of skull and dental cement. Handheld electrical drill was moved to the
1001 lambda point and set the coordinate as (0, 0, 0). Then four holes were drilled by the electrical drill
1002 in the skull. The coordinate of the holes were (-1.27, 0, 0), (-1.27, 5.03, 0), (1.27, 5.03, 0) and (1.27,
1003 0, 0). Then the EEG electrode pins were implanted to the dura under stereotaxic control and the
1004 EMG wires were inserted into the neck muscle and then stick to the skull with dental cement. After
1005 surgery, the mice were housed individually to recover for one week. Then retro-orbital injection of
1006 AAV-PHP.eB was performed. After allowing time for virus expression (2 week for ABC
1007 expression and 3 weeks for ABC-KO), the mice were tethered to a counterbalanced arm (Instech

1008 Laboratories) that allowed free movement and exerted minimal weight for one week before
1009 EEG/EMG recording.
1010
1011 **EEG/EMG recording and data analysis**
1012 Three days of baseline EEG/EMG recording were conducted after mice were acclimated for
1013 one week recording condition. For the ABC-*Ox1r/Ox2r*^{DKO} mice, an additional one week
1014 EEG/EMG recording were conducted feeding with chocolates. The sleep–wake behaviors were
1015 analyzed as previously described with modifications (Funato et al., 2016). EEG/EMG data were
1016 visualized and analyzed using a custom semi-automated staging MatLab (MathWorks)-based
1017 program, followed by visual inspection. Following semi-automated analysis of EEG/EMG data,
1018 EEG signals were subjected to fast Fourier transform analysis for 1 to 30Hz with 1-Hz bins.
1019 Sleep/wake state was staged into NREMS, REMS and wake. NREMS was staged by high
1020 amplitude, delta (1–4 Hz) frequency EEG and low EMG tonus. REMS was characterized based on
1021 theta (6–9Hz)-dominant EEG and EMG muscle atonia. Wake was staged based on the presence of
1022 low amplitude, fast EEG and high amplitude, variable EMG signal. For the NREMS delta power
1023 density analysis, hourly averages of delta density were defined by the ratio of delta power (1–4 Hz)
1024 to total power of NREMS EEG. For the power spectrum analysis of NREMS, REMS and wake, the
1025 EEG power of each frequency bins was expressed as the percentage of total EEG power over all
1026 frequency bins (1–30 Hz) in each state.
1027
1028 **Brain lysate preparation and Immunoblotting**
1029 Mouse brains were quickly dissected and flash frozen in liquid nitrogen. Brain tissues were
1030 homogenized using mortar/pestle with liquid nitrogen and then lysed in ice-cold RIPA buffer
1031 (50mM Tris-HCL pH=7.4, 150mM NaCl, 1% Triton X-100, 0.1% SDS) (Beyotime, P0013B)
1032 freshly supplemented with protease inhibitor (Roche, 11836145001) and phosphatase inhibitor

1033 (Roche, 4906837001) for 30 min and centrifuged at 21,130g for 15 min at 4℃. The supernatant
1034 was transferred to a new tube and boiled at 95℃ for 10 min with SDS-loading buffer. Western
1035 blotting was performed according to standard protocols using the following antibodies. Rabbit
1036 polyclonal anti-SIK3 antibodies were generated using Abcam custom antibody production service.
1037 The following antibodies were purchased from commercial sources: anti-CREB (CST, 9197S),
1038 anti-NeuN (Milipore, ABN78), anti-β-ACTIN (Beyotime, AF003), anti-Tublin J (CST, 5568), anti-
1039 GFP (Beyotime, AG279), anti-Cas9 (Abcam, ab204448), anti-HA (Sigma, H6533), anti-NR1
1040 (Millipore, 05-432), anti-GAPDH (EarthOx, E021010-01), HRP-labeled Goat Anti-Rabbit IgG(H+L)
1041 (Beyotime, A0208), HRP-labeled Goat Anti-Mouse IgG(H+L) (Beyotime, A0216), AP-labeled
1042 Goat Anti-Rabbit IgG (H+L) (Beyotime, A0239), AP-labeled Goat Anti-Mouse IgG(H+L)
1043 (Beyotime, A0258). BeyoECL Plus (Beyotime, P0018M) was used for the coloration of
1044 Horseradish Peroxidase-based secondary antibodies. BCIP/NBT Alkaline Phosphatase Color
1045 Development Kit (Beyotime, C3206) was used for the coloration of Alkaline phosphatase-based
1046 secondary antibodies.
1047
1048 **Immunohistochemistry**
1049 Mice were deeply anesthetized by choral hydrate and perfused transcardially with 0.9%
1050 normal saline followed by 4% paraformaldehyde in PBS. Brains were post-fixed in 4%
1051 paraformaldehyde in PBS at room temperature for at least 4 hours followed by incubation in 30%
1052 sucrose in PBS at room temperature for 24 h. The cryo-protected brains were sectioned at 40
1053 micron on a cryostat microtome (Leica). After washing in PBST(0.3% Triton X-100 in PBS) for 5
1054 min three times, brain sections were incubated in blocking solution (3% BSA, 0.3% Triton X-100
1055 in PBS) at room temperature for 1-h. Then brain sections were incubated with the primary
1056 antibodies overnight at 4 ℃ and immunofluorescence tagged secondary antibodies at room
1057 temperature for 2-h. After staining, the brain sections were mounted on adhesion microscope slides

1058 (Genview) and encapsulated in sealed tablets containing 3 mg/mL DAPI (Solarbio, C0060).The
1059 following antibodies were used: anti-HA (1:500, 11867423001, Roche), anti-NeuN (1:500, ABN78,
1060 Milipore), anti-GFP (1:2000, ab13970, Abcam), Alexa Fluor 555 conjugated goat-anti-rat (1:500,
1061 4417, CST), Alexa Fluor 488 conjugated goat-anti-rabbit (1:500, 111-545-003, Jackson
1062 Immunoresearch), Alexa Fluor 488 conjugated goat-anti-chicken (1:500, ab150169, Abcam).
1063

1064 **RNA extraction and RT-PCR**

1065 Brain tissues from OX1R/OX2R double knockout mice and control mice were quickly
1066 collected in liquid nitrogen. Previously sterilized mortar and pestle were used to pulverize about the
1067 whole brain sample in liquid nitrogen. Until a fine powder was obtained, the samples were quickly
1068 transferred to a new cold 1.5-mL centrifuge tube. Then, 1000 μL TRIzol (Invitrogen, 15596026)
1069 was added and mixed by vortexing the tube to help cell lysis from tissue samples. Centrifuge 5
1070 minutes, 12,000 x g at 4 ℃ to remove high fat content. After incubating 5 minutes at 4 ℃, 200 μL,
1071 chloroform was added to the samples and flipped centrifuge tube to mixing reagents. Incubate 3
1072 minutes and then Centrifuge the samples for 15 minutes at 12,000 x g at 4 ℃. Transfer the Upper
1073 aqueous phase to a new tube and adding 500 μL isopropanol. Flip centrifuge tube to mixing
1074 reagents and incubating 10 minutes. Centrifuge the samples for 10 minutes at 12,000 x g at 4 ℃
1075 and discarding the supernatant. Resuspend the pellet in 1000 μL 75% ethanol and vortex briefly,
1076 then Centrifuge for 5 minutes at 7500 x g at 4 ℃. Discard the supernatant and air dry the RNA
1077 pellet for 10 minutes. Resuspend the pellet with 200 uL RNase-free water. The RNA concentration
1078 of these samples were quantificated by NanoDrop One (Thermo Scientific, ND-ONE-W). 2 ug
1079 RNA per sample were used to reverse transcript the cDNA by QuantScript RT Kit (TIANGEN
1080 Biotech, KR103). 2 x iTaq Universal SYBR Green Supermix (Bio-Rad, 1725125) was used for the
1081 Reverse Transcription-Polymerase Chain Reaction (RT-PCR) by CFX96 Touch qPCR Detection
1082 System (Bio-Rad, 1855196). Data was analysed by CFX Manager software (Bio-Rad).

1083 **Quantification and statistical analysis**

1084 Statistical analysis of EEG/EMG data was performed using GraphPad Prism 8.0.2. Knockout
1085 efficiency measured by Western blot was quantified using ImageJ software. Two-tailed P value
1086 was used for unpaired t-test, one-way ANOVA for multiple comparisons and two-way ANOVA for
1087 multiple comparisons involving two independent variables. Dunnett's test compares every mean to
1088 a control mean. $p < 0.05$ was considered statistically significant.

1089 **REFERENCES**

1090 Allada, R., Cirelli, C., and Sehgal, A. (2017). Molecular mechanisms of sleep homeostasis in flies
1091 and mammals. Cold Spring Harbor Perspectives in Biology *9*.

1092 Aurnhammer, C., Haase, M., Muether, N., Hausl, M., Rauschhuber, C., Huber, I., Nitschko, H.,
1093 Busch, U., Sing, A., Ehrhardt, A.*, et al.* (2012). Universal real-time PCR for the detection and
1094 quantification of adeno-associated virus serotype 2-derived inverted terminal repeat sequences.
1095 Human Gene Therapy Methods *23*, 18-28.

1096 Banks, G.T., Guillaumin, M.C.C., Heise, I., Lau, P., Yin, M., Bourbia, N., Aguilar, C., Bowl, M.R.,
1097 Esapa, C., Brown, L.A.*, et al.* (2020). Forward genetics identifies a novel sleep mutant with sleep
1098 state inertia and REM sleep deficits. Science Advances *6*, eabb3567.

1099 Barco, A., Alarcon, J.M., and Kandel, E.R. (2002). Expression of constitutively active CREB
1100 protein facilitates the late phase of long-term potentiation by enhancing synaptic capture. Cell *108*,
1101 689-703.

1102 Benito, E., and Barco, A. (2010). CREB's control of intrinsic and synaptic plasticity: implications
1103 for CREB-dependent memory models. Trends in Neurosciences *33*, 230-240.

1104 Bentivoglio, M., and Grassi-Zucconi, G. (1997). The pioneering experimental studies on sleep
1105 deprivation. Sleep *20*, 570-576.

1106 Bibb, J.A. (2003). Role of Cdk5 in neuronal signaling, plasticity, and drug abuse. Neuro-Signals *12*,
1107 191-199.

1108 Bleckmann, S.C., Blendy, J.A., Rudolph, D., Monaghan, A.P., Schmid, W., and Schutz, G. (2002).
1109 Activating transcription factor 1 and CREB are important for cell survival during early mouse
1110 development. Molecular and Cellular Biology *22*, 1919-1925.

1111 Borel, F., Kay, M.A., and Mueller, C. (2014). Recombinant AAV as a platform for translating the
1112 therapeutic potential of RNA interference. Molecular Therapy *22*, 692-701.

1113 Castro, D.C., Oswell, C.S., Zhang, E.T., Pedersen, C.E., Piantadosi, S.C., Rossi, M.A., Hunker,
1114 A.C., Guglin, A., Moron, J.A., Zweifel, L.S., *et al.* (2021). An endogenous opioid circuit
1115 determines state-dependent reward consumption. Nature *598*, 646-651.
1116 Ch'ng, T.H., Uzgil, B., Lin, P., Avliyakulov, N.K., O'Dell, T.J., and Martin, K.C. (2012). Activity-
1117 dependent transport of the transcriptional coactivator CRTC1 from synapse to nucleus. Cell *150*,
1118 207-221.
1119 Chan, K.Y., Jang, M.J., Yoo, B.B., Greenbaum, A., Ravi, N., Wu, W.L., Sanchez-Guardado, L.,
1120 Lois, C., Mazmanian, S.K., Deverman, B.E., *et al.* (2017). Engineered AAVs for efficient
1121 noninvasive gene delivery to the central and peripheral nervous systems. Nature Neuroscience *20*,
1122 1172-1179.
1123 Chemelli, R.M., Willie, J.T., Sinton, C.M., Elmquist, J.K., Scammell, T., Lee, C., Richardson, J.A.,
1124 Williams, S.C., Xiong, Y., Kisanuki, Y., *et al.* (1999). Narcolepsy in orexin knockout mice:
1125 molecular genetics of sleep regulation. Cell *98*, 437-451.
1126 Choudhury, S.R., Harris, A.F., Cabral, D.J., Keeler, A.M., Sapp, E., Ferreira, J.S., Gray-Edwards,
1127 H.L., Johnson, J.A., Johnson, A.K., Su, Q., *et al.* (2016). Widespread Central Nervous System
1128 Gene Transfer and Silencing After Systemic Delivery of Novel AAV-AS Vector. Molecular
1129 Therapy *24*, 726-735.
1130 Chrivia, J.C., Kwok, R.P., Lamb, N., Hagiwara, M., Montminy, M.R., and Goodman, R.H. (1993).
1131 Phosphorylated CREB binds specifically to the nuclear protein CBP. Nature *365*, 855-859.
1132 Cirelli, C., and Tononi, G. (1998). Changes in anti-phosphoserine and anti-phosphothreonine
1133 antibody binding during the sleep-waking cycle and after lesions of the locus coeruleus. Sleep
1134 Research Online : SRO *1*, 11-18.
1135 Comb, M., Birnberg, N.C., Seasholtz, A., Herbert, E., and Goodman, H.M. (1986). A cyclic AMP-
1136 and phorbol ester-inducible DNA element. Nature *323*, 353-356.

1137 Conkright, M.D., Canettieri, G., Screaton, R., Guzman, E., Miraglia, L., Hogenesch, J.B., and
1138 Montminy, M. (2003). TORCs: transducers of regulated CREB activity. Molecular Cell *12*, 413-
1139 423.
1140 de Leeuw, C.N., Korecki, A.J., Berry, G.E., Hickmott, J.W., Lam, S.L., Lengyell, T.C., Bonaguro,
1141 R.J., Borretta, L.J., Chopra, V., Chou, A.Y.*, et al.* (2016). rAAV-compatible MiniPromoters for
1142 restricted expression in the brain and eye. Molecular Brain *9*, 52.
1143 de Vivo, L., Bellesi, M., Marshall, W., Bushong, E.A., Ellisman, M.H., Tononi, G., and Cirelli, C.
1144 (2017). Ultrastructural evidence for synaptic scaling across the wake/sleep cycle. Science *355*, 507-
1145 510.
1146 Dembla, M., Wahl, S., Katiyar, R., and Schmitz, F. (2014). ArfGAP3 is a component of the
1147 photoreceptor synaptic ribbon complex and forms an NAD(H)-regulated, redox-sensitive complex
1148 with RIBEYE that is important for endocytosis. Journal of Neuroscience *34*, 5245-5260.
1149 Deverman, B.E., Pravdo, P.L., Simpson, B.P., Kumar, S.R., Chan, K.Y., Banerjee, A., Wu, W.L.,
1150 Yang, B., Huber, N., Pasca, S.P.*, et al.* (2016). Cre-dependent selection yields AAV variants for
1151 widespread gene transfer to the adult brain. Nature Biotechnology *34*, 204-209.
1152 Dickinson, M.E., Flenniken, A.M., Ji, X., Teboul, L., Wong, M.D., White, J.K., Meehan, T.F.,
1153 Weninger, W.J., Westerberg, H., Adissu, H.*, et al.* (2016). High-throughput discovery of novel
1154 developmental phenotypes. Nature *537*, 508-514.
1155 Diering, G.H., Nirujogi, R.S., Roth, R.H., Worley, P.F., Pandey, A., and Huganir, R.L. (2017).
1156 Homer1a drives homeostatic scaling-down of excitatory synapses during sleep. Science *355*, 511-
1157 515.
1158 Dimidschstein, J., Chen, Q., Tremblay, R., Rogers, S.L., Saldi, G.A., Guo, L., Xu, Q., Liu, R., Lu,
1159 C., Chu, J.*, et al.* (2016). A viral strategy for targeting and manipulating interneurons across
1160 vertebrate species. Nature Neuroscience *19*, 1743-1749.

1161 Donlea, J.M., Ramanan, N., and Shaw, P.J. (2009). Use-dependent plasticity in clock neurons
1162 regulates sleep need in Drosophila. Science *324*, 105-108.
1163 Elliott, A.S., Huber, J.D., O'Callaghan, J.P., Rosen, C.L., and Miller, D.B. (2014). A review of
1164 sleep deprivation studies evaluating the brain transcriptome. SpringerPlus *3*, 728.
1165 Feil, R., Brocard, J., Mascrez, B., LeMeur, M., Metzger, D., and Chambon, P. (1996). Ligand-
1166 activated site-specific recombination in mice. Proceedings of the National Academy of Sciences of
1167 the United States of America *93*, 10887-10890.
1168 Fisher, S.P., Godinho, S.I., Pothecary, C.A., Hankins, M.W., Foster, R.G., and Peirson, S.N. (2012).
1169 Rapid assessment of sleep-wake behavior in mice. Journal of Biological Rhythms *27*, 48-58.
1170 Flavell, S.W., Cowan, C.W., Kim, T.K., Greer, P.L., Lin, Y., Paradis, S., Griffith, E.C., Hu, L.S.,
1171 Chen, C., and Greenberg, M.E. (2006). Activity-dependent regulation of MEF2 transcription
1172 factors suppresses excitatory synapse number. Science *311*, 1008-1012.
1173 Flores, A.E., Flores, J.E., Deshpande, H., Picazo, J.A., Xie, X.S., Franken, P., Heller, H.C., Grahn,
1174 D.A., and O'Hara, B.F. (2007). Pattern recognition of sleep in rodents using piezoelectric signals
1175 generated by gross body movements. IEEE Transactions on Bio-medical Engineering *54*, 225-233.
1176 Foust, K.D., Nurre, E., Montgomery, C.L., Hernandez, A., Chan, C.M., and Kaspar, B.K. (2009).
1177 Intravascular AAV9 preferentially targets neonatal neurons and adult astrocytes. Nature
1178 Biotechnology *27*, 59-65.
1179 Franken, P., Chollet, D., and Tafti, M. (2001). The homeostatic regulation of sleep need is under
1180 genetic control. Journal of Neuroscience *21*, 2610-2621.
1181 Funato, H., Miyoshi, C., Fujiyama, T., Kanda, T., Sato, M., Wang, Z., Ma, J., Nakane, S., Tomita,
1182 J., Ikkyu, A.*, et al.* (2016). Forward-genetics analysis of sleep in randomly mutagenized mice.
1183 Nature *539*, 378-383.
1184 Ganguly-Fitzgerald, I., Donlea, J., and Shaw, P.J. (2006). Waking experience affects sleep need in
1185 Drosophila. Science *313*, 1775-1781.

1186 Gierut, J.J., Jacks, T.E., and Haigis, K.M. (2014). Strategies to achieve conditional gene mutation
1187 in mice. Cold Spring Harbor Protocols *2014*, 339-349.
1188 Gonzalez, G.A., and Montminy, M.R. (1989). Cyclic AMP stimulates somatostatin gene
1189 transcription by phosphorylation of CREB at serine 133. Cell *59*, 675-680.
1190 Gradinaru, V. (2020). Expanding the brain researcher's toolkit. Science *369*, 637.
1191 Graves, L.A., Hellman, K., Veasey, S., Blendy, J.A., Pack, A.I., and Abel, T. (2003). Genetic
1192 evidence for a role of CREB in sustained cortical arousal. Journal of Neurophysiology *90*, 1152-
1193 1159.
1194 Graybuck, L.T., Daigle, T.L., Sedeno-Cortes, A.E., Walker, M., Kalmbach, B., Lenz, G.H., Morin,
1195 E., Nguyen, T.N., Garren, E., Bendrick, J.L*., et al.* (2021). Enhancer viruses for combinatorial cell-
1196 subclass-specific labeling. Neuron *109*, 1449-1464 e1413.
1197 He, K., Zhang, X., Ren, S., and Sun, J. (2016). Deep Residual Learning for Image Recognition.
1198 Paper presented at: 2016 IEEE Conference on Computer Vision and Pattern Recognition (CVPR).
1199 Hellman, K., Hernandez, P., Park, A., and Abel, T. (2010). Genetic evidence for a role for protein
1200 kinase A in the maintenance of sleep and thalamocortical oscillations. Sleep *33*, 19-28.
1201 Honda, T., Fujiyama, T., Miyoshi, C., Ikkyu, A., Hotta-Hirashima, N., Kanno, S., Mizuno, S.,
1202 Sugiyama, F., Takahashi, S., Funato, H*., et al.* (2018). A single phosphorylation site of SIK3
1203 regulates daily sleep amounts and sleep need in mice. Proceedings of the National Academy of
1204 Sciences of the United States of America *115*, 10458-10463.
1205 Hsu, P.D., Lander, E.S., and Zhang, F. (2014). Development and applications of CRISPR-Cas9 for
1206 genome engineering. Cell *157*, 1262-1278.
1207 Hu, J.H., Park, J.M., Park, S., Xiao, B., Dehoff, M.H., Kim, S., Hayashi, T., Schwarz, M.K.,
1208 Huganir, R.L., Seeburg, P.H*., et al.* (2010). Homeostatic scaling requires group I mGluR activation
1209 mediated by Homer1a. Neuron *68*, 1128-1142.

1210 Huber, R., Ghilardi, M.F., Massimini, M., Ferrarelli, F., Riedner, B.A., Peterson, M.J., and Tononi,
1211 G. (2006). Arm immobilization causes cortical plastic changes and locally decreases sleep slow
1212 wave activity. Nature Neuroscience *9*, 1169-1176.
1213 Huber, R., Ghilardi, M.F., Massimini, M., and Tononi, G. (2004). Local sleep and learning. Nature
1214 *430*, 78-81.
1215 Hunker, A.C., Soden, M.E., Krayushkina, D., Heymann, G., Awatramani, R., and Zweifel, L.S.
1216 (2020). Conditional Single Vector CRISPR/SaCas9 Viruses for Efficient Mutagenesis in the Adult
1217 Mouse Nervous System. Cell Reports *30*, 4303-4316 e4306.
1218 Ibata, K., Sun, Q., and Turrigiano, G.G. (2008). Rapid synaptic scaling induced by changes in
1219 postsynaptic firing. Neuron *57*, 819-826.
1220 Iourgenko, V., Zhang, W., Mickanin, C., Daly, I., Jiang, C., Hexham, J.M., Orth, A.P., Miraglia, L.,
1221 Meltzer, J., Garza, D.*, et al.* (2003). Identification of a family of cAMP response element-binding
1222 protein coactivators by genome-scale functional analysis in mammalian cells. Proceedings of the
1223 National Academy of Sciences of the United States of America *100*, 12147-12152.
1224 Iwasaki, K., Fujiyama, T., Nakata, S., Park, M., Miyoshi, C., Hotta-Hirashima, N., Ikkyu, A.,
1225 Kakizaki, M., Sugiyama, F., Mizuno, S.*, et al.* (2021). Induction of Mutant Sik3(Sleepy) Allele in
1226 Neurons in Late Infancy Increases Sleep Need. Journal of Neuroscience *41*, 2733-2746.
1227 Jakkamsetti, V., Marin-Valencia, I., Ma, Q., Good, L.B., Terrill, T., Rajasekaran, K., Pichumani, K.,
1228 Khemtong, C., Hooshyar, M.A., Sundarrajan, C.*, et al.* (2019). Brain metabolism modulates
1229 neuronal excitability in a mouse model of pyruvate dehydrogenase deficiency. Science
1230 Translational Medicine *11*.
1231 Jinek, M., Chylinski, K., Fonfara, I., Hauer, M., Doudna, J.A., and Charpentier, E. (2012). A
1232 programmable dual-RNA-guided DNA endonuclease in adaptive bacterial immunity. Science *337*,
1233 816-821.

1234 Kalogiannis, M., Grupke, S.L., Potter, P.E., Edwards, J.G., Chemelli, R.M., Kisanuki, Y.Y.,
1235 Yanagisawa, M., and Leonard, C.S. (2010). Narcoleptic orexin receptor knockout mice express
1236 enhanced cholinergic properties in laterodorsal tegmental neurons. The European Journal of
1237 Neuroscience *32*, 130-142.
1238 Kandel, E.R. (2012). The molecular biology of memory: cAMP, PKA, CRE, CREB-1, CREB-2,
1239 and CPEB. Molecular Brain *5*, 14.
1240 Kapfhamer, D., Valladares, O., Sun, Y., Nolan, P.M., Rux, J.J., Arnold, S.E., Veasey, S.C., and
1241 Bucan, M. (2002). Mutations in Rab3a alter circadian period and homeostatic response to sleep loss
1242 in the mouse. Nature Genetics *32*, 290-295.
1243 Kohlmeier, K.A., Tyler, C.J., Kalogiannis, M., Ishibashi, M., Kristensen, M.P., Gumenchuk, I.,
1244 Chemelli, R.M., Kisanuki, Y.Y., Yanagisawa, M., and Leonard, C.S. (2013). Differential actions of
1245 orexin receptors in brainstem cholinergic and monoaminergic neurons revealed by receptor
1246 knockouts: implications for orexinergic signaling in arousal and narcolepsy. Frontiers in
1247 Neuroscience *7*, 246.
1248 Konermann, S., Lotfy, P., Brideau, N.J., Oki, J., Shokhirev, M.N., and Hsu, P.D. (2018).
1249 Transcriptome Engineering with RNA-Targeting Type VI-D CRISPR Effectors. Cell *173*, 665-676
1250 e614.
1251 Lisman, J., Yasuda, R., and Raghavachari, S. (2012). Mechanisms of CaMKII action in long-term
1252 potentiation. Nature Reviews Neuroscience *13*, 169-182.
1253 Liu, D., and Dan, Y. (2019). A Motor Theory of Sleep-Wake Control: Arousal-Action Circuit.
1254 Annual Review of Neuroscience *42*, 27-46.
1255 Liu, S., Fu, S., Wang, G., Cao, Y., Li, L., Li, X., Yang, J., Li, N., Shan, Y., Cao, Y.*, et al.* (2021).
1256 Glycerol-3-phosphate biosynthesis regenerates cytosolic NAD(+) to alleviate mitochondrial disease.
1257 Cell Metabolism *33*, 1974-1987 e1979.

1258 Lo, C.C., Chou, T., Penzel, T., Scammell, T.E., Strecker, R.E., Stanley, H.E., and Ivanov, P. (2004).
1259 Common scale-invariant patterns of sleep-wake transitions across mammalian species. Proceedings
1260 of the National Academy of Sciences of the United States of America *101*, 17545-17548.
1261 Luoni, M., Giannelli, S., Indrigo, M.T., Niro, A., Massimino, L., Iannielli, A., Passeri, L., Russo, F.,
1262 Morabito, G., Calamita, P.*, et al.* (2020). Whole brain delivery of an instability-prone Mecp2
1263 transgene improves behavioral and molecular pathological defects in mouse models of Rett
1264 syndrome. eLife *9*.
1265 Mich, J.K., Graybuck, L.T., Hess, E.E., Mahoney, J.T., Kojima, Y., Ding, Y., Somasundaram, S.,
1266 Miller, J.A., Kalmbach, B.E., Radaelli, C.*, et al.* (2021). Functional enhancer elements drive
1267 subclass-selective expression from mouse to primate neocortex. Cell Reports *34*, 108754.
1268 Mikhail, C., Vaucher, A., Jimenez, S., and Tafti, M. (2017). ERK signaling pathway regulates sleep
1269 duration through activity-induced gene expression during wakefulness. Science Signaling *10*.
1270 Montminy, M.R., Sevarino, K.A., Wagner, J.A., Mandel, G., and Goodman, R.H. (1986).
1271 Identification of a cyclic-AMP-responsive element within the rat somatostatin gene. Proceedings of
1272 the National Academy of Sciences of the United States of America *83*, 6682-6686.
1273 Nonaka, M., Kim, R., Fukushima, H., Sasaki, K., Suzuki, K., Okamura, M., Ishii, Y., Kawashima,
1274 T., Kamijo, S., Takemoto-Kimura, S.*, et al.* (2014). Region-specific activation of CRTC1-CREB
1275 signaling mediates long-term fear memory. Neuron *84*, 92-106.
1276 Oishi, Y., Williams, R.H., Agostinelli, L., Arrigoni, E., Fuller, P.M., Mochizuki, T., Saper, C.B.,
1277 and Scammell, T.E. (2013). Role of the medial prefrontal cortex in cataplexy. Journal of
1278 Neuroscience *33*, 9743-9751.
1279 Pack, A.I., Galante, R.J., Maislin, G., Cater, J., Metaxas, D., Lu, S., Zhang, L., Von Smith, R., Kay,
1280 T., Lian, J.*, et al.* (2007). Novel method for high-throughput phenotyping of sleep in mice.
1281 Physiological Genomics *28*, 232-238.

1282 Pardo, L., Valor, L.M., Eraso-Pichot, A., Barco, A., Golbano, A., Hardingham, G.E., Masgrau, R.,
1283 and Galea, E. (2017). CREB Regulates Distinct Adaptive Transcriptional Programs in Astrocytes
1284 and Neurons. Scientific Reports *7*, 6390.
1285 Plath, N., Ohana, O., Dammermann, B., Errington, M.L., Schmitz, D., Gross, C., Mao, X.,
1286 Engelsberg, A., Mahlke, C., Welzl, H.*, et al.* (2006). Arc/Arg3.1 is essential for the consolidation
1287 of synaptic plasticity and memories. Neuron *52*, 437-444.
1288 Platt, R.J., Chen, S., Zhou, Y., Yim, M.J., Swiech, L., Kempton, H.R., Dahlman, J.E., Parnas, O.,
1289 Eisenhaure, T.M., Jovanovic, M.*, et al.* (2014). CRISPR-Cas9 knockin mice for genome editing
1290 and cancer modeling. Cell *159*, 440-455.
1291 Port, F., Strein, C., Stricker, M., Rauscher, B., Heigwer, F., Zhou, J., Beyersdorffer, C., Frei, J.,
1292 Hess, A., Kern, K.*, et al.* (2020). A large-scale resource for tissue-specific CRISPR mutagenesis in
1293 Drosophila. eLife *9*.
1294 Pulicherla, N., Shen, S., Yadav, S., Debbink, K., Govindasamy, L., Agbandje-McKenna, M., and
1295 Asokan, A. (2011). Engineering liver-detargeted AAV9 vectors for cardiac and musculoskeletal
1296 gene transfer. Molecular Therapy *19*, 1070-1078.
1297 Rechtschaffen, A., Bergmann, B.M., Everson, C.A., Kushida, C.A., and Gilliland, M.A. (1989).
1298 Sleep deprivation in the rat: X. Integration and discussion of the findings. Sleep *12*, 68-87.
1299 Rial Verde, E.M., Lee-Osbourne, J., Worley, P.F., Malinow, R., and Cline, H.T. (2006). Increased
1300 expression of the immediate-early gene arc/arg3.1 reduces AMPA receptor-mediated synaptic
1301 transmission. Neuron *52*, 461-474.
1302 Ruppert, S., Cole, T.J., Boshart, M., Schmid, E., and Schutz, G. (1992). Multiple mRNA isoforms
1303 of the transcription activator protein CREB: generation by alternative splicing and specific
1304 expression in primary spermatocytes. The EMBO Journal *11*, 1503-1512.

1305 Saitoh, A., Shin, H.W., Yamada, A., Waguri, S., and Nakayama, K. (2009). Three homologous
1306 ArfGAPs participate in coat protein I-mediated transport. Journal of Biological Chemistry *284*,
1307 13948-13957.
1308 Sanjana, N.E., Shalem, O., and Zhang, F. (2014). Improved vectors and genome-wide libraries for
1309 CRISPR screening. Nature Methods *11*, 783-784.
1310 Saper, C.B., Fuller, P.M., Pedersen, N.P., Lu, J., and Scammell, T.E. (2010). Sleep state switching.
1311 Neuron *68*, 1023-1042.
1312 Saper, C.B., Scammell, T.E., and Lu, J. (2005). Hypothalamic regulation of sleep and circadian
1313 rhythms. Nature *437*, 1257-1263.
1314 Scammell, T.E., Arrigoni, E., and Lipton, J.O. (2017). Neural Circuitry of Wakefulness and Sleep.
1315 Neuron *93*, 747-765.
1316 Seeburg, D.P., Feliu-Mojer, M., Gaiottino, J., Pak, D.T., and Sheng, M. (2008). Critical role of
1317 CDK5 and Polo-like kinase 2 in homeostatic synaptic plasticity during elevated activity. Neuron *58*,
1318 571-583.
1319 Sehgal, A., and Mignot, E. (2011). Genetics of sleep and sleep disorders. Cell *146*, 194-207.
1320 Shaw, P.J., Tononi, G., Greenspan, R.J., and Robinson, D.F. (2002). Stress response genes protect
1321 against lethal effects of sleep deprivation in Drosophila. Nature *417*, 287-291.
1322 Shaywitz, A.J., and Greenberg, M.E. (1999). CREB: a stimulus-induced transcription factor
1323 activated by a diverse array of extracellular signals. Annual Review of Biochemistry *68*, 821-861.
1324 Shepherd, J.D., Rumbaugh, G., Wu, J., Chowdhury, S., Plath, N., Kuhl, D., Huganir, R.L., and
1325 Worley, P.F. (2006). Arc/Arg3.1 mediates homeostatic synaptic scaling of AMPA receptors.
1326 Neuron *52*, 475-484.
1327 Short, J.M., Wynshaw-Boris, A., Short, H.P., and Hanson, R.W. (1986). Characterization of the
1328 phosphoenolpyruvate carboxykinase (GTP) promoter-regulatory region. II. Identification of cAMP
1329 and glucocorticoid regulatory domains. Journal of Biological Chemistry *261*, 9721-9726.

1330 Silva-Pinheiro, P., Cerutti, R., Luna-Sanchez, M., Zeviani, M., and Viscomi, C. (2020). A Single
1331 Intravenous Injection of AAV-PHP.B-hNDUFS4 Ameliorates the Phenotype of Ndufs4 (-/-) Mice.
1332 Molecular Therapy Methods & Clinical Development *17*, 1071-1078.
1333 Sonntag, T., Moresco, J.J., Vaughan, J.M., Matsumura, S., Yates, J.R., 3rd, and Montminy, M.
1334 (2017). Analysis of a cAMP regulated coactivator family reveals an alternative phosphorylation
1335 motif for AMPK family members. PloS One *12*, e0173013.
1336 Sunagawa, G.A., Sumiyama, K., Ukai-Tadenuma, M., Perrin, D., Fujishima, H., Ukai, H.,
1337 Nishimura, O., Shi, S., Ohno, R.I., Narumi, R.*, et al.* (2016). Mammalian Reverse Genetics without
1338 Crossing Reveals Nr3a as a Short-Sleeper Gene. Cell Reports *14*, 662-677.
1339 Suzuki, K., Tsunekawa, Y., Hernandez-Benitez, R., Wu, J., Zhu, J., Kim, E.J., Hatanaka, F.,
1340 Yamamoto, M., Araoka, T., Li, Z.*, et al.* (2016). In vivo genome editing via CRISPR/Cas9
1341 mediated homology-independent targeted integration. Nature *540*, 144-149.
1342 Tabebordbar, M., Lagerborg, K.A., Stanton, A., King, E.M., Ye, S., Tellez, L., Krunnfusz, A.,
1343 Tavakoli, S., Widrick, J.J., Messemer, K.A.*, et al.* (2021). Directed evolution of a family of AAV
1344 capsid variants enabling potent muscle-directed gene delivery across species. Cell *184*, 4919-4938
1345 e4922.
1346 Takahashi, J.S., Pinto, L.H., and Vitaterna, M.H. (1994). Forward and reverse genetic approaches
1347 to behavior in the mouse. Science *264*, 1724-1733.
1348 Tatsuki, F., Sunagawa, G.A., Shi, S., Susaki, E.A., Yukinaga, H., Perrin, D., Sumiyama, K., Ukai-
1349 Tadenuma, M., Fujishima, H., Ohno, R.*, et al.* (2016). Involvement of Ca(2+)-Dependent
1350 Hyperpolarization in Sleep Duration in Mammals. Neuron *90*, 70-85.
1351 Tian, D., Wenlock, S., Kabir, M., Tzotzos, G., Doig, A.J., and Hentges, K.E. (2018). Identifying
1352 mouse developmental essential genes using machine learning. Disease Models & Mechanisms *11*.

1353 Tindi, J.O., Chavez, A.E., Cvejic, S., Calvo-Ochoa, E., Castillo, P.E., and Jordan, B.A. (2015).
1354 ANKS1B Gene Product AIDA-1 Controls Hippocampal Synaptic Transmission by Regulating
1355 GluN2B Subunit Localization. Journal of Neuroscience *35*, 8986-8996.
1356 Tononi, G., and Cirelli, C. (2014). Sleep and the price of plasticity: from synaptic and cellular
1357 homeostasis to memory consolidation and integration. Neuron *81*, 12-34.
1358 Torregrosa, T., Lehman, S., Hana, S., Marsh, G., Xu, S., Koszka, K., Mastrangelo, N., McCampbell,
1359 A., Henderson, C.E., and Lo, S.C. (2021). Use of CRISPR/Cas9-mediated disruption of CNS cell
1360 type genes to profile transduction of AAV by neonatal intracerebroventricular delivery in mice.
1361 Gene Therapy *28*, 456-468.
1362 Tsien, J.Z., Chen, D.F., Gerber, D., Tom, C., Mercer, E.H., Anderson, D.J., Mayford, M., Kandel,
1363 E.R., and Tonegawa, S. (1996). Subregion- and cell type-restricted gene knockout in mouse brain.
1364 Cell *87*, 1317-1326.
1365 Vaccaro, A., Kaplan Dor, Y., Nambara, K., Pollina, E.A., Lin, C., Greenberg, M.E., and Rogulja, D.
1366 (2020). Sleep Loss Can Cause Death through Accumulation of Reactive Oxygen Species in the Gut.
1367 Cell *181*, 1307-1328 e1315.
1368 Vakilian, H., Mirzaei, M., Sharifi Tabar, M., Pooyan, P., Habibi Rezaee, L., Parker, L., Haynes,
1369 P.A., Gourabi, H., Baharvand, H., and Salekdeh, G.H. (2015). DDX3Y, a Male-Specific Region of
1370 Y Chromosome Gene, May Modulate Neuronal Differentiation. Journal of Proteome Research *14*,
1371 3474-3483.
1372 Wang, H., Yang, H., Shivalila, C.S., Dawlaty, M.M., Cheng, A.W., Zhang, F., and Jaenisch, R.
1373 (2013). One-step generation of mice carrying mutations in multiple genes by CRISPR/Cas-
1374 mediated genome engineering. Cell *153*, 910-918.
1375 Wang, Z., Ma, J., Miyoshi, C., Li, Y., Sato, M., Ogawa, Y., Lou, T., Ma, C., Gao, X., Lee, C.*, et al.*
1376 (2018). Quantitative phosphoproteomic analysis of the molecular substrates of sleep need. Nature
1377 *558*, 435-439.

1378 Webb, J.M., and Fu, Y.H. (2021). Recent advances in sleep genetics. Current Opinion in
1379 Neurobiology *69*, 19-24.
1380 Weber, F., and Dan, Y. (2016). Circuit-based interrogation of sleep control. Nature *538*, 51-59.
1381 Weiergraber, M., Henry, M., Hescheler, J., Smyth, N., and Schneider, T. (2005).
1382 Electrocorticographic and deep intracerebral EEG recording in mice using a telemetry system.
1383 Brain Research Brain Research Protocols *14*, 154-164.
1384 Wimmer, M.E., Cui, R., Blackwell, J.M., and Abel, T. (2021). Cyclic AMP response element-
1385 binding protein is required in excitatory neurons in the forebrain to sustain wakefulness. Sleep *44*.
1386 Xiao, D., Zhang, W., Wang, Q., Li, X., Zhang, Y., Rasouli, J., Casella, G., Ciric, B., Curtis, M.,
1387 Rostami, A.*, et al.* (2021). CRISPR-mediated rapid generation of neural cell-specific knockout
1388 mice facilitates research in neurophysiology and pathology. Molecular Therapy Methods &
1389 Clinical Development *20*, 755-764.
1390 Xie, K., Minkenberg, B., and Yang, Y. (2015). Boosting CRISPR/Cas9 multiplex editing capability
1391 with the endogenous tRNA-processing system. Proceedings of the National Academy of Sciences
1392 of the United States of America *112*, 3570-3575.
1393 Yaghouby, F., Donohue, K.D., O'Hara, B.F., and Sunderam, S. (2016). Noninvasive dissection of
1394 mouse sleep using a piezoelectric motion sensor. Journal of Neuroscience Methods *259*, 90-100.
1395 Yamaguchi, H., and de Lecea, L. (2019). In vivo cell type-specific CRISPR gene editing for sleep
1396 research. Journal of Neuroscience Methods *316*, 99-102.
1397 Yang, Y., Wang, L., Bell, P., McMenamin, D., He, Z., White, J., Yu, H., Xu, C., Morizono, H.,
1398 Musunuru, K.*, et al.* (2016). A dual AAV system enables the Cas9-mediated correction of a
1399 metabolic liver disease in newborn mice. Nature Biotechnology *34*, 334-338.
1400 Yin, L., Maddison, L.A., Li, M., Kara, N., LaFave, M.C., Varshney, G.K., Burgess, S.M., Patton,
1401 J.G., and Chen, W. (2015). Multiplex Conditional Mutagenesis Using Transgenic Expression of
1402 Cas9 and sgRNAs. Genetics *200*, 431-441.

1403 Zell, V., Steinkellner, T., Hollon, N.G., Warlow, S.M., Souter, E., Faget, L., Hunker, A.C., Jin, X.,
1404 Zweifel, L.S., and Hnasko, T.S. (2020). VTA Glutamate Neuron Activity Drives Positive
1405 Reinforcement Absent Dopamine Co-release. Neuron *107*, 864-873 e864.
1406 Zetsche, B., Heidenreich, M., Mohanraju, P., Fedorova, I., Kneppers, J., DeGennaro, E.M.,
1407 Winblad, N., Choudhury, S.R., Abudayyeh, O.O., Gootenberg, J.S.*, et al.* (2017). Multiplex gene
1408 editing by CRISPR-Cpf1 using a single crRNA array. Nature Biotechnology *35*, 31-34.
1409 Zhang, X.L., Poschel, B., Faul, C., Upreti, C., Stanton, P.K., and Mundel, P. (2013). Essential role
1410 for synaptopodin in dendritic spine plasticity of the developing hippocampus. Journal of
1411 Neuroscience *33*, 12510-12518.
1412 Zhong, G., Wang, H., Li, Y., Tran, M.H., and Farzan, M. (2017). Cpf1 proteins excise CRISPR
1413 RNAs from mRNA transcripts in mammalian cells. Nature Chemical Biology *13*, 839-841.
1414